

A RE-REANALYSIS OF THE EÖTVÖS EXPERIMENT AND
TIME-VARIATION OF NUCLEAR DECAY RATES

A Dissertation

Submitted to the Faculty

of

Purdue University

by

Michael J. Muetherthies

In Partial Fulfillment of the

Requirements for the Degree

of

Doctor of Philosophy

August 2019

Purdue University

West Lafayette, Indiana

THE PURDUE UNIVERSITY GRADUATE SCHOOL
STATEMENT OF DISSERTATION APPROVAL

Dr. Ephraim Fischbach, Chair

Department of Physics and Astronomy

Dr. Virgil Barnes

Department of Physics and Astronomy

Dr. Mark Haugan

Department of Physics and Astronomy

Dr. Andrew Hirsch

Department of Physics and Astronomy

Approved by:

Dr. John Finley

Head of Department of Physics and Astronomy

For my family, for always supporting me.

ACKNOWLEDGMENTS

I would like to thank my advisor, Ephraim Fischbach, for his guidance and support during my tenure at Purdue. He helped my transition from naive aerospace engineer to competent physicist and has taught me many valuable lessons. I would also like to thank Dr. Virgil Barnes, Dr. Andrew Hirsch, and Dr. Mark Haugan for participating on my committee and counseling me over the years.

I would also like to thank Dr. Dennis Krause and Andrew Longman for their assistance and for many lively discussions over the course of my research.

I would also like to thank the Purdue School of Aeronautics and Astronautics for their support as a teaching assistant and NASA for their support under the Space Technology Research Fellowship (NSTRF). While I eventually switched projects, the freedom offered by NSTRF was invaluable for determining what I ultimately wanted to study. I have had a bit of a convoluted path through graduate school, but I have always been fortunate to have faculty members interested in my skills and abilities, so I would like to thank Dr. James Longuski and Dr. John Cushman for taking me under their wings during my early graduate days.

Over my years at Purdue, I have had the pleasure of meeting and befriending a great many people during my undergraduate and graduate schooling at Purdue. While there are too many people to adequately list here, I would be remiss if I did not mention Jason Liu. From being in the same group during Boiler Gold Rush, to being next-door neighbors in Earhart Hall, to being classmates in Aeronautics and Astronautics Engineering, to finally being my roommate and helping pay the mortgage for the past eight years, you have been with me since literally day one at Purdue and I am more grateful for your friendship than words can adequately express.

I owe, by far, the biggest debt to my family, especially my Mom and Dad. They have supported my emotionally and financially throughout my schooling. They have

always believed in me, even when I did not believe in myself. I would like to thank my brother, for the long Skype chats and gaming sessions, which have been great stress relievers over the years. My parents, siblings, grandparents, aunts/uncles, and cousins have always remain interested in my research (or at least pretended to be, for my sake), even when I have difficulty explaining it. My grandparents have always kept me in their prayers, especially during the long drives between Iowa and Indiana. Unfortunately, Grandma Marie, Grandpa, and Neil did not quite make it to see me finish my dissertation. On a happier note, I would also like to mention little Mollie, who joined the world just in time for me to still be “Uncle Mike” and not “Dr. Mike.” The unwavering support of my my entire family (including distant relatives I do not get to see often enough) has been appreciated throughout my entire schooling, but especially so in the last few months as the prospect of finishing school and finding a job has been mildly panic inducing.

TABLE OF CONTENTS

	Page
LIST OF TABLES	x
LIST OF FIGURES	xi
ABBREVIATIONS	xv
ABSTRACT	xvi
1 Introduction	1
1.1 Fifth Force/Non-Newtonian Gravity	1
1.2 Time-Varying Nuclear Decay Rates	3
1.3 Organization of this Work	5
2 The Eötvös Experiment: From Equivalence Principle Violation to Fifth Force Searches	7
2.1 Equivalence Principle Violation	7
2.2 Pre-Eötvös Experiments	8
2.2.1 Double Pendulum - Newton and Bessel	8
2.2.2 The Guyòt Experiment	9
2.2.3 The Torsion Balance and the Eötvös Experiment	11
2.2.4 Post-Eötvös: Roll, Krotkov, and Dicke	15
2.3 Weak Equivalence Principle and Fifth Forces	15
2.3.1 A Reanalysis of the Eötvös Experiment	18
2.3.2 Eöt-Wash (E-W) Experiment	21
2.3.3 The MICROSCOPE Experiment	22
2.3.4 The Eötvös Experiment Endures	24
3 A Re-Reanalysis of the Eötvös Experiment: Arbitrary Forces in Torsion Balance Experiments	26
3.1 Eötvös Experiment	30

	Page
3.2 The Eöt-Wash Experiment	44
3.3 Scalar-Vector Force Model	46
3.3.1 Case 1: $\bar{\xi}_V > \bar{\xi}_S, \lambda_S > \lambda_V$	50
3.3.2 Case 2: $\bar{\xi}_S > \bar{\xi}_V, \lambda_V > \lambda_S$	54
3.4 Discussion	55
4 Fifth Forces in the MICROSCOPE Experiment	60
4.1 The MICROSCOPE Satellite	60
4.2 Dynamics of Drag-Free Satellites	60
4.3 Data Analysis	65
4.4 Drag Due to Background Particles	66
4.5 Comparison with MICROSCOPE	68
4.5.1 Orbital Elements	68
4.5.2 Results and Discussion	69
5 Time-Varying Nuclear Decay Rates: Review of Past Experiments	73
5.1 Falkenberg ^3H	74
5.2 PTB $^{226}\text{Ra}/^{152}\text{Eu}$	75
5.3 BNL ^{32}Si	76
5.4 Parkhomov $^{60}\text{Co}/^{90}\text{Sr}/^{239}\text{Pu}$	77
5.5 Purdue ^{54}Mn	77
5.6 Mercury MESSENGER	78
5.7 Summary	80
6 Perturbations of Nuclear Decay Rates	83
6.1 Theory	83
6.1.1 β Decay	84
6.1.2 Electron Capture	86
6.2 Modified Decay Energy	87
6.2.1 β decay	87

	Page
6.2.2 Electron capture	90
6.3 Modified Dispersion Relations	91
6.3.1 β decay	92
6.3.2 Electron capture	93
6.4 Time Dependence of the Perturbations	93
6.4.1 Earth-Sun Distance	94
6.4.2 Earth Orbital Velocity	95
6.5 Neutrino Index of Refraction	96
6.5.1 Dispersionless Models	97
6.5.2 Dispersive Models	98
6.5.3 Anomalous Dispersion	102
6.6 Future Experiments	102
6.6.1 Multiple Neutrino Emission	102
6.6.2 Neutrinoless Double Beta Decay	103
6.6.3 Torsion Balance Experiments	104
6.6.4 Mass Problem	104
7 Decay Rate Suppression by the Pauli Exclusion Principle	106
7.1 Thermal Neutrinos	107
7.2 Non-Thermal Neutrinos	109
7.2.1 PEP Suppression Factor	109
7.2.2 Simple Example	112
7.2.3 A (Slightly) More Complicated Example	112
7.3 Discussion	114
8 Conclusions and Future Work	115
8.1 Overview of Major Results	115
8.1.1 Fifth Force/Non-Newtonian Gravity	115
8.1.2 Time-variation in Nuclear Decay Rates	116
8.2 Future Work	118

	Page
8.2.1 Fifth Force/Non-Newtonian Gravity	118
8.2.2 Time-variation in Nuclear Decay Rates	119
REFERENCES	120
A Alternate Parameterization of Arbitrary Forces in Torsion Balance Experiments	125
B Reference Frames and Frame Rotations	128
B.1 Reference Frames and Conversions	128
B.1.1 Space-Based Reference Frames	128
B.1.2 Earth-Based Reference Frame	128
B.1.3 Body Reference Frames	130
B.1.4 Frame Conversions	130
B.2 Velocity of the MICROSCOPE Test Mass	131
B.2.1 Velocity of the Sun through the galaxy	131
B.2.2 Orbital Velocity	132
B.2.3 Total Velocity	133
C Derivation of the Matrix Element for Beta Decay of a Polarized Neutron	134
D Solution to the Lepton Tensor Traces	139
D.1 $Tr(\gamma^\mu \gamma^\kappa \gamma^\nu \gamma^\tau)$	139
D.2 $-Tr(\gamma^\mu \gamma^\kappa \gamma^\nu \gamma^5 \gamma^\tau)$	139
D.3 $-Tr(\gamma^\mu \gamma^5 \gamma^\kappa \gamma^\nu \gamma^\tau)$	140
D.4 $Tr(\gamma^\mu \gamma^5 \gamma^\kappa \gamma^\nu \gamma^5 \gamma^\tau)$	140
D.5 Full Solution	140
E Computation of the Beta Decay Integral	141
E.1 $I_1 = \int x \sqrt{x^2 - 1} dx$	141
E.2 $I_2 = \int x^2 \sqrt{x^2 - 1} dx$	142
E.3 $I_3 = \int x^3 \sqrt{x^2 - 1} dx$	143
E.4 Full Results	143
VITA	145

LIST OF TABLES

Table	Page
2.1 Measurements of $\Delta\kappa$ from EPF [2] and calculations of $\Delta(B/\mu)$ from Fischbach et al. [34] used in the curve fitting.	19
3.1 Notation differences between EPF (Ref. [2]) and this work.	29
5.1 Experiments showing changes to radioactive decay rates with distance from the Sun, along with properties of the isotopes, and the computed oscillation amplitude, ξ	81
6.1 Measurements of neutrino (and anti-neutrino) speeds from various experiments.	98
6.2 Computed values for the real and imaginary parts of the index of refraction for $M_0 = 5$ MeV and $\gamma = 0.05$ MeV.	101

LIST OF FIGURES

Figure	Page
2.1 Schematic of Newton's Pendulum Experiment. Reproduced from [7].	8
2.2 Representation of the N-E-D reference frame.	10
2.3 The Guyòt experiment. Reproduced from [7].	12
2.4 Schematic of a two mass torsion balance. Reproduced from [7].	13
2.5 Drawing of the torsion balance used in EPF experiment [2].	14
2.6 Drawing of the torsion balance used in the RKD experiment [4]. The three masses arranged at the corner of the triangle eliminate gravity gradients that were intrinsic to The EPF measurements.	16
2.7 Plot of $\Delta\kappa$ vs $\Delta(B/\mu)$ for the Eötvös experiment. The solid line shows the linear curve fit of the data. The data are listed in Table 2.1. The plot was reproduced from [35].	20
2.8 A drawing of the torsion balance used by Eöt-Wash taken from [35]. This entire apparatus was mounted on a turntable and rotated to eliminate any intrinsic twist in the fiber.	23
2.9 A drawing of the four masses attached to the fiber. Two of the masses are aluminum while the other two are beryllium.	24
3.1 Representation of the N-E-D reference frame.	27
3.2 The transformations from the NED frame to the body frame.	29
3.3 Side view of the Eötvös Experiment.	30
3.4 Top view of the Eötvös Experiment.	31
3.5 Side view of the Eöt-Wash Experiment.	45
3.6 Reduced Eötvös parameter for the Eötvös experiment for various values of α_1 , ζ_1 , and λ_V	52
3.7 Reduced Eötvös parameter for the Eöt-Wash experiment for various values of α_1 , ζ_1 , and λ_V	53
3.8 The top plot shows zeros of $\bar{\eta}_{EW}$. The bottom plot shows the values of $\bar{\eta}_{EPF}$ at the zeros of $\bar{\eta}_{EW}$	54

Figure	Page
3.9 Reduced Eötvös parameter for the Eötvös experiment for various values of α_2 , ζ_2 , and λ_S	56
3.10 Reduced Eötvös parameter for the Eöt-Wash experiment for various values of α_2 , ζ_2 , and λ_S	57
3.11 The top plot shows zeros of η_{EW} for Case 2. The bottom plot shows value of $\bar{\eta}_{EPF}$ at the zeros of $\bar{\eta}_{EW}$	58
4.1 A one-dimensional schematic of a drag free satellite. If the test mass moves forward relative to the spacecraft, the aft thrusters fire, accelerating the spacecraft. If the test mass moves after relative to the spacecraft, the froward thrusters fire, decelerating the spacecraft. This process generalizes to three dimensions	62
4.2 The two test masses for the MICROSCOPE satellite with fixed orientation. The two masses drift due to a composition dependent force or a WEP violation.	63
4.3 Simulated result of the differential acceleration of the STEP Experiment [17]. The top plot shows the signal with the WEP violation due to $\Delta\kappa$ and the bottom plot lacks a WEP violation. The difference is the slight peak at $\omega/\omega_0 = 3$. The remaining peaks are due to the orbit, gravity gradients, and effective spring constants. [17]. To test for WEP violation, we would look for the peak at $3\omega_0$	66
4.4 The expected results for background particles fixed relative to the galaxy. The left plot has satellite spin rate of 2.0432×10^{-3} Hz and the plot on the right has a spin rate of 0.5885×10^{-3} Hz, as in Figure 4.6. The red and green lines show the locations of a WEP violation and gravity gradient, respectively.	70
4.5 The expected results for background particles that rotate with the galaxy. The left plot has satellite spin rate of 2.0432×10^{-3} Hz and the plot on the right has a spin rate of 0.5885×10^{-3} Hz, as in Figure 4.6. The red and green lines show the locations of a WEP violation and gravity gradient, respectively.	71
4.6 The results from two different runs of the MICROSCOPE Experiment [37]. The left plot has satellite spin rate of 2.0432×10^{-3} Hz, the plot on the right has a spin rate of 0.5885×10^{-3} Hz, and both plots have an orbital frequency of 0.16818×10^{-3} Hz. The frequency of an expected WEP violation is f_{EP} . The gravity gradient signal is located at $2f_{EP}$. Note the lack of peak at f_{EP} , indicating no WEP violation (to the level of the noise). 72	72

Figure	Page
5.1 Plot of the data from the Falkenberg experiment along with bounded curve, taken from [38]. The horizontal axis represents days since January 1, 1981. The vertical axis represents the detrended data (exponential removed).	74
5.2 Normalized decay rates of ^{152}Eu from [31]. The vertical dotted lines indicate January 1st every five years. The vertical axis measures the normalized decay rates, but it is presented as a change in the efficiency of the detector. The oscillations have a period of ~ 1 yr and an amplitude of $\sim 10^{-3}$.	75
5.3 Normalized decay rates of ^{226}Ra and $1/R^2$ plotted versus time. The decay rates are measured relative to the left axis and $1/R^2$ is measured relative to right axis.	76
5.4 The raw $^{32}\text{Si}/^{36}\text{Cl}$ data from BNL plotted with the $1/R^2$ data (from [32]). The scale for $^{32}\text{Si}/^{36}\text{Cl}$ is given on the left axis while the scale for $1/R^2$ is given on the right axis. We see good qualitative agreement between the two curves.	77
5.5 From top to bottom, normalized decay rates of ^{60}Co , ^{90}Sr , and ^{239}Pu from Parkhomov [39].	78
5.6 Data from the Purdue ^{54}Mn experiment between 2008 and 2012 (unpublished, from [40]). The vertical lines represent locations of perihelion and aphelion. We see that the data have a general upward trend, which appears to correlate to the upward trend in the number of sunspots during the observation period. In addition to the upward trend, the data appear to oscillate with an estimated period of ~ 1 yr with an amplitude of $\sim 10^{-3}$.	79
6.1 The fractional change for the perturbation of the form $V \sim a^n$. We see that lower values of n are well behaved as a gets large, but the curves diverge as $a \rightarrow 1$, which is undesired.	88
6.2 The fractional change for the perturbation of the form $V \sim (a - 1)^n$. We see that $n = 0$ and $n = 1$ are well behaved as a gets large, but $n = 0$ diverges as $a \rightarrow 1$	89
6.3 The first- and second- order corrections from a perturbation of the form $V = \epsilon q$. We see that $\Gamma^{(1)}/\Gamma^{(0)}$ is fairly flat over the range of q values considered.	91
6.4 The real and imaginary parts of the index of refraction, $n(E)$ and $\kappa(E)$ assuming $\epsilon = 0.01$ and $\gamma/M_0 = 0.01$	100

Figure	Page
6.5 The neutrino group velocity (blue) for $\epsilon_0 = \gamma/M_0 = 0.01$. (a), and zooming in on the region of anomalous dispersion (b). The red line in (a) is the the imaginary part of the refractive index which shows absorption is largest in the region of anomalous dispersion.	103
B.1 The relationship between the inertial frame and the perifocal frame. Ω is the longitude of the ascending node, i is the inclination and θ^* is the argument of periapsis. The perifical frame is related to the local orbital frame by the true anomaly, ν	129

ABBREVIATIONS

BNL	Brookhaven National Laboratory
E-W	Eöt-Wash
ECI	Earth-Centered Inertial
EFP	Eötvös, Eötvös, Fekete, and Pekár
N-E-D	North-East-Down Frame
PEP	Pauli Exclusion Principle
pp	proton-proton fusion chain
PSD	Power Spectrum Density
PTB	Physikalisch-Technische Bundesanstalt
RKD	Roll, Krotkov, and Dicke

ABSTRACT

Mueterthies, Michael J. Ph.D., Purdue University, August 2019. A Re-Reanalysis of the Eötvös Experiment and Time-Variation of Nuclear Decay Rates. Major Professor: Ephraim Fischbach.

We consider the existence of a force that could produce a non-null result in the Eötvös experiment while producing a null result in the Eöt-Wash experiment. We introduce a general force, in the form of its Taylor series expansion, and determine the response of each experiment to that force. We can then determine which terms of the expansion are important to each experiment. A trial force, in the form of a mixed vector-scalar interaction is introduced and we analyze the resulting Eötvös parameters for various values of the strengths and ranges of the interactions. We find that under certain conditions the Eötvös parameter for the Eöt-Wash experiment can be made zero while the Eötvös parameter for the Eötvös experiment is nonzero.

Next, we examine the possibility of a wind force appearing in the MICROSCOPE experiment. This wind would be due to the satellite's motion through a particle background which couples to the differential accelerometer through a baryon-number dependent interaction. We determine the signal that would be measured by MICROSCOPE satellite and compare the power spectrum density of this signal to the published power spectrum density of the experiment.

Additionally, we present a new theoretical framework for the time-variation of nuclear decay rates. This new framework is motivated by the results of numerous experiments which show a periodicity of one year. The fractional decay rate of these experiments are constant, regardless of isotope. We find that a novel neutrino interaction, in the form of an index of refraction, successfully generates the constant fractional decay rates. Using the optical theorem and the relativistic Breit-Wigner

distribution makes the index of refraction consistent with neutrino speed measurements. We conclude by describing other systems where the index of refraction could create observable oscillations.

Finally, we consider the suppression of beta decay rates through the Pauli exclusion principle due to the presence of background cosmic and solar neutrinos. We derive the suppression factor for both thermalized and non-thermalized neutrinos.

1. INTRODUCTION

1.1 Fifth Force/Non-Newtonian Gravity

The idea of universality of free fall (UFF) has its origins in the unhistorical story of Galileo dropping masses off the Leaning Tower of Pisa. In reality, he used an inclined plane to test whether objects fall at the same rate. This concept was further codified as the Weak Equivalence Principle (WEP) by Isaac Newton [1] when he set out to measure whether the gravitational and inertial masses of an object were identical. Newton and later Bessel [2] used the period of different pendulums to measure the WEP violation. Guyòt [2] later tried to measure and WEP violation using the angle of a plumb bob relative to a liquid mercury surface.

The next big stride in the study of WEP violations and the impetus for part of this work was the experiment of Eötvös, Pekár and Fekete (EPF) [2]. Over the span of several years, EPF measure the differential acceleration of a number of materials using the recently-invented torsion balance, which proved to be significantly more sensitive than previous versions. Strangely, the results of the experiment were not published for several years, eventually being published in 1922, three years after the death of Eötvös. The paper claims that the results were consistent with no effect, but later work calls that result into doubt.

In the 1950's the work of Lee and Yang [3] showed that additional, short range forces could mimic violations of the weak equivalence principle or universality of free fall. Lee and Yang's focus shifted to parity violation and they did not return to WEP violations. However, their work spurred renewed interest in WEP experiments. Roll, Krotkov, and Dicke [4], Braginskii and Panov [5], and Keiser and Faller [6] performed torsion balance experiments using the Sun as the source in 1964, 1971, and 1982, respectively.

Perhaps the biggest stimulus for the revival of WEP/UFF/fifth force experiments was the work of Fischbach et al. in 1986 [7]. They went back and reanalyzed the published results of Eötvös, Pekár and Fekete from 1922 [2]. Fischbach et al. reconsidered the problem from the perspective of a baryon-number dependent Yukawa force and not a WEP violation. They found a clear correlation between baryon number and the measured results of EPF at a level of 8σ .

The results of Fischbach et al. sparked even more experiments, most now specifically looking for new forces. In the years since the Fischbach paper, the Eö-Wash group [8] [9] [10] has performed a number of torsion balance experiments searching for new forces using a number of sources, from the hills near the University of Washington campus in Seattle, to the Sun and the center of the galaxy. The Eöt-Wash group has not found an evidence for new forces.

In addition to torsion balance experiments, other groups have performed Galileo (or free fall experiments). The groups have included Niebauer, HcHugh and Faller in 1987 [11], Kuroda and Mio in 1989 [12] and 1990 [13] and Carusotto et al. in 1992 [14]. These experiments used laser interferometry to measure the differential rotation rate of test mass with two different compositions. None of these groups reported positive results. Thieberger in 1987 [15] and Bizzeti in 1989 [16] used buoyant forces on floating balls to search for a fifth force. Thieberger reported a positive result while Bizzeti reported a negative result. Despite other authors trying to explain Thieberger's results as being due to systemic effects, Thieberger has stood by his results. While interesting, we will not be focusing on the Thieberger experiment in this work.

Searches for violation of WEP and UFF and searches for new forces continue this day. To obtain even more accuracy, groups have begun proposing space-based missions such as STEP [17], which was eventually cancelled and MICROSCOPE [18] which launched in 2016.

Despite numerous attempts, no one has been able to explain why the Eötvös experiment has a correlation to baryon number, a concept that did not exist when the

experiment was performed. In this work we will focus on comparing the Eötvös experiment to the most precise modern torsion balance experiments, namely the Eötvash experiment.

The term fifth force is a bit of a misnomer, invented by the press. Most students are taught that there are four forces: gravity, electromagnetic, weak nuclear force, and strong nuclear force. However, any particle exchange can give rise to a force. Meson exchanges bind neutrons and protons together in the nucleus. neutrino-antineutrino exchange can give rise to long range forces and become particularly important in neutron stars. Higgs bosons, axions, and W and Z bosons could also give rise to forces. For this reason it is probably more apt to refer to the forces considered in this work as “non-Newtonian gravity”, but we will keep the “fifth force” nomenclature, as it is popular parlance and it rolls off the tongue more easily.

1.2 Time-Varying Nuclear Decay Rates

Becquerel’s [19] discovery of radioactivity in 1896 sparked a flurry of research in the early 20th century. Many sources of radioactivity were discovered and many experiments were performed to determine the variability of nuclear decay rates; by 1930, no change in decay rates had been discovered and they were thought to be constant [20].

Developments such as quantum theory and Fermi’s [21] weak interaction provided a foundation for theoretical investigation into the constancy of decay rates. Consider the process of electron capture, a proton captures an orbiting electron, converting into a neutron and emitting an electron neutrino. We must note positron emission also involves the conversion of a proton into a neutron. In this case, instead of capturing an electron, a positron is emitted in the final state. Any isotope that can undergo positron emission has the potential to decay via electron capture; however, there are isotopes where the mass difference between the initial (“parent”) nucleus and the final (“daughter”) nucleus is insufficient to produce a positron. These isotopes can

only decay by capturing an electron, which obviously requires orbiting electrons to be present. If we remove electrons from the atom, the decay rate decreases, as there are fewer electrons to capture; if we fully ionize the atom, decay is not possible. This effect was used to isolate the contribution from positron emission [22] and to study the K-orbit electron capture [23]. We see a similar phenomenon in electron emission. ^{163}Dy is normally a stable element, but when fully ionized, $^{163}\text{Dy}^{66+}$ decays by emitting an electron into a low lying orbital with a half-life of 47 days [24].

The examples above are quite drastic as they involving removing nearly all of the atom's electrons. There also exist more subtle modifications to the decay rates. Emery [25] discussed the influence of pressure and temperature on the radioactive decay, particularly electron capture. Chemical bonds can affect decay rates; Wang et al. measured the decay rate of ^7Be inside a metal and found a 1% change in the decay rates. To accurately measure the mass of the electron neutrino, the KATRIN experiment must account for the molecular effects in the decay of tritium [26]. Matese and O'Connell [27] and Fasio-Canuto [28] showed that incredibly strong magnetic fields (strong enough to quantize the emitted electrons into Landau Levels) could significantly alter decay rates.

The recent interest in time-varying nuclear decay rates began with a desire to test the inherent randomness of nuclear decays [29]. In an effort to design an experiment, Fischbach found a paper by Alburger, Harbottle, and Norton [30] at Brookhaven National Laboratory (BNL) who compared the decay of ^{32}Si to ^{36}Cl . Their data showed unexpected time oscillations. Further research uncovered the work of Siegert, Schrader, and Schötzig [31] (PTB) who compared the decay of Eu isotopes to that of ^{226}Ra with both ^{152}Eu and ^{226}Ra showing oscillations. Analysis of both sets of data showed strong correlation with $1/R(t)^2$, where $R(t)$ is the Earth-Sun distance. [32]. These correlations, and correlations between the two data sets during the time they were simultaneously operating, point to the effect coming from the Sun as opposed to environmental effects. A power spectrum analysis of the data revealed several other

periods associated with the Sun, including the solar rotation period, providing further evidence of solar influences.

The puzzling oscillations in the BNL and PTB data led to an experiment at Purdue to measure the decay of ^{54}Mn . This experiment provided perhaps the most compelling evidence of solar influences on decay rates. A large solar flare occurred that appears to be correlated with a perturbation in the measured decay of the Mn sample during the same time period [33]. Care was taken to eliminate possible flare-induced environmental effects to reach the conclusion that the dip in the decay rate was caused by the solar flare. The flare also serendipitously may have revealed information about the form of the perturbation. When the dip in the decay data occurred, Purdue was on the night side of the planet, meaning that whatever particle was responsible for the perturbation must have traveled through the Earth unaffected. Particles that best fit this description are neutrinos. It was proposed that the perturbation comes from a novel neutrino-neutrino interaction. The magnitude of the perturbation would depend on the flux of neutrinos at the experiment location. The flux of solar neutrinos falls off as $1/R^2$, matching the behavior of the BNL and PTB experiments. It is presumed that the physical process that creates solar flares also creates a burst of neutrinos, accounting for the dip during the December 2006 solar flare.

1.3 Organization of this Work

The remainder of this work proceeds as follows. Chapter 2 will review the early experiments and modern torsion balance experiments that searched for equivalence principle violations, and fifth force. Chapter 3 will be our attempt to reconcile the Eötvös results with the Eöt-Wash results by modeling a general force in each experiment. Chapter 4 will investigate whether the MICROSCOPE Experiment can measure a background wind force. Beginning with Chapter 5, we switch gears, and begin consider the time-varying nuclear decay rates. Chapter 5 will give a review of the experiments showing oscillations of one year and we tabulate relevant data. In Chap-

ter 6 we consider two possibilities for perturbing the decay rates and consider their ramifications. In Chapter 7, we consider the perturbation due to the Pauli blocking of background neutrinos. Chapter 8 will summarize the results and give suggestions for future work. Finally, the work ends with several Appendices containing math computations that might be of interest to the reader, but that may distract from the flow of the main chapters.

2. THE EÖTVÖS EXPERIMENT: FROM EQUIVALENCE PRINCIPLE VIOLATION TO FIFTH FORCE SEARCHES

2.1 Equivalence Principle Violation

Today, we associate the Eötvös experiment with fifth force searches, but it has its roots in searches for violations of the universality of free fall (UFF), today referred to as the weak equivalence principle (WEP). Tests for the violation of UFF have their origin of the rolling ball tests of Galileo, but it was the work of Isaac Newton that allowed a mathematical description of the problem. Newton's second law of motion relates the acceleration, \vec{a} , of an object of mass, m_I , to the force, \vec{F} applied as shown in Eq. (2.1),

$$m_I \vec{a} = \vec{F}. \quad (2.1)$$

Newton's Law of universal gravitation states that the force of gravity on an object is proportional to the local gravitational field, $\vec{g}(\vec{r})$, with the proportionality constant being the mass, m_G ,

$$\vec{F}_{grav} = m_G \vec{g}(r). \quad (2.2)$$

We can combine Eqs. (2.1) and (2.2) to describe the motion of a body in the local gravitational field, where m_I is defined as the inertial mass and m_G is defined as the gravitational mass.

$$m_I \vec{a} = m_G \vec{g}(r). \quad (2.3)$$

Both sides of this equation have a mass term, and the question can be posed as to whether these masses are the same. The inertial mass has its origin in a body's resistance to its acceleration, while gravitational mass comes from coupling to the gravitational field. Galileo's experiments on the universality of free fall tell us that the two masses should be identical, but Galileo's experiments have a very limited

precision and we cannot guarantee the conclusions beyond that precision. Therefore, we label the two masses as m_I and m_G and consider other experiments.

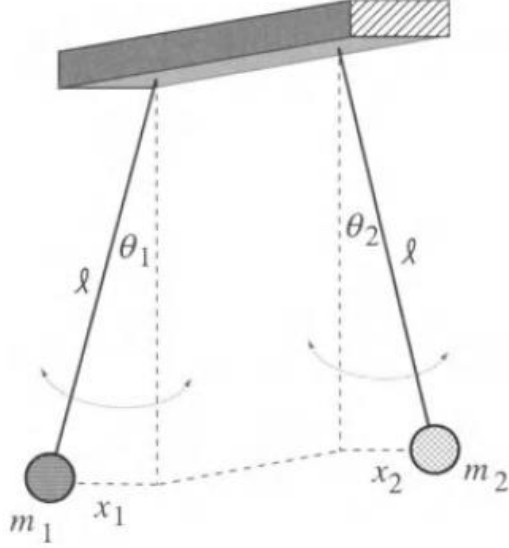


Fig. 2.1. Schematic of Newton's Pendulum Experiment. Reproduced from [7].

2.2 Pre-Eötvös Experiments

2.2.1 Double Pendulum - Newton and Bessel

Isaac Newton himself performed the first test of the weak equivalence principle [1]. His experiment consisted to two pendulums with the same length and mass, but constructed with different materials. The dynamics of the pendulums are given by

$$m_{I,j} \ell^2 \ddot{\theta}_j = -m_{G,j} g \ell \sin \theta_j, \quad (2.4)$$

$$\ddot{\theta}_j = -\frac{m_{G,j} g}{m_{I,j} \ell} \sin \theta_j, \quad (2.5)$$

$$= -\Omega_j \sin \theta_j, \quad (2.6)$$

where $j = 1, 2$ refer to the two test masses.

The periods of the pendulums are

$$T_j = \frac{2\pi}{\Omega} = 2\pi \sqrt{\frac{m_{I,j}}{m_{G,j}}} \sqrt{\frac{\ell}{g}}. \quad (2.7)$$

Hence, the shift in the periods due to the appearance of the fifth force interactions is given by

$$\frac{\Delta T_{12}}{T} = \sqrt{\frac{m_{I,1}}{m_{G,1}}} - \sqrt{\frac{m_{I,2}}{m_{G,2}}}, \quad (2.8)$$

where T the unperturbed period. If we now introduce the common parameterization for the WEP violation,

$$m_{G,j} = m_{I,j} (1 + \kappa_j), \quad (2.9)$$

then we can finally write the relative WEP violation parameter in terms of the measured period difference

$$\Delta\kappa_{12} = -2 \frac{\Delta T_{12}}{T}. \quad (2.10)$$

.

Newton performed the dual pendulum experiment and found a limit of the WEP parameter of $\Delta\kappa_{12} \leq \left| \frac{1}{1,000} \right|$, while Bessel repeated the experiment and extended the lower bound to $\Delta\kappa_{12} \leq \left| \frac{1}{60,000} \right|$ (Reported in [2]).

2.2.2 The Guyòt Experiment

The next evolution of WEP violation experiments was the experiment of Guyòt, shown in Fig. 2.3. The motivation behind this experiment is the fact that when suspended, a plumb bob points in the direction of the total force vector. This is not simply towards the center of the Earth, but slightly displaced due to the centrifugal force from the Earth's rotation. Thus, the angle of the bob will be determined by an inertial term (centrifugal) and a gravitational term, so a WEP violation can result in different materials hanging at different angles.

We will work in a North-East-Down frame, as shown in Fig. 2.2. The \hat{N} vector points from the local location towards the North Pole of the Earth, \hat{D} points toward the center of Earth, and \hat{E} points toward the East, completing a right-handed vector

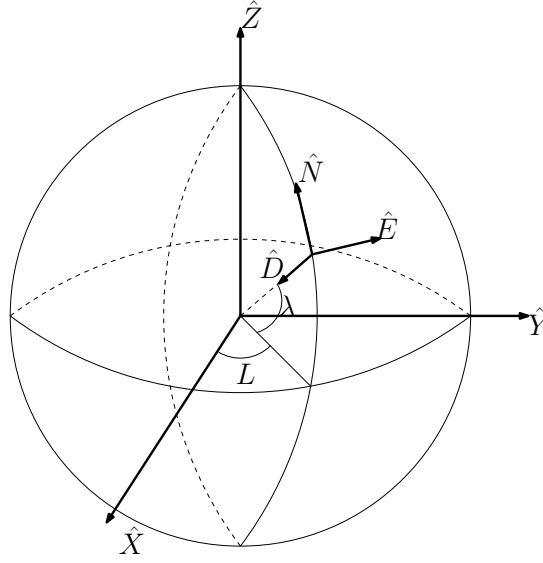


Fig. 2.2. Representation of the N-E-D reference frame.

set. The X-Y-Z and N-E-D frames are related by a 3-2 rotation through the angles of longitude and latitude, respectively. The longitude and latitude do not change. The X-Y-Z frame is an Earth fixed frame which rotates relative to the inertial frame with a rate

$$\vec{\omega} = \Omega_{\oplus} \hat{z} = \Omega_{\oplus} c_{\lambda} \hat{N} - \Omega_{\oplus} s_{\lambda} \hat{D}, \quad (2.11)$$

where $c_{\lambda} = \cos \lambda$ and $s_{\lambda} = \sin \lambda$. The total force on the plumb bob is

$$\begin{aligned} \vec{F}_{tot} &= m_G g_N \hat{D} - m_I \vec{\omega} \times \vec{\omega} \times (-R_{\oplus} \vec{D}) \\ &= (m_G g_N - m_I R_{\oplus} \Omega_{\oplus}^2 c_{\lambda}^2) \hat{D} - m_I R_{\oplus} \Omega_{\oplus}^2 c_{\lambda} s_{\lambda} \hat{N} \\ &= F_{tot} c_{\beta} \hat{D} - F_{tot} s_{\beta} \hat{N}, \end{aligned} \quad (2.12)$$

where we introduced the magnitude of the total force and the angle β between the total force and the \hat{D} vector. Then,

$$\tan \beta = \frac{m_I R_{\oplus} \Omega_{\oplus}^2 c_{\lambda} s_{\lambda}}{m_G g_N - m_I R_{\oplus} \Omega_{\oplus}^2 c_{\lambda}^2}. \quad (2.13)$$

Since the inertial component is much smaller than the gravitational component, we can simplify the denominator and approximate $\tan \beta \approx \beta$, so that

$$\begin{aligned}\beta &\approx \frac{m_I R_\oplus \Omega_\oplus^2 c_\lambda s_\lambda}{m_G g_N} \\ &= (1 - \kappa) \frac{R_\oplus^3 \Omega_\oplus^2}{GM_\oplus} c_\lambda s_\lambda.\end{aligned}\tag{2.14}$$

We see that the presence of κ makes β composition-dependent, so that comparing two materials, we find

$$\Delta\beta = -\Delta\kappa \frac{R_\oplus^3 \Omega_\oplus^2}{GM_\oplus} c_\lambda s_\lambda.\tag{2.15}$$

The Guyòt experiment, shown in Fig. 2.3, consisted of a pendant suspended over a vat of mercury. The surface of the mercury will align perpendicular to its local vertical, so $\Delta\beta$ is a measure of the angle that the pendant makes with the mercury normal, visualized using the reflection of the pendant on the mercury surface. While Guyòt initially found a nonzero $\Delta\beta$, he eventually concluded that he was finding a null result.

2.2.3 The Torsion Balance and the Eötvös Experiment

The next step forward with in the study of the weak equivalence principle was the introduction of the torsion balance. Originally built to measure very small electrostatic and gravitational forces between objects, the sensitivity of torsion balances proved to be very useful in the study of inertial and gravitational masses.

The simplest torsion balance, shown in Fig. 2.4, essentially consists of two of Guyòt's pendants. Instead of trying to find a difference in their hanging angles as in Eq. 2.15, the pendants are hung from a rigid bar that is suspended by a stiff wire. The difference in accelerations felt by the two pendants results in a torque about the wire, causing the wire to twist, which is easier to observe than the relative angle of the two pendulums.

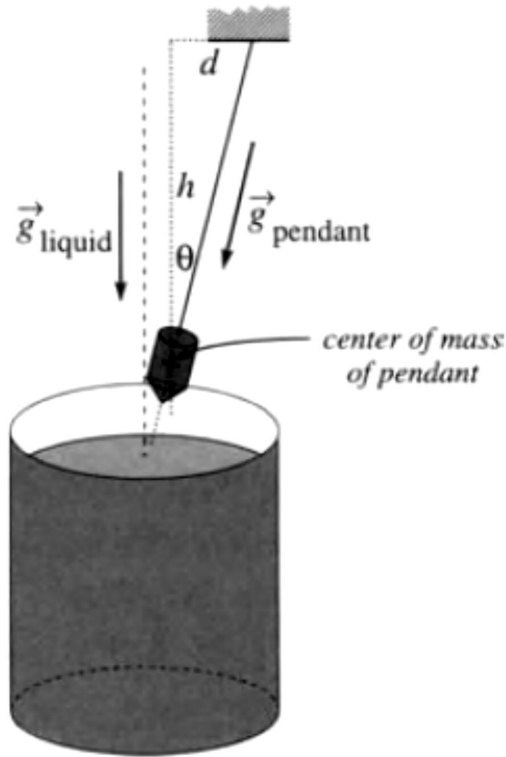


Fig. 2.3. The Guyot experiment. Reproduced from [7].

One drawback of the torsion balance is that any intrinsic twist in the fiber can give a false positive. This problem can be mitigated by taking two measurements 180 degrees apart; the intrinsic twist will give a contribution in the same direction for both measurements, while the actual signal will switch sign. Taking the difference of the two signals will then eliminate the intrinsic twist.

The Eötvös experiment of Eötvös, Fekete, and Pekár (EPF), was the first experiment to use torsion balances to attempt to observe a WEP violation. Lorand Eötvös (1848-1919) was a Hungarian physicist, considered to be a very careful experimentalist. Eötvös began his experiments in 1889, reporting a $\Delta\kappa < 1/20,000,000$. He returned to the problem in 1904, performing a set of observations until 1909. He used a variety of materials and compared most to a copper standard. Interestingly, Eötvös

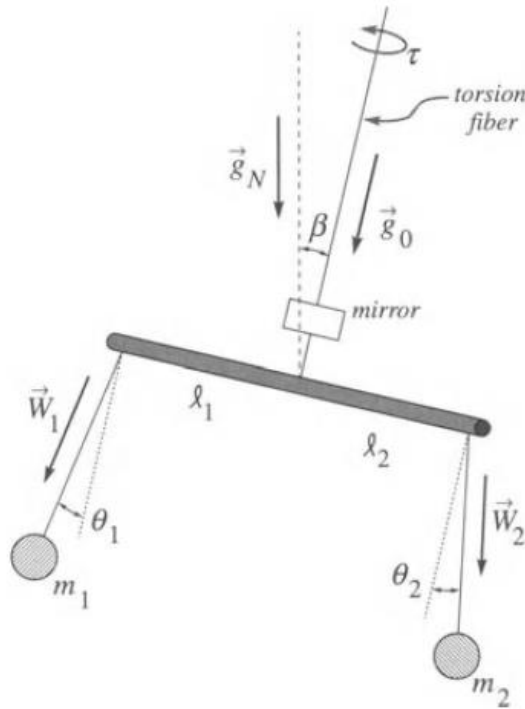


Fig. 2.4. Schematic of a two mass torsion balance. Reproduced from [7].

did not publish his results. In fact, the results were published by his aides in 1922 after Eötvös passed away in 1919.

A drawing of the torsion balances used by Eötvös is shown in Fig. 2.5. This specific design has some drawbacks. In addition to intrinsic twist, gravity gradients can also masquerade as positive WEP signals and must be dealt with carefully. If we consider the drawing of the Eötvös balance, we see that the two masses are held at two vertical heights, which makes the balance susceptible to vertical gradients. The fact that the balance only has a twofold symmetry means that it is susceptible to gradients in the plane of the balance as well. While modern experiments go to great lengths to eliminate gravity gradients, the Eötvös torsion balance was specifically designed to measure gravity gradients. His balance was originally built to measure gradients in order to locate gravitational anomalies associated with buried oil fields. To eliminate the gravity gradients inherent in measurements, Eötvös was forced to

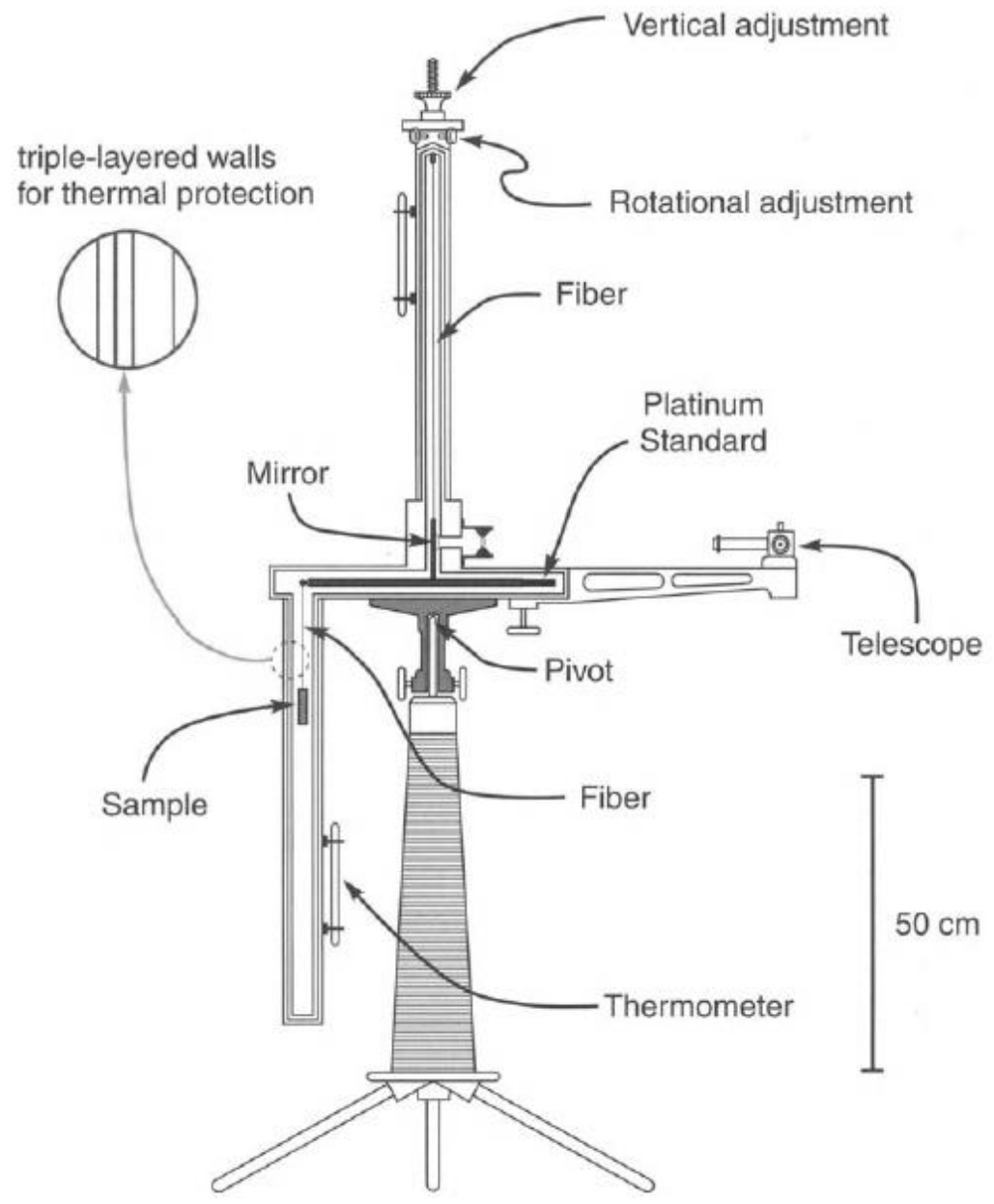


Fig. 2.5. Drawing of the torsion balance used in EPF experiment [2].

combine measurements in multiple directions and with multiple materials, a process that will be described in Chapter 3.

2.2.4 Post-Eötvös: Roll, Krotkov, and Dicke

In 1964, Roll, Krotkov, and Dicke (RKD) performed a torsion balance experiment to improve the limits on WEP violation as found by Eötvös. Mindful of some of the drawbacks of the Eötvös balance, RKD designed their balance to eliminate as much of the gravity gradients as possible. They used three samples, two identical and one of a different composition mounted on the corners of an equilateral triangle which eliminated the in plane gradients. The three masses were also at the same height, eliminating the vertical gravity gradients. To combat the intrinsic twist in the wire, previous experiments were forced to rotate the torsion balance 180 degrees, which introduced noise and error into the measurements. To avoid that noise, RKD use the Sun as the source of the gravitational field instead of the Earth. The rotation of the Earth then moves the source from one side of the apparatus to the other, allowing RKD to eliminate intrinsic twist in the wire by subtracting measurements taken 12 hours apart, with no need to move the apparatus. RKD were able to achieve results on the order of $\Delta\kappa \lesssim 10^{-11}$ for gold-aluminum and copper-lead chloride.

2.3 Weak Equivalence Principle and Fifth Forces

In 1955, Lee and Yang [3] showed that an additional force coupling to baryon number could appear as an apparent violation of WEP, which implied that all of the experiments mentioned above could be recast as searches for extra forces. To see this consider that any search for short range forces will require samples being brought close together. While the samples can be kept electrically neutral to avoid electromagnetic forces, we cannot eliminate the gravitational field. So as we consider the physics of the experiment we must include both the Newtonian gravity and a

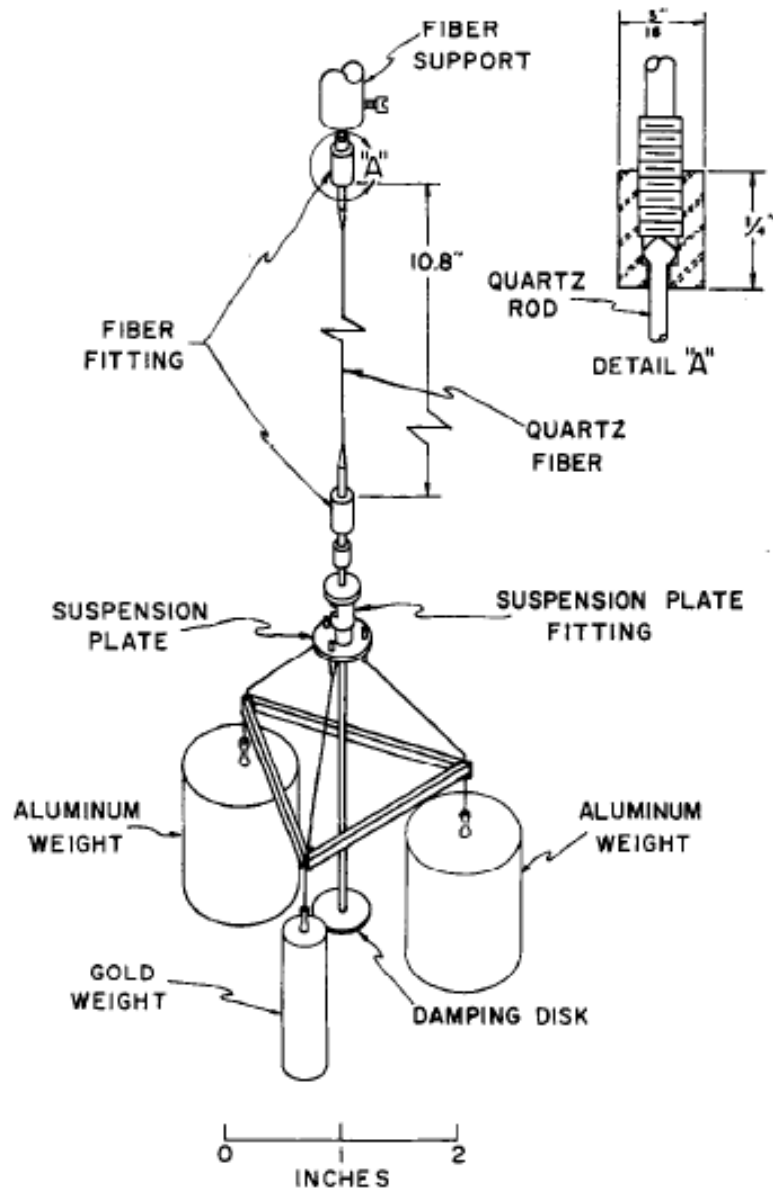


Fig. 2.6. Drawing of the torsion balance used in the RKD experiment [4]. The three masses arranged at the corner of the triangle eliminate gravity gradients that were intrinsic to The EPF measurements.

possible non-gravitational fifth-force. The potential energy of such a system, where the additional interaction is in the form of a simple Yukawa, it given by

$$V_N(\vec{r}) = -G \frac{m_i m_j}{r}, \quad (2.16)$$

$$V_5(\vec{r}) = \pm f^2 \frac{Q_{5i} Q_{5j}}{r} e^{-r/\lambda}. \quad (2.17)$$

The sign on V_5 depends on the interaction (attractive for scalar and tensor, attractive for vector). The total potential energy of the system is then

$$\begin{aligned}
V_{tot}(\vec{r}) &= V_N(\vec{r}) + V_5(\vec{r}) \\
&= -G \frac{m_i m_j}{r} \pm f^2 \frac{Q_{5i} Q_{5j}}{r} e^{-r/\lambda} \\
&= -G \frac{m_i m_j}{r} \left(1 \mp \frac{f^2 Q_{5i} Q_{5j}}{G m_i m_j} e^{-r/\lambda} \right) \\
&= -G \frac{m_i m_j}{r} (1 + \alpha_{ij} e^{-r/\lambda}), \tag{2.18}
\end{aligned}$$

with

$$\alpha_{ij} = \mp \frac{f^2 Q_{5i} Q_{5j}}{G m_i m_j} = \mp \frac{Q_{5i}}{\mu_i} \frac{Q_{5j}}{\mu_j} \xi = \mp q_{5i} q_{5j} \xi, \tag{2.19}$$

$$\mu_k = \frac{m_k}{m_H}, \tag{2.20}$$

$$\xi = \frac{f^2}{G m_H^2}. \tag{2.21}$$

In our original Yukawa potential, the ‘‘fifth force charge’’ Q_{5k} ; however, since we will be comparing the accelerations of different particles, the actual ‘‘charge’’ is more appropriately Q_{5k}/m_k . So, we rewrite the particle masses in terms of the hydrogen mass ($m_k = \mu_k m_H$) so that our ‘‘proper’’ fifth force charge, $q_{5k} = Q_{5k}/\mu_k$, becomes unitless.

Taking the gradient of Eq. (2.18), we can find the total force acting on the sample

$$\vec{F}_{tot} = -\nabla V_{tot} = -G \frac{m_i m_j}{r^2} \hat{r} \left[1 + \alpha_{ij} \left(1 + \frac{r}{\lambda} \right) e^{-r/\lambda} \right]. \tag{2.22}$$

Using the definition of the local gravitational field

$$\vec{g}(r) = -\frac{G m_i}{r^2} \hat{r},$$

we then have

$$\vec{F}_{tot} = m_j \vec{a} = m_j \left[1 + \alpha_{ij} \left(1 + \frac{r}{\lambda} \right) e^{-r/\lambda} \right] \vec{g}. \tag{2.23}$$

Comparing Eqs. (2.3) and (2.23), we can write the ratio of the effective gravitational mass and the inertial mass as

$$\frac{m_G}{m_I} = 1 + \kappa = \left[1 + \alpha_{ij} \left(1 + \frac{r}{\lambda} \right) e^{-r/\lambda} \right]. \tag{2.24}$$

We can also write Eq. (2.22) as

$$\vec{F}_{tot}(\vec{r}) = -G(r) \frac{m_i m_j}{r^2} \hat{r} \quad (2.25)$$

$$G(r) = G_\infty \left[1 + \alpha_{ij} \left(1 + \frac{r}{\lambda} \right) e^{-r/\lambda} \right]. \quad (2.26)$$

Here, the Yukawa factor $e^{-r/\lambda}$ appears to modify Newton's gravitational constant. There remains the composition dependence in α_{ij} , so different experiments would obtain different results. However, Eq. (2.26) is still valid for composition independent-forces. Any WEP-violation experiments, or variable- G - experiments, are also inherently searches for short-range fifth forces. The variable- G experiments are not covered in this work, but we mention their presence for the sake of completeness.

2.3.1 A Reanalysis of the Eötvös Experiment

The 1955 work of Lee and Yang eventually led Fischbach et. al [7] to undertake a reanalysis of Eötvös Experiment to look for evidence of fifth forces. Their model assumed a baryon-number dependent Yukawa potential

$$V_5 = \xi \left(\frac{B}{\mu} \right)_i \left(\frac{B}{\mu} \right)_\oplus \frac{e^{-R_\oplus/\lambda}}{r}. \quad (2.27)$$

Since some of the samples were molecules comprised of different atoms, care had to be taken when defining B/μ . The total baryon number and total mass for the entire sample was simply the baryon number and mass for each atom multiplied by the number of atoms of that species

$$\frac{B}{\mu} = \frac{\sum_{i=1}^k n_i B_i}{\sum_{i=1}^k n_i \mu_i}. \quad (2.28)$$

It should be noted that EPF would never have been able to search for this force as the concepts of baryon number and Yukawa potentials would not be introduced until the 1930's and 1950's, respectively.

Fischbach et. al began by translating the EPF paper from German to English. They then compiled the Eötvös' measured values of $\Delta\kappa$ for the various samples, which are tabulated in Table 2.1.

Table 2.1.
Measurements of $\Delta\kappa$ from EPF [2] and calculations of $\Delta(B/\mu)$ from Fischbach et al. [34] used in the curve fitting.

Samples	$10^9 \Delta\kappa$	$10^5 \Delta(B/\mu)$
Magnalium-Pt	4 ± 1	+50.0
Brass-Pt	1 ± 2	+93.2
Cu-Pt	4 ± 2	+94.3
Ag-Fe-SO ₄	0	0.0
CuSO ₄ (dissolution)	2 ± 2	0.0
Snakewood-Pt	-1 ± 2	-50.9
Asbestos-Cu	-3 ± 2	-74.0
CuSO ₄ · 5H ₂ O-Cu	-5 ± 2	-85.7
CuSO ₄ (sol'n)-Cu	-7 ± 2	-146.3
H ₂ O-Cu	-10 ± 2	-171.8
Tallow-Cu	-6 ± 2	-203.1

If we compare the torque expected from a WEP violation to the torque expected from a fifth force signal, we can relate the measured values of $\Delta\kappa$ to the computed values of $\Delta(B/\mu)$

$$\begin{aligned} \Delta\kappa &= \left[\frac{f^2 \epsilon(R_{\oplus}/\lambda)}{Gm_H^2} \left(\frac{B}{\mu} \right)_{\oplus} \right] \Delta \left(\frac{B}{\mu} \right) \\ &= a \Delta \left(\frac{B}{\mu} \right) + b. \end{aligned} \quad (2.29)$$

Here $\epsilon(R_{\oplus}/\lambda)$ is the spatial dependence of the Yukawa potential integrated over the source (Earth). In the second line we have introduced arbitrary parameters a and b that can be determined from a curve fit of the $\Delta\kappa$ - $\Delta(B/\mu)$ data. The parameter a then relates the strength of the interaction f to its length scale λ , while parameter b should be nominally zero.

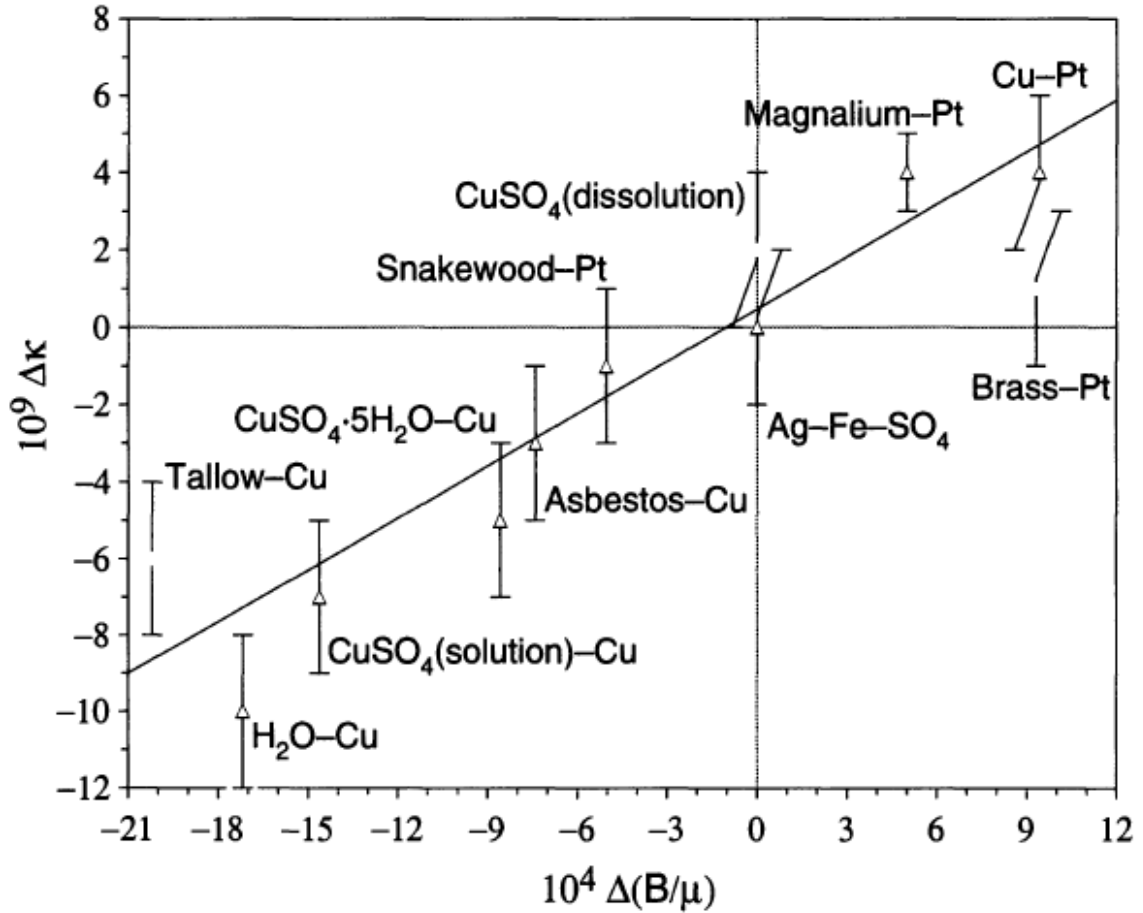


Fig. 2.7. Plot of $\Delta\kappa$ vs $\Delta(B/\mu)$ for the Eötvös experiment. The solid line shows the linear curve fit of the data. The data are listed in Table 2.1. The plot was reproduced from [35].

The plot of the $\Delta\kappa$ - $\Delta(B/\mu)$ data along with its curve fit is shown in Fig. 2.7. In their initial paper, Fischbach et al. determined from the fit

$$a = (5.65 \pm 0.71) \times 10^{-6}$$

$$b = (0.48 \pm 0.64) \times 10^{-9}$$

$$\chi^2 = 2.1 \text{ (5 degrees of freedom),}$$

while in [35] the values were updated to

$$\begin{aligned} a &= (4.51 \pm 0.56) \times 10^{-6} \\ b &= (0.47 \pm 0.55) \times 10^{-9} \\ \chi^2 &= 10.4 \text{ (9 degrees of freedom).} \end{aligned}$$

We note that the updated value of the constant a differs from zero by eight standard deviations, while b is consistent with zero. Fischbach et. al concluded that this result supported the existence of an unseen force coupling to baryon number. This conclusion prompted a large number of experiments over the last 30 years to test for WEP violations or to directly search for new forces (See Fischbach and Talmadge [35] for a discussion of the various experiments). Two of the most prominent groups are the Eöt-Wash group of the University of Washington and the MICROSCOPE collaboration. Their experiments will be discussed below.

2.3.2 Eöt-Wash (E-W) Experiment

The original Eöt-Wash [8] experiment was performed near a hill on the University of Washington Campus. The choice of placing the apparatus near a local mass distribution may seem odd (EPF placed their apparatus in the basement of a building), but the local mass may actually lead to higher sensitivities. The gravitational force, and any Yukawa force with the Earth as a source point in the down (\hat{D}) direction. If we aligned the fiber of the torsion balance with the down direction as well, these forces would not be able to cause a torque as torsion balances are sensitive only to forces in the plane of the balance. Due to the centripetal force arising from the Earth's rotation, the fiber is instead aligned along the local vertical which deviates from down by the small angle β . Thus, a portion of the gravitational and Earth Yukawa forces end up lying in the plane of the torsion balance, but they are suppressed by a factor of $\sin \beta$ which is small. Alternatively, a force in the North or East directions is suppressed by $\cos \beta$ which is approximately one. Thus, most modern experiments use a

large local mass distribution (a hill or mountain) or laboratory masses in searches for WEP violations and fifth forces.

A drawing of the torsion balance used by Eöt-Wash is shown in Fig. 2.8 with a enlarged picture of the test masses shown in Fig. 2.9. This balance has numerous improvements over previous experiments. Instead of using three mass like RGD, Eöt-Wash used four masses (two aluminum, two beryllium). This makes the balance insensitive to higher gravitational multipole moments. The test masses themselves are machined in such a way as to have the same exterior dimensions despite differences in density. The entire balance is placed inside a vacuum chamber to eliminate air currents and the chamber is mounted on a turntable. The turntable helps to eliminate the intrinsic twist in the wire without having to move the apparatus by hand, introducing more noise. This rotation also helps with data analysis as they can simply read off the Fourier component with the same frequency as the turntable. Finally, the entire apparatus was given a thin coating in gold to eliminate electrostatic forces.

2.3.3 The MICROSCOPE Experiment

MICROSCOPE is a satellite-based experiment that launched in 2016 to search for a WEP violation using the Earth as a source. The space environment eliminates many of the disturbances seen on the Earth, and a special control system compensates for the drag due to the atmosphere, solar wind, and solar radiation pressure, giving the experiment an expected accuracy of 10^{-15} .

The experiment uses a differential accelerometer consisting of two concentric cylinders of differing materials. As the satellite and test masses orbit the Earth, the control system eliminates the unwanted forces, allowing the center of mass of the three bodies to follow a geodesic path. This orbit is roughly circular, so the inertial force balances gravity. This is true for the center of mass of the three bodies, but not for each body individually. The test masses will drift from the total center of mass and we can

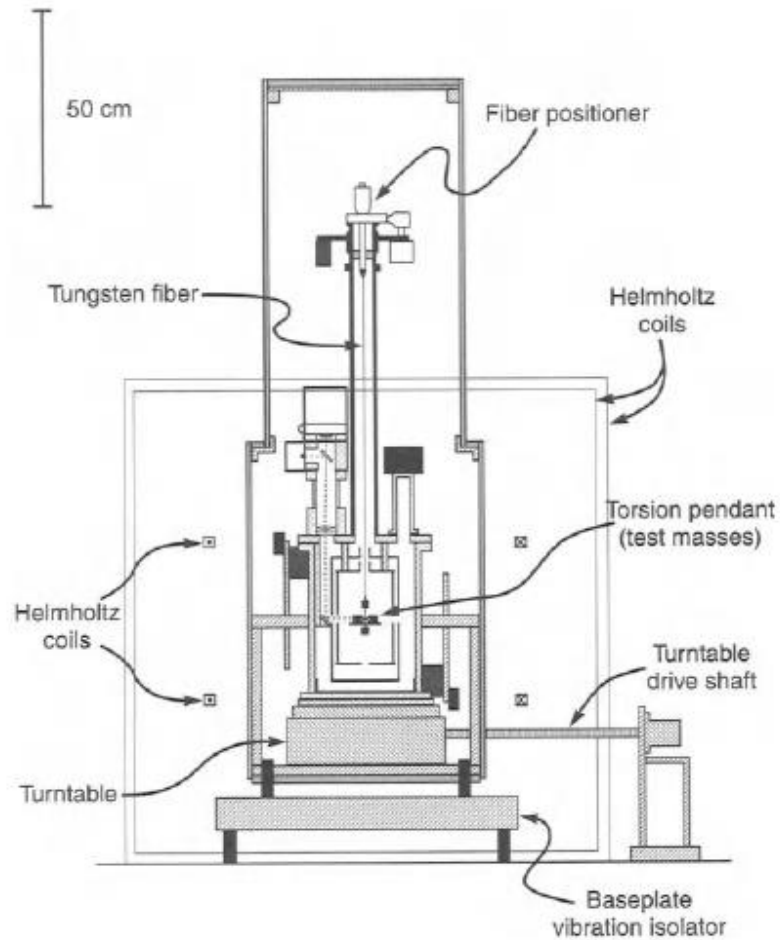


Fig. 2.8. A drawing of the torsion balance used by Eöt-Wash taken from [35]. This entire apparatus was mounted on a turntable and rotated to eliminate any intrinsic twist in the fiber.

measure its acceleration, which will be proportional to the WEP violating factor κ . Thus $\Delta\kappa$ can be obtained by taking the difference in the two accelerometers.

The initial results from the MICROSCOPE experiment are consistent with no WEP violation. As with the other experiments discussed the MICROSCOPE experiment could also be tasked with searching for new forces. These searches did not reveal any new forces and served to put stricter limits on the strength and range of any short-range force. We will revisit this idea and consider a short-range force that couples

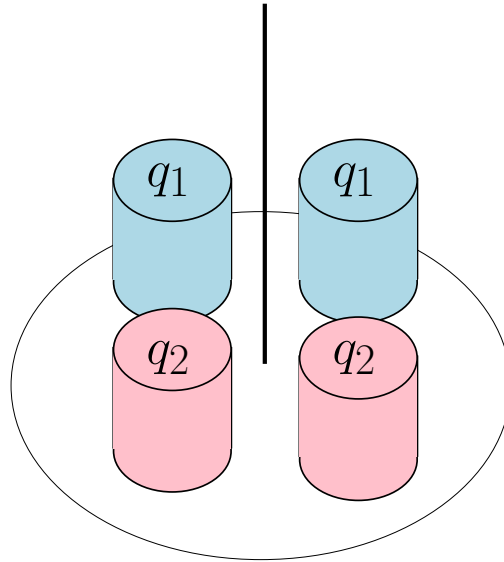


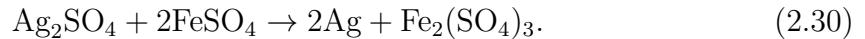
Fig. 2.9. A drawing of the four masses attached to the fiber. Two of the masses are aluminum while the other two are beryllium.

to a background field through which the apparatus moves. This will be discussed in Chapter 4.

2.3.4 The Eötvös Experiment Endures

In the years since the reanalysis of the Eötvös experiment by Fischbach et. al, many experiments have been performed to confirm or deny Fischbach's conclusion that buried in Eötvös' data is evidence for a baryon-number dependent forces. Most of these experiments returned null results. Some gave positive results, but these were either attributed to errors or were set aside in favor of results such as Eöt-Wash. During this time though, no one has made a convincing argument to explain why Eötvös' results correlate with baryon number. Some of the suggested explanations include convection, thermal gradients, the presence of the experimenter affecting the balance, and changes in gravity gradients due to rainfall. These suggestions have been refuted based in part on Eötvös' reputation as a meticulous experimenter, but

also based on the fact that none of these suggested causes would yield an eight standard deviation correlation with baryon number. Bod et. al [36] defend Eötvös' reputation as an careful scientist, specifically mentioning the torsion balance being placed on stone piers sunk deep into the ground to limit vibrations, and the balance being allowed to equilibrate for two days before taking measurements. The most fascinating evidence is the data point for Ag-Fe-SO₄, which was taken before and after the reaction



The reactants were suspended in liquid, but after the reaction, the silver precipitates out and collects on the bottom of the container. This would change the center of mass of the sample, and would couple to the vertical gravity gradients giving a different answer for the reactants and products. The fact that this data point is quoted at zero leads observers to believe that Eötvös and his associates were careful enough to catch this complication, and implies that they should have also recognized and corrected for most systemic perturbations.

Unfortunately, as everyone involved in the Eötvös experiment has long since passed away, and an exact re-enactment of the experiment is impossible 100 years later, we can never know with absolute certainty that a systemic effect was not present in the experiment. Nevertheless, the eight standard deviation affect is striking.

It should be noted that no group has "repeated" the Eötvös experiment. All modern experiments used custom-made balances specifically designed to eliminate spurious forces. Perhaps this is the key: although it seems almost blasphemous to describe an experiment as "too well-designed", perhaps there is a force that can survive Eötvös' software program, but is eliminated by the additional symmetries of the RKD and Eöt-Wash experiments. This concept will be explored in more detail in Chapter 3.

3. A RE-REANALYSIS OF THE EÖTVÖS EXPERIMENT: ARBITRARY FORCES IN TORSION BALANCE EXPERIMENTS

In order to determine whether a force exists that could appear in the Eotvös experiment, but not in later experiments such as Eöt-Wash, we need the most general form of the response to both apparatus to outside forces.

We introduce a baryon-number dependent force of the form

$$F_{5i} = \xi G m q \bar{q}_{source} \left[\mathcal{F}_{5i}(\vec{R}) + \mathcal{D}_{5ij}(\vec{R}) r_j + \dots \right], \quad (3.1)$$

where q is the baryon to mass number ratio, \bar{q} is the average charge of the source, \vec{R} is the coordinate of the pivot point of the torsion balance, and \vec{r} is the coordinate relative to the pivot point. Eq. (3.1) is the Taylor series expansion of the force. If we introduce the potential $V_5 = \xi G m q \bar{q}_{source} \mathcal{V}_5$, then \mathcal{F}_{5i} is the gradient of \mathcal{V}_5 , while \mathcal{D}_{5ij} would be the gradient of \mathcal{F}_{5i} : $\mathcal{F}_{5i} = -\partial_i \mathcal{V}_5$; $\mathcal{D}_{5ij} = \partial_j \mathcal{F}_{5i} = -\partial_i \partial_j \mathcal{V}_5$, and $\partial_i = \frac{\partial}{\partial R_i}$.

To simplify the notation we introduce $f_{5i} = \xi G \bar{q}_{source} \mathcal{F}_{5i}$ and $d_{5ij} = \xi G \bar{q}_{source} \mathcal{D}_{5ij}$. Since we are treating our torsion balance experiments as extended sources, we need to allow the fifth force charge to vary with position, and we replace the mass with the differential mass: $m q \rightarrow q(\vec{r}) dm(\vec{r})$. We can then write the force on the differential element as

$$dF_{5i} = q(\vec{r}) dm(\vec{r}) (f_{5i} + d_{5ij} r_j + \dots), \quad (3.2)$$

where we have further introduced $f_{5i} = \mathcal{F}_{5i}(\vec{R})/m_H$, $d_{5ij} = \mathcal{D}_{5ij}(\vec{R})/m_H$, and $q = B/\mu$. We make q a function of \vec{r} to allow the composition of the sample to change with position. In addition to the fifth force, we will also have the gravitational force and the centripetal force due to the rotation of the Earth. The total force is then

$$F_{tot,i} = F_{grav,i} + F_{cent,i} + m \bar{q} f_{5i} + m \bar{q} \ell_j d_{5ij}, \quad (3.3)$$

where $m = \int dm$, $\bar{q} = \int q(\vec{r})dm(\vec{r})/m$, and $\bar{\ell}_j = \int q(\vec{r})r_j dm(\vec{r})/m\bar{q}$,

We must now introduce the reference frames relevant to the system. The first reference frame is a local North-East-Down (N-E-D) Frame for our experiments as shown in Figure 3.1. Our forces are defined in this frame. In the N-E-D frame, we align the axis of the torsion balance with the local vertical, found by hanging a plumb bob. We can then define the rotation axis of the torsion balance as

$$\hat{b}_3 = \frac{\vec{F}_{tot}}{|\vec{F}_{tot}|}. \quad (3.4)$$

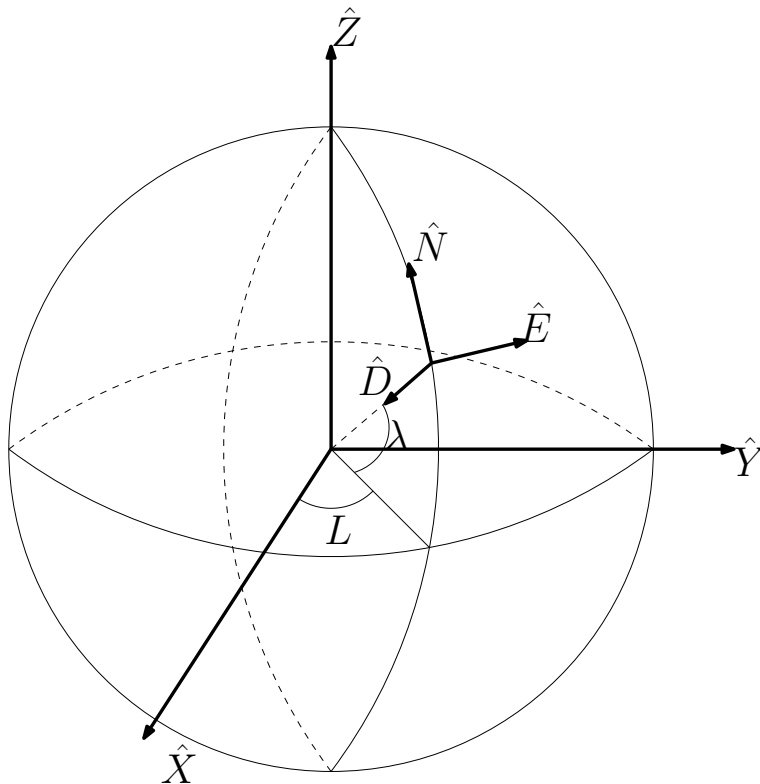


Fig. 3.1. Representation of the N-E-D reference frame.

The \hat{b}_1 -axis will be along the axis of the torsion balance when the twist is zero. We also want this axis to be roughly towards North, so we can define the \hat{b}_2 -axis, the axis perpendicular to the torsion balance as

$$\hat{b}_2 = \frac{\hat{b}_3 \times \hat{N}}{|\hat{b}_3 \times \hat{N}|}. \quad (3.5)$$

Finally, we introduce the \hat{B}_1 axis

$$\hat{b}_1 = \hat{b}_2 \times \hat{b}_3. \quad (3.6)$$

The \hat{B} frame is space-fixed in the zero-twist orientation of the beam and makes an angle β with the NED frame. We also introduce the body fixed x-y-z frame which is a rotation of the \hat{b} frame by the angle θ .

$$\begin{aligned} \hat{N} &= \hat{x}c_\phi c_\beta - \hat{y}s_\phi c_\beta - \hat{z}s_\beta \\ \hat{E} &= \hat{x}s_\phi + \hat{y}c_\phi \end{aligned} \quad (3.7)$$

$$\hat{D} = \hat{x}c_\phi s_\beta - \hat{y}s_\phi s_\beta + \hat{z}c_\beta \quad (3.8)$$

The frame relations are also sketched in Figure 3.2.

To find the torque on the torsion balance, we use the Lagrangian formulation

$$\frac{d}{dt} \left(\frac{\partial \mathcal{L}}{\partial \dot{\phi}} \right) - \frac{\partial \mathcal{L}}{\partial \phi} = Q_\phi, \quad (3.9)$$

where Q_ϕ is the generalized force,

$$\begin{aligned} dQ_\phi &= \frac{\partial r_i}{\partial \phi} \cdot d\mathcal{F}_{5i} \\ &= q(\vec{r}) dm(\vec{r}) \left(f_{5i} \frac{\partial r_i}{\partial \phi} + d_{5ij} r_j \frac{\partial r_i}{\partial \phi} \right) \\ &= q(\vec{r}) \rho(\vec{r}) dV \left(f_{5i} \frac{\partial r_i}{\partial \phi} + d_{5ij} r_j \frac{\partial r_i}{\partial \phi} \right). \end{aligned} \quad (3.10)$$

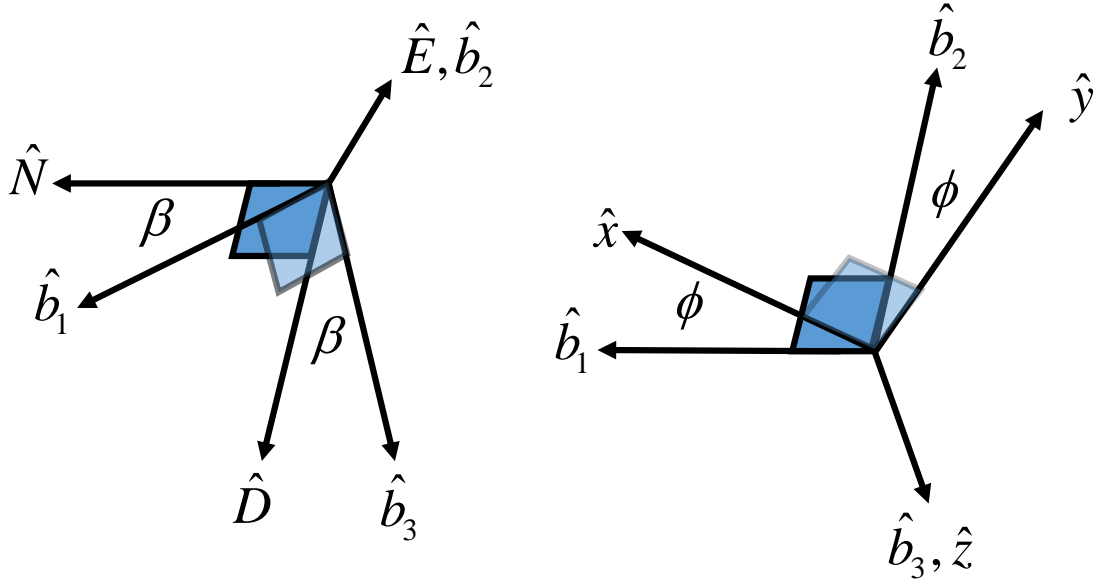


Fig. 3.2. The transformations from the NED frame to the body frame.

Table 3.1.

Notation differences between EPF (Ref. [2]) and this work.

This work	EPF	Description
I	K	Moment of Inertia
V_{grav}	$-U$	Gravitational Potential Energy
δ	L	Observation scale length
L	ℓ_a	Torsion Balance length
m	M_a	Sample mass
β	ϵ	Plumb bob angle
σ	$m = n_E - n_W$	East-West observation difference

We note that \vec{r} is the same \vec{r} that is in Eq. (3.1), the position of the particle in the N-E-D frame. This position can be written as

$$\begin{aligned}
 \vec{r} &= x\hat{x} + y\hat{y} + z\hat{z} \\
 &= (xc_\phi c_\beta - ys_\phi c_\beta - zs_\beta)\hat{N} + (xs_\phi + yc_\phi)\hat{E} \\
 &\quad + (xc_\phi s_\beta - ys_\phi s_\beta + zc_\beta)\hat{D}.
 \end{aligned} \tag{3.11}$$

It is straightforward to show that the derivative of \vec{r} is

$$\frac{\partial \vec{r}}{\partial \phi} = (-xs_\phi c_\beta - yc_\phi c_\beta) \hat{N} + (xc_\phi - ys_\phi) \hat{E} + (-xs_\phi s_\beta - yc_\phi s_\beta) \hat{D}. \quad (3.12)$$

3.1 Eötvös Experiment

We begin with the Eötvös experiment. We note that we have made changes to the notation of Ref. [2] to be more consistent with current practices. A summary of the changes are listed in Table 3.1. The Eötvös experiment contained two masses. Mass 1 was located along the balance towards North and hung a distance h below the balance. Mass 2 was located along the balance towards the South and was located at the same height as balance.

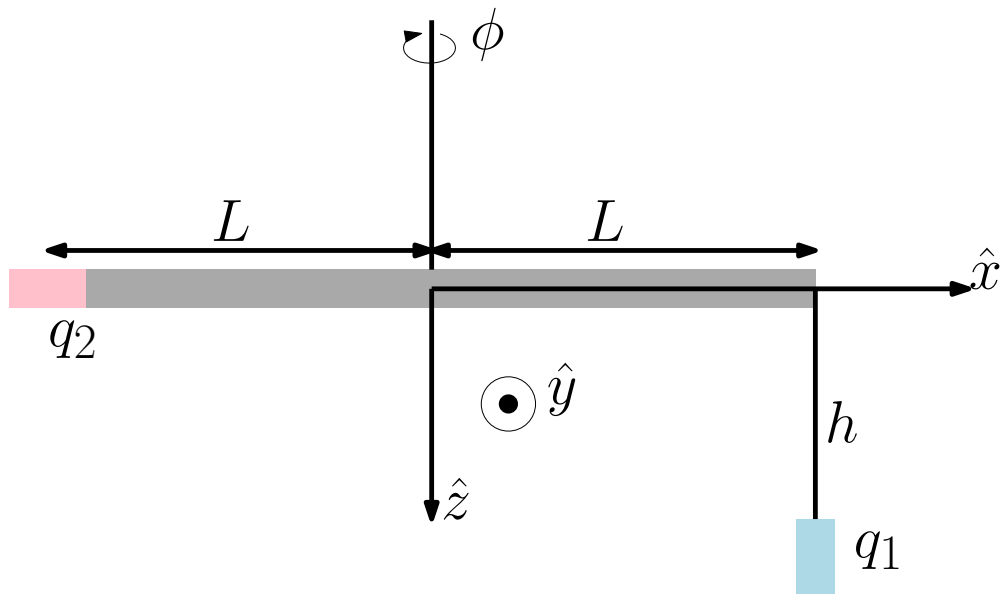


Fig. 3.3. Side view of the Eötvös Experiment.

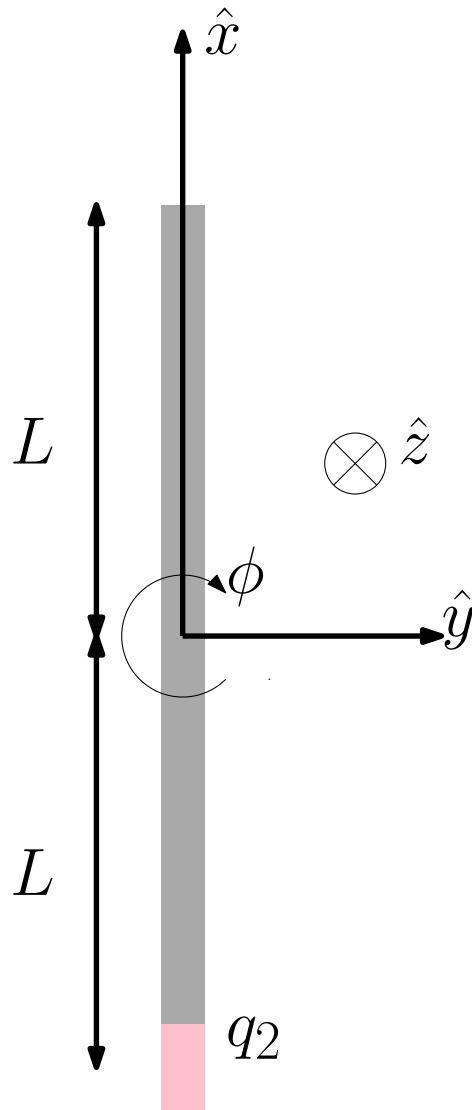


Fig. 3.4. Top view of the Eötvös Experiment.

We can write the product of the fifth force charge and the mass density of the Eötvös experiment as

$$q(\vec{r})\rho(\vec{r}) = q_1\delta(x-L)\delta(y)\delta(z-h) + q_2\delta(x+L)\delta(y)\delta(z). \quad (3.13)$$

The torque on the fiber can then be written as

$$\begin{aligned}
T_5 = & -(q_1 - q_2)mLc_\beta s_\phi f_{5x} + (q_1 - q_2)mLc_\phi f_{5y} - (q_1 - q_2)mLs_\beta s_\phi f_{5z} \\
& -(q_1 + q_2)\frac{I}{2}c_\beta^2 c_\phi s_\phi d_{5xx} + q_1mLhs_\beta c_\beta s_\phi d_{5xx} \\
& +(q_1 + q_2)\frac{I}{2}c_\beta c_\phi^2 d_{5yx} - q_1mLhs_\beta c_\phi d_{5yx} \\
& -(q_1 + q_2)\frac{I}{2}c_\beta s_\beta c_\phi s_\phi d_{5zx} + q_1mLhs_\beta^2 s_\phi d_{5zx} \\
& -(q_1 + q_2)\frac{I}{2}c_\beta s_\phi^2 d_{5xy} + (q_1 + q_2)\frac{I}{2}c_\phi s_\phi d_{5yy} - (q_1 + q_2)\frac{I}{2}s_\beta s_\phi^2 d_{5zy} \\
& -(q_1 + q_2)\frac{I}{2}c_\beta s_\beta c_\phi s_\phi d_{5xz} - q_1mLhc_\beta^2 s_\phi d_{5xz} \\
& +(q_1 + q_2)\frac{I}{2}s_\beta c_\phi^2 d_{5yz} + q_1mLhc_\beta c_\phi d_{5yz} \\
& -(q_1 + q_2)\frac{I}{2}s_\beta^2 c_\phi s_\phi d_{5zz} - q_1mLhs_\beta c_\beta s_\phi d_{5zz}. \tag{3.14}
\end{aligned}$$

We also need the gravitational and centrifugal force vectors. We have two ways of proceeding. First, we could form the Lagrangian using the gravitational potential energy and the effective potential energy for the centripetal force. Then we expand the Lagrangian to second order in \vec{r} , and finally apply Eq. (3.9) to find the torque. Alternatively, we can use the results from Eq. (3.14) to quickly deduce the remaining terms, as Eq. (3.14) was written generically. We simply let $q_1 = q_2 = 1$, $f_i = -\partial_i V_{grav} + F_{cent,i}/m$, and $d_{ij} = -\partial_i \partial_j V_{grav}$ where V_{grav} is the gravitational potential. Then, the Newtonian contribution to the torque is

$$\begin{aligned}
T_{grav} = & Ic_\beta^2 c_\phi s_\phi \partial_x^2 V_{grav} - mLhs_\beta c_\beta s_\phi \partial_x^2 V_{grav} - Ic_\beta (c_\phi^2 - s_\phi^2) \partial_x \partial_y V_{grav} \\
& + mLhs_\beta c_\phi \partial_x \partial_y V_{grav} + 2Ic_\beta s_\beta c_\phi s_\phi \partial_x \partial_z V_{grav} + mLh(c_\beta^2 \\
& - s_\beta^2) s_\phi \partial_x \partial_z V_{grav} - Ic_\phi s_\phi \partial_y^2 V_{grav} - Is_\beta (c_\phi^2 - s_\phi^2) \partial_y \partial_z V_{grav} \\
& - mLc_\beta c_\phi \partial_y \partial_z V_{grav} + Is_\beta^2 c_\phi s_\phi \partial_z^2 V_{grav} + mLhs_\beta c_\beta s_\phi \partial_z^2 V_{grav}. \tag{3.15}
\end{aligned}$$

Letting s_β be small and approximating $c_\beta \approx 1$, the gravitational terms simplify to

$$\begin{aligned}
T_{grav} \approx & \left[-I(\partial_y^2 V_{grav} - \partial_x^2 V_{grav}) \frac{s_{2\phi}}{2} - I\partial_x \partial_y V_{grav} c_{2\phi} \right. \\
& \left. + mLh\partial_x \partial_z V_{grav} s_\phi - mLh\partial_y \partial_z V_{grav} c_\phi \right] \\
& - I\partial_y \partial_z V_{grav} s_\beta c_{2\phi} + mLh\partial_x \partial_y V_{grav} s_\beta c_\phi \\
& - mLh\partial_x^2 V_{grav} s_\beta s_\phi + I\partial_x \partial_z V_{grav} s_\beta s_{2\phi} \\
& + + mLh\partial_z^2 V_{grav} s_\beta s_\phi
\end{aligned} \tag{3.16}$$

The first five terms (in square brackets) match Eötvös (up to a sign) while the remaining five terms do not appear in Eötvös, as they contain s_β multiplied by gravity gradients which are neglected.

The total torque can then be written as

$$\begin{aligned}
T_{total} = & \left[-I(\partial_y^2 V_{grav} - \partial_x^2 V_{grav}) \frac{s_{2\phi}}{2} - I\partial_x \partial_y V_{grav} c_{2\phi} \right. \\
& \left. + mLh\partial_x \partial_z V_{grav} s_\phi - mLh\partial_y \partial_z V_{grav} c_\phi \right] \\
& + \left[q_+ \frac{I}{4} (d_{5yy} - d_{5xx}) s_{2\phi} + q_+ \frac{I}{4} (d_{5yx} + d_{5xy}) c_{2\phi} \right. \\
& - q_1 mLhd_{5xz} s_\phi + q_1 mLhd_{5yz} c_\phi - q_- mLf_{5z} s_\beta s_\phi \\
& + q_+ \frac{I}{4} (d_{5yz} + d_{5zy}) s_\beta c_{2\phi} - q_1 mLhd_{5yx} s_\beta c_\phi \\
& + q_1 mLhd_{5xx} s_\beta s_\phi - q_+ \frac{I}{4} (d_{5xz} + d_{5zx}) s_\beta s_{2\phi} \\
& \left. - q_1 mLhs_\beta s_\phi d_{5zz} \right] \\
& + \left[-q_- mLf_{5x} s_\phi + q_- mLf_{5y} c_\phi \right. \\
& \left. + q_+ \frac{I}{4} (d_{5yx} - d_{5xy}) + q_+ \frac{I}{4} (d_{5yz} - d_{5zy}) s_\beta \right].
\end{aligned} \tag{3.17}$$

To easily compare our results to those of Eötvös, we adopt a convention where we list the ‘‘Eötvös’’ terms in the first set of square brackets, followed by our new ‘‘non-Eötvös’’ terms. We will include the f_{5z} term with the ‘‘Eötvös’’ terms since the force of interest WEP-violating gravitational term in the \hat{D} -direction. It follows that the first two lines of Eq. (3.17) match the terms in Eq. (8) of Ref. [2].

We now introduce the measure scale value n , the constant n_0 , the length L , and the torsion constant τ of the wire and write the torque as

$$T_{total} = \tau \frac{n_0 - n}{2\delta} \quad (3.18)$$

Then, the measured quantity is

$$\begin{aligned} n_0 - n = & \left[-\frac{\delta}{\tau} I (\partial_y^2 V_{grav} - \partial_x^2 V_{grav}) s_{2\phi} - \frac{2\delta}{\tau} I \partial_x \partial_y V_{grav} c_{2\phi} \right. \\ & \left. + \frac{2\delta}{\tau} mLh \partial_x \partial_z V_{grav} s_\phi - \frac{2\delta}{\tau} mLh \partial_y \partial_z V_{grav} c_\phi \right] \\ & + \left[q_+ \frac{\delta I}{\tau 2} (d_{5yy} - d_{5xx}) s_{2\phi} + q_+ \frac{\delta I}{\tau 2} (d_{5yx} + d_{5xy}) c_{2\phi} \right. \\ & - q_1 \frac{2\delta}{\tau} mLh d_{5xz} s_\phi + q_1 \frac{2\delta}{\tau} mLh d_{5yz} c_\phi - q_- \frac{2\delta}{\tau} mL f_{5z} s_\beta s_\phi \\ & + q_+ \frac{\delta I}{\tau 2} (d_{5yz} + d_{5zy}) s_\beta c_{2\phi} - q_1 \frac{2\delta}{\tau} mLh d_{5yx} s_\beta c_\phi \\ & + q_1 \frac{2\delta}{\tau} mLh d_{5xx} s_\beta s_\phi - q_+ \frac{\delta I}{\tau 2} (d_{5xz} + d_{5zx}) s_\beta s_{2\phi} \\ & \left. - q_1 \frac{2\delta}{\tau} mLh d_{5zz} s_\beta s_\phi \right] \\ & + \left[-q_- \frac{2\delta}{\tau} mL f_{5x} s_\phi + q_- \frac{2\delta}{\tau} mL f_{5y} c_\phi \right. \\ & \left. + q_+ \frac{\delta I}{\tau 2} (d_{5yx} - d_{5xy}) + q_+ \frac{\delta I}{\tau 2} (d_{5yz} - d_{5zy}) s_\beta \right]. \quad (3.19) \end{aligned}$$

Eötvös measured the scale value in four orientations: North (N), East (E), South (S), and West (W). When the apparatus is pointed toward the north, the deflection of the balance from North is simply due to the intrinsic twist in the wire. Thus,

$$\phi_N = \Delta\alpha \quad (3.20)$$

$$s_{\phi_N} = \Delta\alpha \quad (3.21)$$

$$s_{2\phi_N} = 2\Delta\alpha \quad (3.22)$$

$$c_{\phi_N} = 1 \quad (3.23)$$

$$c_{2\phi_N} = 1 \quad (3.24)$$

Then,

$$\begin{aligned}
n_0 - n_N = & \left[-\frac{2\delta}{\tau} I (\partial_y^2 V_{grav} - \partial_x^2 V_{grav}) \Delta\alpha - \frac{2\delta}{\tau} I \partial_x \partial_y V_{grav} \right. \\
& \left. + \frac{2\delta}{\tau} m L h \partial_x \partial_z V_{grav} \Delta\alpha - \frac{2\delta}{\tau} m L h \partial_y \partial_z V_{grav} \right] \\
& + \left[q_+ \frac{\delta}{\tau} I (d_{5yy} - d_{5xx}) \Delta\alpha + q_+ \frac{\delta}{\tau} I d_{5yx} \right. \\
& - q_1 \frac{2\delta}{\tau} m L h d_{5xz} \Delta\alpha + q_1 \frac{2\delta}{\tau} m L h d_{5yz} \\
& \left. + q_+ \frac{\delta}{\tau} I d_{5yz} s_\beta - q_1 \frac{2\delta}{\tau} m L h d_{5yx} s_\beta \right] \\
& + \left[-q_- \frac{2\delta}{\tau} m L f_{5x} \Delta\alpha + q_- \frac{2\delta}{\tau} m L f_{5y} \right]. \tag{3.25}
\end{aligned}$$

When the apparatus is pointed in the Eastern direction, the deflection of the beam balance from North is due to a combination of the intrinsic twist, the difference in the measurements n_N and n_E , and a factor of $\frac{\pi}{2}$ due to physically moving the balance.

Thus

$$\phi_E = \Delta\alpha + \frac{n_N - n_E}{2\delta} + \frac{\pi}{2} \tag{3.26}$$

$$s_{\phi_E} = 1 \tag{3.27}$$

$$s_{2\phi_E} = -2 \left(\Delta\alpha + \frac{n_N - n_E}{2\delta} \right) \tag{3.28}$$

$$c_{\phi_E} = - \left(\Delta\alpha + \frac{n_N - n_E}{2\delta} \right) \tag{3.29}$$

$$c_{2\phi_E} = -1 \tag{3.30}$$

$$\begin{aligned}
n_0 - n_E = & \left[\frac{2\delta}{\tau} I (\partial_y^2 V_{grav} - \partial_x^2 V_{grav}) \left(\Delta\alpha + \frac{n_N - n_E}{2\delta} \right) + \frac{2\delta}{\tau} I \partial_x \partial_y V_{grav} \right. \\
& + \frac{2\delta}{\tau} m L h \partial_x \partial_z V_{grav} + \frac{2\delta}{\tau} m L h \partial_y \partial_z V_{grav} \left. \left(\Delta\alpha + \frac{n_N - n_E}{2\delta} \right) \right] \\
& + \left[-q_+ \frac{\delta}{\tau} I (d_{5yy} - d_{5xx}) \left(\Delta\alpha + \frac{n_N - n_E}{2\delta} \right) - q_+ \frac{\delta}{\tau} I d_{5xy} \right. \\
& - q_1 \frac{2\delta}{\tau} m L h d_{5xz} - q_1 \frac{2\delta}{\tau} m L h d_{5yz} \left. \left(\Delta\alpha + \frac{n_N - n_E}{2\delta} \right) \right. \\
& - q_- \frac{2\delta}{\tau} m L f_{5z} s_\beta - q_+ \frac{\delta}{\tau} I d_{5zy} s_\beta \\
& \left. + q_1 \frac{2\delta}{\tau} m L h d_{5xx} s_\beta - q_1 \frac{2\delta}{\tau} m L h d_{5zz} s_\beta \right] \\
& + \left[-q_- \frac{2\delta}{\tau} m L f_{5x} - q_- \frac{2\delta}{\tau} m L f_{5y} \left(\Delta\alpha + \frac{n_N - n_E}{2\delta} \right) \right] \quad (3.31)
\end{aligned}$$

Rotating the apparatus to point in the Southern direction yields

$$\phi_S = \Delta\alpha + \frac{n_N - n_S}{2\delta} + \pi \quad (3.32)$$

$$s_{\phi_S} = - \left(\Delta\alpha + \frac{n_N - n_S}{2\delta} \right) \quad (3.33)$$

$$s_{2\phi_S} = 2 \left(\Delta\alpha + \frac{n_N - n_S}{2\delta} \right) \quad (3.34)$$

$$c_{\phi_S} = -1 \quad (3.35)$$

$$c_{2\phi_S} = 1, \quad (3.36)$$

and,

$$\begin{aligned}
n_0 - n_S = & \left[-\frac{2\delta}{\tau} I (\partial_y^2 V_{grav} - \partial_x^2 V_{grav}) \left(\Delta\alpha + \frac{n_N - n_S}{2\delta} \right) - \frac{2\delta}{\tau} I \partial_x \partial_y V_{grav} \right. \\
& \left. - \frac{2\delta}{\tau} m L h \partial_x \partial_z V_{grav} \left(\Delta\alpha + \frac{n_N - n_S}{2\delta} \right) + \frac{2\delta}{\tau} m L h \partial_y \partial_z V_{grav} \right] \\
& \left[+q_+ \frac{\delta}{\tau} I (d_{5yy} - d_{5xx}) \left(\Delta\alpha + \frac{n_N - n_S}{2\delta} \right) + q_+ \frac{\delta}{\tau} I d_{5yx} \right. \\
& + q_1 \frac{2\delta}{\tau} m L h d_{5xz} \left(\Delta\alpha + \frac{n_N - n_S}{2\delta} \right) - q_1 \frac{2\delta}{\tau} m L h d_{5yz} \\
& \left. + q_+ \frac{\delta}{\tau} I d_{5yz} s_\beta + q_1 \frac{2\delta}{\tau} m L h d_{5yx} s_\beta \right] \\
& + \left[q_- \frac{2\delta}{\tau} m L f_{5x} \left(\Delta\alpha + \frac{n_N - n_S}{2\delta} \right) - q_- \frac{2\delta}{\tau} m L f_{5y} \right]. \quad (3.37)
\end{aligned}$$

Finally, rotating the apparatus to point in the Western direction yields

$$\phi_W = \Delta\alpha + \frac{n_N - n_W}{2\delta} + \frac{3\pi}{2} \quad (3.38)$$

$$s_{\phi_W} = -1 \quad (3.39)$$

$$s_{2\phi_W} = -2 \left(\Delta\alpha + \frac{n_N - n_W}{2\delta} \right) \quad (3.40)$$

$$c_{\phi_W} = \left(\Delta\alpha + \frac{n_N - n_W}{2\delta} \right) \quad (3.41)$$

$$c_{2\phi_W} = -1 \quad (3.42)$$

and,

$$\begin{aligned} n_0 - n_W = & \left[\frac{2\delta}{\tau} I (\partial_y^2 V_{grav} - \partial_x^2 V_{grav}) \left(\Delta\alpha + \frac{n_N - n_W}{2\delta} \right) + \frac{2\delta}{\tau} I \partial_x \partial_y V_{grav} \right. \\ & \left. - \frac{2\delta}{\tau} mLh \partial_x \partial_z V_{grav} - \frac{2\delta}{\tau} mLh \partial_y \partial_z V_{grav} \left(\Delta\alpha + \frac{n_N - n_W}{2\delta} \right) \right] \\ & + \left[-q_+ \frac{\delta}{\tau} I (d_{5yy} - d_{5xx}) \left(\Delta\alpha + \frac{n_N - n_W}{2\delta} \right) - q_+ \frac{\delta}{\tau} I d_{5xy} \right. \\ & + q_1 \frac{2\delta}{\tau} mLh d_{5xz} + q_1 \frac{2\delta}{\tau} mLh d_{5yz} \left(\Delta\alpha + \frac{n_N - n_W}{2\delta} \right) \\ & + q_- \frac{2\delta}{\tau} mL f_{5z} s_\beta - q_+ \frac{\delta}{\tau} I d_{5zy} s_\beta \\ & \left. - q_1 \frac{2\delta}{\tau} mLh d_{5xx} s_\beta + q_1 \frac{2\delta}{\tau} mLh d_{5zz} s_\beta \right] \\ & + \left[q_- \frac{2\delta}{\tau} mL f_{5x} + q_- \frac{2\delta}{\tau} mL f_{5y} \left(\Delta\alpha + \frac{n_N - n_W}{2\delta} \right) \right]. \quad (3.43) \end{aligned}$$

To eliminate the contribution from gravity gradients, we combine measurements.

We start by introducing $\sigma = n_N - n_S$, where

$$\begin{aligned}
\sigma &= \left[-\frac{2\delta}{\tau} I(\partial_y^2 V_{grav} - \partial_x^2 V_{grav}) \left(\frac{n_N - n_S}{2\delta} \right) \right. \\
&\quad \left. - \frac{2\delta}{\tau} mLh \partial_x \partial_z V_{grav} \left(2\Delta\alpha + \frac{n_N - n_S}{2\delta} \right) + \frac{4\delta}{\tau} mLh \partial_y \partial_z V_{grav} \right] \\
&\quad + \left[q_+ \frac{\delta}{\tau} I(d_{5yy} - d_{5xx}) \left(\frac{n_N - n_S}{2\delta} \right) + q_1 \frac{4\delta}{\tau} mLh d_{5yx} s_\beta \right. \\
&\quad \left. + q_1 \frac{2\delta}{\tau} mLh d_{5xz} \left(2\Delta\alpha + \frac{n_N - n_S}{2\delta} \right) - q_1 \frac{4\delta}{\tau} mLh d_{5yz} \right] \\
&\quad + \left[q_- \frac{2\delta}{\tau} mL f_{5x} \left(2\Delta\alpha + \frac{n_N - n_S}{2\delta} \right) - q_- \frac{4\delta}{\tau} mL f_{5y} \right] \\
&= \frac{4\delta}{\tau} mLh \left(\partial_y \partial_z V_{grav} - q_1 d_{5yz} - q_- \frac{f_{5y}}{h} \right) \\
&\quad - \frac{2\delta}{\tau} I \left[(\partial_y^2 V_{grav} - \partial_x^2 V_{grav}) - \frac{q_+}{2} (d_{5yy} - d_{5xx}) \right] \frac{n_N - n_S}{2\delta} \\
&\quad - \frac{2\delta}{\tau} mLh \left(\partial_x \partial_z V_{grav} - q_1 d_{5xz} - q_- \frac{f_{5x}}{h} \right) \left(2\Delta\alpha + \frac{n_N - n_S}{2\delta} \right) \\
&\quad + q_1 \frac{4\delta}{\tau} mLh s_\beta d_{5yx}. \tag{3.44}
\end{aligned}$$

Then, we now introduce $\nu = n_E - n_W$, where

$$\begin{aligned}
\nu &= \left[\frac{2\delta}{\tau} I (\partial_y^2 V_{grav} - \partial_x^2 V_{grav}) \left(\frac{n_E - n_W}{2\delta} \right) \right. \\
&\quad \left. - \frac{4\delta}{\tau} mLh \partial_x \partial_z V_{grav} - \frac{2\delta}{\tau} mLh \partial_y \partial_z V_{grav} \left(2\Delta\alpha + \frac{2n_N - n_E - n_W}{2\delta} \right) \right] \\
&\quad + \left[-q_+ \frac{\delta}{\tau} I (d_{5yy} - d_{5xx}) \left(\frac{n_E - n_W}{2\delta} \right) + q_- \frac{4\delta}{\tau} mL f_{5z} s_\beta \right. \\
&\quad \left. + q_1 \frac{4\delta}{\tau} mLh d_{5xz} + q_1 \frac{2\delta}{\tau} mLh d_{5yz} \left(2\Delta\alpha + \frac{2n_N - n_E - n_W}{2\delta} \right) \right. \\
&\quad \left. - q_1 \frac{4\delta}{\tau} mLh d_{5xx} s_\beta + q_1 \frac{4\delta}{\tau} mLh d_{5zz} s_\beta \right] \\
&\quad + \left[q_- \frac{4\delta}{\tau} mL f_{5x} + q_- \frac{2\delta}{\tau} mL f_{5y} \left(2\Delta\alpha + \frac{2n_N - n_E - n_W}{2\delta} \right) \right] \\
&= -\frac{4\delta}{\tau} mLh \left(\partial_x \partial_z V_{grav} - q_1 d_{5xz} - q_- \frac{f_{5x}}{h} \right) \\
&\quad + \frac{2\delta}{\tau} I \left[(\partial_y^2 V_{grav} - \partial_x^2 V_{grav}) - \frac{q_+}{2} (d_{5yy} - d_{5xx}) \right] \frac{n_E - n_W}{2\delta} \\
&\quad - \frac{2\delta}{\tau} mLh \left(\partial_y \partial_z V_{grav} - q_1 d_{5yz} - q_- \frac{f_{5y}}{h} \right) \left(2\Delta\alpha + \frac{2n_N - n_E - n_W}{2\delta} \right) \\
&\quad + q_- \frac{4\delta}{\tau} mL s_\beta f_{5z} + q_1 \frac{4\delta}{\tau} MLh s_\beta d_{5zz} - q_1 \frac{4\delta}{\tau} MLh s_\beta d_{5xx}. \tag{3.45}
\end{aligned}$$

Equations (3.44) and (3.45) match Eqs. (14) and (15) in the original EPF work [2]. In the final step of both equations, however, we have deviated from our convention of grouping the Eötvös contributions at the beginning of the equation, to instead group the terms in a way as to make the next step of the analysis a bit easier, the computation of ν/σ . In the original analysis of Eötvös, ν contained the WEP-violating term of interest along with gravity-gradient terms, while σ contained only gravity-gradients. Therefore, they used σ to attempt to remove the gravity gradients. To this end, Eötvös divided ν by σ . When we computed Eqs. (3.44) and (3.45), we

intentionally grouped like terms. Here, we take this a step further and introduce some additional parameters. Let

$$\tau \frac{\sigma}{2\delta} = C_1 - C_2 \frac{n_N - n_S}{2\delta} - C_3 \left(2\Delta\alpha + \frac{n_N - n_S}{2\delta} \right) + C_4 s_\beta, \quad (3.46)$$

$$\tau \frac{\nu}{2\delta} = -D_1 + D_2 \frac{n_E - n_W}{2\delta} - D_3 \left(2\Delta\alpha + \frac{2n_N - n_E - n_W}{2\delta} \right) + D_4 s_\beta, \quad (3.47)$$

with

$$C_1 = 2mLh \left(\partial_y \partial_z V_{grav} - q_1 d_{5yz} - q_- \frac{f_{5y}}{h} \right), \quad (3.48)$$

$$C_2 = I \left[(\partial_y^2 V_{grav} - \partial_x^2 V_{grav}) - \frac{q_+}{2} (d_{5yy} - d_{5xx}) \right], \quad (3.49)$$

$$C_3 = mLh \left(\partial_x \partial_z V_{grav} - q_1 d_{5xz} - q_- \frac{f_{5x}}{h} \right), \quad (3.50)$$

$$C_4 = 2q_1 mLh d_{5yx}, \quad (3.51)$$

$$\begin{aligned} D_1 &= 2mLh \left(\partial_x \partial_z V_{grav} - q_1 d_{5xz} - q_- \frac{f_{5x}}{h} \right) \\ &= 2C_3, \end{aligned} \quad (3.52)$$

$$\begin{aligned} D_2 &= I \left[(\partial_y^2 V_{grav} - \partial_x^2 V_{grav}) - \frac{q_+}{2} (d_{5yy} - d_{5xx}) \right] \\ &= C_2, \end{aligned} \quad (3.53)$$

$$\begin{aligned} D_3 &= mLh \left(\partial_y \partial_z V_{grav} - q_1 d_{5yz} - q_- \frac{f_{5y}}{h} \right) \\ &= \frac{1}{2} C_1, \end{aligned} \quad (3.54)$$

$$D_4 = 2q_- mL f_{5z} + 2q_1 mLh d_{5zz} - 2q_1 mLh d_{5xx}. \quad (3.55)$$

We chose the definitions of the C 's and D 's so that they would all have the same approximate magnitude. We assume, for the moment, that the d_5 's are roughly the same order of magnitude as the gravity gradients. We also assume that \vec{f}_5/h is of this same magnitude. We know that h and L are of the same order, thus I and mLh are as well. We now consider Eqs. (3.46) and (3.47). We know that $\Delta\alpha$ and s_β are

small, and we know that δ is larger than n_N , n_E , n_S , and n_W , so we can define the lowest order approximations of σ and ν as

$$\tau \frac{\sigma}{2\delta} \approx C_1 = 2mLh \left(\partial_y \partial_z V_{grav} - q_1 d_{5yz} - q_- \frac{f_{5y}}{h} \right), \quad (3.56)$$

$$\tau \frac{\nu}{2\delta} \approx -D_1 = -2mLh \left(\partial_x \partial_z V_{grav} - q_1 d_{5xz} - q_- \frac{f_{5x}}{h} \right). \quad (3.57)$$

Based on the preceding discussion, we can compute our equivalent to Eötvös' ν/σ term

$$\begin{aligned} \frac{\nu}{\sigma} &= \frac{-D_1 + C_2 \frac{n_E - n_W}{2\delta} - C_1 \left(\Delta\alpha + \frac{2n_N - n_E - n_W}{4\delta} \right) + D_4 s_\beta}{C_1 - C_2 \frac{n_N - n_S}{2\delta} - D_1 \left(\Delta\alpha + \frac{n_N - n_S}{4\delta} \right) + C_4 s_\beta} \\ &= \frac{-D_1 + C_2 \frac{n_E - n_W}{2\delta} - C_1 \left(\Delta\alpha + \frac{2n_N - n_E - n_W}{4\delta} \right) + D_4 s_\beta}{C_1 \left(1 - \frac{C_2}{C_1} \frac{n_N - n_S}{2\delta} - \frac{D_1}{C_1} \left(\Delta\alpha + \frac{n_N - n_S}{4\delta} \right) + \frac{C_4}{C_1} s_\beta \right)} \\ &\approx \left(-\frac{D_1}{C_1} + \frac{C_2}{C_1} \frac{n_E - n_W}{2\delta} - \left(\Delta\alpha + \frac{2n_N - n_E - n_W}{4\delta} \right) + \frac{D_4}{C_1} s_\beta \right) \\ &\quad \times \left(1 + \frac{C_2}{C_1} \frac{n_N - n_S}{2\delta} + \frac{D_1}{C_1} \left(\Delta\alpha + \frac{n_N - n_S}{4\delta} \right) - \frac{C_4}{C_1} s_\beta \right) \\ &\approx -\frac{D_1}{C_1} + \frac{C_2}{C_1} \frac{n_E - n_W}{2\delta} - \left(\Delta\alpha + \frac{2n_N - n_E - n_W}{4\delta} \right) + \frac{D_4}{C_1} s_\beta \\ &\quad - \frac{D_1}{C_1} \frac{C_2}{C_1} \frac{n_N - n_S}{2\delta} - \left(\frac{D_1}{C_1} \right)^2 \left(\Delta\alpha + \frac{n_N - n_S}{4\delta} \right) + \frac{D_1}{C_1} \frac{C_4}{C_1} s_\beta. \end{aligned} \quad (3.58)$$

We can use our approximations (3.56) and (3.57) to simplify Eq. (3.58). In every term except the first term, we can replace D_1/C_1 with $-\nu/\sigma$ and we can replace C_1 with $\tau\sigma/2\delta$ (we are essentially trying to eliminate C_1 and solve for D_1/C_1 in terms of σ and ν). We also use the definitions $\sigma = n_N - n_S$ and $\nu = n_E - n_W$ to write

$$\begin{aligned} \frac{\nu}{\sigma} &= -\frac{D_1}{C_1} + \frac{2C_2}{\tau} \frac{\nu}{\sigma} - \left(\frac{\nu^2}{\sigma^2} + 1 \right) \Delta\alpha - \frac{2n_N - n_E - n_W}{4\delta} \\ &\quad - \frac{\nu^2}{\sigma^2} \frac{\sigma}{4\delta} + \frac{2\delta}{\sigma\tau} D_4 s_\beta - \frac{\nu}{\sigma} \frac{2\delta}{\sigma\tau} C_4 s_\beta. \end{aligned} \quad (3.59)$$

We need to further simplify this term. Since f_{5i}/h and d_{5ij} are much smaller than the gravity gradient terms, we can approximate σ and ν as simply the gravity gradient terms at lowest order.

$$\tau \frac{\sigma}{2\delta} \approx 2mLh \partial_y \partial_z V_{grav}, \quad (3.60)$$

$$\tau \frac{\nu}{2\delta} \approx -2mLh \partial_x \partial_z V_{grav}. \quad (3.61)$$

Next, we can approximate the first term in Eq. (3.59) as

$$\begin{aligned} \frac{D_1}{C_1} &= \frac{(\partial_x \partial_z V_{grav} - q_1 d_{5xz} - q_- \frac{f_{5x}}{h})}{(\partial_y \partial_z V_{grav} - q_1 d_{5yz} - q_- \frac{f_{5y}}{h})} \\ &= \frac{(\partial_x \partial_z V_{grav} - q_1 d_{5xz} - q_- \frac{f_{5x}}{h})}{\partial_y \partial_z V_{grav}} \left(1 - \frac{q_1 d_{5yz} + q_- \frac{f_{5y}}{h}}{\partial_y \partial_z V_{grav}} \right)^{-1} \\ &\approx \frac{\partial_x \partial_z V_{grav}}{\partial_y \partial_z V_{grav}} - \frac{q_1 d_{5xz} + q_- \frac{f_{5x}}{h}}{\partial_y \partial_z V_{grav}} + \frac{\partial_x \partial_z V_{grav}}{\partial_y \partial_z V_{grav}} \frac{q_1 d_{5yz} + q_- \frac{f_{5y}}{h}}{\partial_y \partial_z V_{grav}} \\ &\approx \frac{\partial_x \partial_z V_{grav}}{\partial_y \partial_z V_{grav}} - q_1 \frac{1}{\partial_y \partial_z V_{grav}} \left(d_{5xz} - \frac{\partial_x \partial_z V_{grav}}{\partial_y \partial_z V_{grav}} d_{5yz} \right) \\ &\quad + \frac{q_-}{h} \frac{1}{\partial_y \partial_z V_{grav}} \left(f_{5x} - \frac{\partial_x \partial_z V_{grav}}{\partial_y \partial_z V_{grav}} f_{5y} \right). \end{aligned} \quad (3.62)$$

We can use Eq. (3.60) to replace $(\partial_y \partial_z V_{grav})^{-1}$ in terms of σ and $(\partial_x \partial_z V_{grav}/\partial_y \partial_z V_{grav})$ with $(-\nu/\sigma)$ in the second and third terms. Again, we cannot make this substitution in the first term as our ultimate goal is to eliminate the gravity gradients, so we are trying to solve for $(\partial_x \partial_z V_{grav}/\partial_y \partial_z V_{grav})$ in terms of D_1/C_1 which is approximately ν/σ from before. Then,

$$\begin{aligned} \frac{D_1}{C_1} &\approx \frac{\partial_x \partial_z V_{grav}}{\partial_y \partial_z V_{grav}} - q_1 \frac{4\delta}{\sigma\tau} mLh \left(d_{5xz} + \frac{\nu}{\sigma} d_{5yz} \right) \\ &\quad + q_- \frac{4\delta}{\sigma\tau} mL \left(f_{5x} + \frac{\nu}{\sigma} f_{5y} \right), \end{aligned} \quad (3.63)$$

and we can substitute Eq. (3.63) into Eq. (3.59) to yield

$$\begin{aligned}
\frac{\nu}{\sigma} = & \left[-\frac{\partial_x \partial_z V_{grav}}{\partial_y \partial_z V_{grav}} + \frac{2I}{\tau} \frac{\nu}{\sigma} \left(\partial_y^2 V_{grav} - \partial_x^2 V_{grav} \right) - \left(\frac{\nu^2}{\sigma^2} + 1 \right) \Delta\alpha \right. \\
& \left. - \frac{\nu^2}{\sigma^2} \frac{\sigma}{4\delta} - \frac{2n_N - n_E - n_W}{4\delta} \right] \\
& + \left[q_- \frac{4\delta}{\sigma\tau} mLs_\beta f_{5z} + q_1 \frac{4\delta}{\sigma\tau} mLh \left(d_{5xz} + \frac{\nu}{\sigma} d_{5yz} \right) \right. \\
& \left. - q_+ \frac{I}{\tau} \frac{\nu}{\sigma} (d_{5yy} - d_{5xx}) - q_1 \frac{4\delta}{\sigma\tau} mLhs_\beta \left(d_{5xx} + \frac{\nu}{\sigma} d_{5yx} - d_{5zz} \right) \right] \\
& + \left[q_- \frac{4\delta}{\sigma\tau} mL \left(f_{5x} + \frac{\nu}{\sigma} f_{5y} \right) \right]. \tag{3.64}
\end{aligned}$$

We have now returned to our convention of grouping the Eötvös terms first. We notice that we still have unwanted and unknown gravity gradient terms in our equations. However, the rest of the terms are known. (Several terms are multiplied by σ and ν , but at this point, those are experimentally known.) To eliminate the gradients, the sample q_1 is replaced with the sample q'_1 and the measurements are repeated and a new term $\frac{\nu'}{\sigma'}$ is computed. We then subtract the two calculated values (assuming ν and σ do not change much between the measurements) and we cancel the gravity gradients to lowest working order.

$$\begin{aligned}
\frac{\nu}{\sigma} - \frac{\nu'}{\sigma'} = & \left[- \left(\frac{\nu^2}{\sigma^2} + 1 \right) (\Delta\alpha - \Delta\alpha') \right] \\
& + \left[\Delta q \frac{4\delta}{\sigma\tau} mLs_\beta f_{5z} \right] \\
& + \left[\Delta q \frac{4\delta}{\sigma\tau} mL \left(f_{5x} + \frac{\nu}{\sigma} f_{5y} \right) \right. \\
& \left. - \Delta q \frac{I}{\tau} \frac{\nu}{\sigma} (d_{5yy} - d_{5xx}) \right. \\
& \left. + \Delta q \frac{4\delta}{\sigma\tau} mLh \left(d_{5xz} + \frac{\nu}{\sigma} d_{5yz} \right) \right. \\
& \left. - \Delta q \frac{4\delta}{\sigma\tau} mLhs_\beta \left(d_{5xx} + \frac{\nu}{\sigma} d_{5yx} - d_{5zz} \right) \right]. \tag{3.65}
\end{aligned}$$

In Eq. (3.65), $\Delta q = q_1 - q'_1$ and the first bracket corresponds to Eq. (18) of EPF [2]. The ultimate goal of the Eötvös experiment was to measure the differences

in the WEP violating parameters for the different substances, referred to as $\kappa_a - \kappa'_a$, and from Eq. (19) of [2],

$$\begin{aligned} \kappa_a - \kappa'_a &= \frac{\sigma\tau}{4\sigma m L g s_\beta} \left(\frac{\nu}{\sigma} - \frac{\nu'}{\sigma'} \right) \\ &\quad + \frac{\sigma\tau}{4\sigma m L g s_\beta} \left(\frac{\nu^2}{\sigma^2} + 1 \right) (\Delta\alpha - \Delta\alpha'). \end{aligned} \quad (3.66)$$

This parameter, which is represented by η in modern works and referred to as the ‘‘Eötvös Parameter,’’ can be written in terms of our fifth force by combining Eq. (19) of [2] with Eq. (3.65) above:

$$\begin{aligned} \eta_{EPF} &= \Delta\kappa_{s\beta} = \frac{\sigma\tau}{4\sigma m L g} \left(\frac{\nu}{\sigma} - \frac{\nu'}{\sigma'} \right) \\ &\quad + \frac{\sigma\tau}{4\sigma m L g} \left(\frac{\nu^2}{\sigma^2} + 1 \right) (\Delta\alpha - \Delta\alpha') \\ &= \Delta q \frac{f_{5z}}{g} s_\beta + \Delta q \frac{1}{g} \left(f_{5x} + \frac{\nu}{\sigma} f_{5y} \right) \\ &\quad - \Delta q \frac{L}{g} \frac{\nu}{2\delta} (d_{5yy} - d_{5xx}) \\ &\quad + \Delta q \frac{h}{g} \left(d_{5xz} + \frac{\nu}{\sigma} d_{5yz} \right) \\ &\quad - \Delta q \frac{h}{g} s_\beta \left(d_{5xx} + \frac{\nu}{\sigma} d_{5yx} - d_{5zz} \right). \end{aligned} \quad (3.67)$$

3.2 The Eöt-Wash Experiment

The Eöt-Wash experiment of Stubbs et al. [8] consists of four masses, two of each sample. They form two perpendicular fifth-force dipoles and an overall mass quadrupole.

The fifth-force charge times the mass density can be written as

$$\begin{aligned} q(\vec{r}) \rho(\vec{r}) &= q_1 m [\delta(x-L) \delta(y) \delta(z) + \delta(x) \delta(y-L) \delta(z)] \\ &\quad + q_2 m [\delta(x+L) \delta(y) \delta(z) + \delta(x) \delta(y+L) \delta(z)]. \end{aligned} \quad (3.68)$$

For the E-W experiment, we start with Eq. (3.17) for the torque, then let $\phi \rightarrow \phi + \pi/2$, and add it to the original expression, and if we set $h = 0$, then the fifth force torque, T_5 is given by,

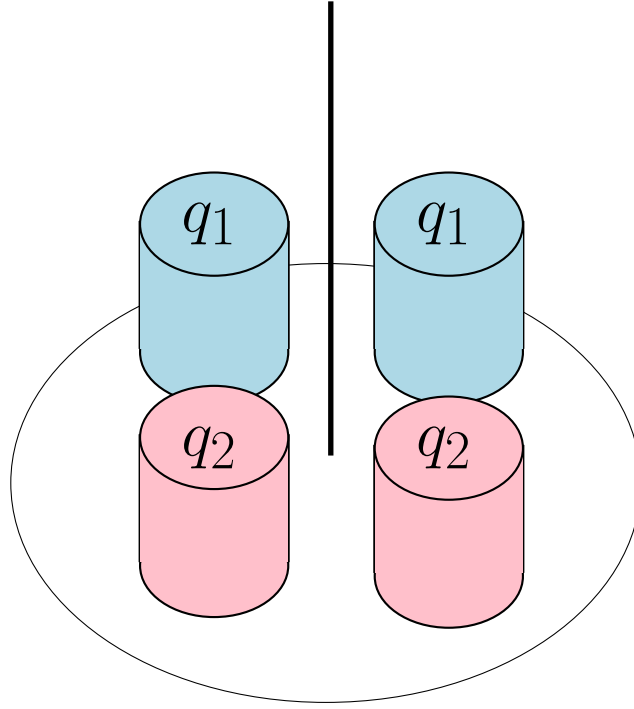


Fig. 3.5. Side view of the Eöt-Wash Experiment.

$$\begin{aligned}
T_5 &= -(q_1 - q_2)mL(s_\phi + c_\phi)f_{5x} - (q_1 - q_2)mL(s_\phi - c_\phi)f_{5y} - (q_1 - q_2)mLs_\beta(s_\phi + c_\phi)f_{5z} \\
&\quad - (q_1 + q_2)\frac{I}{2}(d_{5yx} - d_{5xy}) + (q_1 + q_2)\frac{I}{2}s_\beta(d_{5yz} - d_{5zy}) \\
&= -(q_1 - q_2)mL\sqrt{2}(f_{5x} + s_\beta f_{5z})\cos\left(\phi - \frac{\pi}{4}\right) - (q_1 - q_2)mL\sqrt{2}f_{5y}\sin\left(\phi - \frac{\pi}{4}\right) \\
&\quad - (q_1 + q_2)\frac{I}{2}(d_{5yx} - d_{5xy}) + (q_1 + q_2)\frac{I}{2}s_\beta(d_{5yz} - d_{5zy}). \tag{3.69}
\end{aligned}$$

To eliminate any inherent twist in the fiber we define $\bar{T}(\phi) = T_5(\phi) - T_5(\phi + \pi)$,

$$\begin{aligned}
\bar{T} &= -(q_1 - q_2)mL2\sqrt{2}(f_{5x} + s_\beta f_{5z})\cos\left(\phi - \frac{\pi}{4}\right) - (q_1 - q_2)mL2\sqrt{2}f_{5y}\sin\left(\phi - \frac{\pi}{4}\right) \\
&= -(q_1 - q_2)mL2\sqrt{2}\sqrt{(f_{5x} + s_\beta f_{5z})^2 + f_{5y}^2}\cos(\phi + \delta), \tag{3.70}
\end{aligned}$$

$$\delta = \tan^{-1}\left(\frac{f_{5y}}{f_{5x} + s_\beta f_{5z}}\right) - \frac{\pi}{4}. \tag{3.71}$$

We can identify the acceleration difference $\Delta a = (q_1 - q_2)\sqrt{2}\sqrt{(f_{5x} + s_\beta f_{5z})^2 + f_{5y}^2}$, and then, the Eötvös parameter becomes

$$\begin{aligned}\eta_{EW} &= \frac{\Delta a}{g} = \Delta q \frac{\sqrt{2}}{g} \sqrt{(f_{5x} + s_\beta f_{5z})^2 + f_{5y}^2}, \\ \eta_{EPF} &= \Delta q \frac{f_{5z}}{g} s_\beta + \Delta q \frac{1}{g} \left(f_{5x} + \frac{\nu}{\sigma} f_{5y} \right) \\ &\quad - \Delta q \frac{L}{g} \frac{\nu}{2\delta} (d_{5yy} - d_{5xx}) \\ &\quad + \Delta q \frac{h}{g} \left(d_{5xz} + \frac{\nu}{\sigma} d_{5yz} \right) \\ &\quad - \Delta q \frac{h}{g} s_\beta \left(d_{5xx} + \frac{\nu}{\sigma} d_{5yx} - d_{5zz} \right).\end{aligned}\tag{3.72}$$

$$\tag{3.73}$$

3.3 Scalar-Vector Force Model

Based on the results above, we can specify a set of requirements for a fifth force model aimed at accounting for the EPF data:

1. The interaction is proportional to baryon number, B ,
2. The interaction is short range, on the order of $1 \text{ m} \lesssim \lambda \lesssim 1 \text{ km}$,
3. The torque due to the force, f_{5i} , is zero in the E-W experiment,
4. The torque due to the gradients, d_{5ij} , is nonzero in the EPF experiment.

The first requirement is trivial to implement. The second requirement can be fulfilled by a Yukawa potential, meaning a massive force-carrier. The third and fourth requirements need additional attention. Requiring the the force to be small at some point (item 3), but not another (item 4) is the same as requiring that the potential has a minimum at that point. As an example, we can consider the quadratic potential $V = \frac{1}{2}m\omega^2(x - x_0)^2$. This potential has a minimum at $x = x_0$. At this point, the force, $F_x = m\omega^2(x - x_0)$, vanishes, while the derivative of the force, $d_{xx} = m\omega^2$ is nonzero, fulfilling requirements three and four. The question now becomes how do we obtain a quadratic potential from elementary particle physics. We recall that

an arbitrary function Taylor expanded about an equilibrium point behaves like a quadratic function. Although the Yukawa potential does not have an equilibrium point, if we introduce a second Yukawa with opposite sign, we have a function that indeed does contain a minimum. Microscopically this function would arise if the interaction were due to the exchange of scalar and vector bosons coupling to baryon number, whose potential energies naturally enter with opposite signs,

$$V_S(\vec{r}) = -Gm_i m_j q_i q_j \frac{\xi_S}{r} e^{-r/\lambda_S}, \quad (3.74)$$

$$V_V(\vec{r}) = Gm_i m_j q_i q_j \frac{\xi_V}{r} e^{-r/\lambda_V}. \quad (3.75)$$

where $q_k = B_k/\mu_k$ is our Baryon-number dependent charge and, we have used the notation introduced in Chapter 2 and Fischbach et al. [7].

We can now integrate over the mass distributions. The Earth serves as the sole source for the Eötvös experiment, and one of two sources for the Eöt-Wash experiment. We model the Earth as a uniform sphere with the experimental apparatus located a distance z above the surface. We let $m_j \rightarrow dm_j = \rho_{\oplus} d^3r'$ and then we integrate over the volume of the Earth ($k = \{V, S\}$)

$$V_k = \pm G m_i q_i \xi_k \int d^3r' \rho(\vec{r}') q_{\oplus}(\vec{r}') \frac{e^{-|\vec{r}-\vec{r}'|/\lambda_k}}{|\vec{r}-\vec{r}'|}. \quad (3.76)$$

The uniform sphere assumption means we can take ρ_{\oplus} and q_{\oplus} to be constant. Then, using spherical coordinates,

$$\begin{aligned} V_k &= \pm G \rho_{\oplus} m_i q_i q_{\oplus} \xi_k \int_0^{2\pi} d\phi' \int_0^{R_{\oplus}} dr' r'^2 \\ &\quad \times \int_0^{\pi} d\theta' \sin \theta' \frac{e^{-\sqrt{r'^2+r^2-2rr'\cos\theta'}/\lambda_k}}{\sqrt{r'^2+r^2-2rr'\cos\theta'}}. \end{aligned} \quad (3.77)$$

Let $u = \sqrt{r'^2+r^2-2rr'\cos\theta'}$, then $du = rr' \sin\theta' d\theta' / \sqrt{r'^2+r^2-2rr'\cos\theta'}$, and integrating over ϕ' , we have

$$\begin{aligned} V_k &= \pm 2\pi \frac{G \rho_{\oplus} m_i}{r} q_i q_{\oplus} \xi_k \int_0^{R_{\oplus}} dr' r' \int_{|r-r'|}^{r+r'} du e^{-u/\lambda_k} \\ &= \pm 2\pi \frac{G \rho_{\oplus} m_i \lambda_k}{r} q_i q_{\oplus} \xi_k \int_0^R dr' r' \left(e^{-|r-r'|/\lambda_k} - e^{-(r+r')/\lambda_k} \right). \end{aligned} \quad (3.78)$$

Since $r = R_\oplus + z$, $r - r'$ is always positive, we can drop the absolute value. Then,

$$\begin{aligned}
V_k &= \pm 2\pi \frac{G\rho_\oplus m_i \lambda_k}{R_\oplus + z} q_i q_\oplus \xi_k e^{-(R_\oplus + z)\lambda_k} \int_0^{R_\oplus} dr' r' \left(e^{r'/\lambda_k} - e^{-r'/\lambda_k} \right) \\
&= \pm 2\pi \frac{G\rho_\oplus m_i \lambda_k^3}{R_\oplus + z} q_i q_\oplus \xi_k e^{-(R_\oplus + z)\lambda_k} \\
&\quad \times \left[\left(\frac{r'}{\lambda_k} - 1 \right) e^{r'/\lambda_k} + \left(\frac{r'}{\lambda_k} + 1 \right) e^{-r'/\lambda_k} \right] \Big|_{r'=0}^{r'=R_\oplus} \\
&= \pm 2\pi \frac{G\rho_\oplus m_i \lambda_k^3}{R_\oplus + z} q_i q_\oplus \xi_k e^{-(R_\oplus + z)\lambda_k} \\
&\quad \times \left[\left(\frac{R_\oplus}{\lambda_k} - 1 \right) e^{R_\oplus/\lambda_k} + \left(\frac{R_\oplus}{\lambda_k} + 1 \right) e^{-R_\oplus/\lambda_k} \right] \\
&= \pm \frac{3GM_\oplus m_i}{2} \frac{q_i q_\oplus \xi_k}{R_\oplus + z} \left(\frac{\lambda_k}{R_\oplus} \right)^2 e^{-z/\lambda_k} \\
&\quad \times \left[\left(1 - \frac{\lambda_k}{R_\oplus} \right) + \left(1 + \frac{\lambda_k}{R_\oplus} \right) e^{-2R_\oplus/\lambda_k} \right]. \tag{3.79}
\end{aligned}$$

Since the apparatus is close to the surface ($z \ll R_\oplus$), and the force is short range ($\lambda_k \ll R_\oplus$), we can simplify Eq. (3.79) to read,

$$V_k = \pm \frac{3GM_\oplus m_i}{2} \frac{q_i q_\oplus \xi_k}{R_\oplus} \left(\frac{\lambda_k}{R_\oplus} \right)^2 e^{-z/\lambda_k}. \tag{3.80}$$

The total potential and force are then given by,

$$V_{tot} = \frac{3GM_\oplus m_i}{2} \frac{q_i q_\oplus}{R_\oplus} \left[\xi_V \left(\frac{\lambda_V}{R_\oplus} \right)^2 e^{-z/\lambda_V} - \xi_S \left(\frac{\lambda_S}{R_\oplus} \right)^2 e^{-z/\lambda_S} \right], \tag{3.81}$$

$$\begin{aligned}
\vec{F}_{tot} &= \frac{3GM_\oplus m_i}{2} \frac{q_i q_\oplus}{R_\oplus^2} \left[\xi_V \left(\frac{\lambda_V}{R_\oplus} \right) e^{-z/\lambda_V} - \xi_S \left(\frac{\lambda_S}{R_\oplus} \right) e^{-z/\lambda_S} \right] \hat{z} \\
&= \frac{3}{2} g_N m_i q_i q_\oplus (\bar{\xi}_V e^{-z/\lambda_V} - \bar{\xi}_S e^{-z/\lambda_S}) \hat{z}, \tag{3.82}
\end{aligned}$$

where we have introduced the gravitational acceleration due to Earth, and we have defined $\bar{\xi}_V = \xi_V (\lambda_V/R_\oplus)$. We must stop and consider the unit vector \hat{z} in Eq. (3.82). When we integrated over Earth, we used a standard spherical reference frame and our apparatus was located radially away from the center of the Earth at a distance of $R + z$. In our N-E-D frame (Figure 3.1) this direction corresponds to $-\hat{D}$. Thus we must replace \hat{z} with $-\hat{D}$ in Eq. (3.82).

The second source for the E-W experiment was a hill located north of the apparatus. We model this hill as an infinite half plane with the apparatus located a distance

z above the plane. We assume that the hill has the same q and ρ as the Earth and we write the mass element at $dm_j = \rho_{\oplus} r' dr' d\phi' dz'$ in cylindrical coordinates. Then,

$$\begin{aligned} V_k &= \pm G \rho_{\oplus} m_i q_i q_{\oplus} \xi_k \int_0^{2\pi} d\phi' \int_{-\infty}^0 dz' \\ &\quad \times \int_0^{\infty} dr' r' \frac{e^{-\sqrt{r'^2 + (z-z')^2}/\lambda_k}}{\sqrt{r'^2 + (z-z')^2}}. \end{aligned} \quad (3.83)$$

Let $u = \sqrt{r'^2 + (z-z')^2}$, then $du = r' dr' / \sqrt{r'^2 + (z-z')^2}$, and (integrating over ϕ')

$$\begin{aligned} V_k &= \pm 2\pi G \rho_{\oplus} m_i q_i q_{\oplus} \xi_k \int_{-\infty}^0 dz' \int_{|z-z'|}^{\infty} du e^{-u/\lambda_k} \\ &= \pm 2\pi G \rho_{\oplus} m_i q_i q_{\oplus} \xi_k \lambda_k \int_{-\infty}^0 dz' e^{-|z-z'|/\lambda_k}. \end{aligned}$$

Since z is positive and z' is always negative, we can drop the absolute value and write

$$\begin{aligned} V_k &= \pm 2\pi G \rho_{\oplus} m_i q_i q_{\oplus} \xi_k \lambda_k e^{-z/\lambda_k} \int_{-\infty}^0 dz' e^{z'/\lambda_k} \\ &= \pm 2\pi G \rho_{\oplus} m_i q_i q_{\oplus} \xi_k \lambda_k^2 e^{-z/\lambda_k} \\ &= \pm \frac{3}{2} g_N m_i q_i q_{\oplus} \bar{\xi}_k \lambda_k e^{-z/\lambda_k}, \end{aligned} \quad (3.84)$$

where we introduced some of the simplifications from before. We see that the potential for the hill and the Earth have the same form. This makes sense since the short range of the force means the apparatus only ‘‘sees’’ the Earth in its immediate vicinity, and at that distance the Earth appears flat like an infinite plane. The force from the hill will then be equal to Eq. (3.82), but we must be careful about symbols and vectors again. In our model, the apparatus was located a distance z above the semi-infinite plane. In reality, the apparatus was a distance x to the south, so we must replace z in Eq. (3.82) with x and \hat{z} with $-\hat{N}$.

The forces from the Earth and the hill are then

$$\vec{F}_{\oplus} = -\frac{3}{2} g_N m_i q_i q_{\oplus} (\bar{\xi}_V e^{-z/\lambda_V} - \bar{\xi}_S e^{-z/\lambda_S}) \hat{D}, \quad (3.85)$$

$$\vec{F}_{\text{hill}} = -\frac{3}{2} g_N m_i q_i q_{\oplus} (\bar{\xi}_V e^{-x/\lambda_V} - \bar{\xi}_S e^{-x/\lambda_S}) \hat{N}. \quad (3.86)$$

We can find the equilibrium position of these functions by setting the force equal to zero,

$$\begin{aligned}
0 &= \frac{3}{2} g_N m_i q_i q_\oplus (\bar{\xi}_V e^{-z_{equil}/\lambda_V} - \bar{\xi}_S e^{-z_{equil}/\lambda_S}) \hat{z} \\
&= (\bar{\xi}_V e^{-z_{equil}/\lambda_V} - \bar{\xi}_S e^{-z_{equil}/\lambda_S}) \\
\rightarrow z_{equil} &= \frac{\lambda_S \lambda_V}{\lambda_S - \lambda_V} \ln \left(\frac{\bar{\xi}_V}{\bar{\xi}_S} \right) \\
&= \left(\frac{1}{\lambda_V} - \frac{1}{\lambda_S} \right)^{-1} \ln \left(\frac{\bar{\xi}_V}{\bar{\xi}_S} \right). \tag{3.87}
\end{aligned}$$

Since z_{equil} or x_{equil} must be positive, we have two possibilities

$$\frac{1}{\lambda_V} - \frac{1}{\lambda_S} > 0, \frac{\bar{\xi}_V}{\bar{\xi}_S} > 1 \tag{3.88}$$

$$\frac{1}{\lambda_V} - \frac{1}{\lambda_S} < 0, \frac{\bar{\xi}_V}{\bar{\xi}_S} < 1 \tag{3.89}$$

3.3.1 Case 1: $\bar{\xi}_V > \bar{\xi}_S, \lambda_S > \lambda_V$

We can rewrite the positivity conditions as

$$\frac{\bar{\xi}_S}{\bar{\xi}_V} < 1, \tag{3.90}$$

$$\frac{\lambda_V}{\lambda_S} < 1. \tag{3.91}$$

We introduce parameters $\alpha_1 = \bar{\xi}_S/\bar{\xi}_V$ and $\zeta_1 =$

$\lambda_{\lambda_V}/\lambda_S$ which are bounded between zero and one. We can then write the relevant phenomenological coefficients from Eq. (3.1) as

$$f_{5x} = -\frac{3}{2} g_N q_\oplus \bar{\xi}_V (e^{-x/\lambda_V} - \alpha_1 e^{-x\zeta_1/\lambda_V}), \tag{3.92}$$

$$f_{5z} = -\frac{3}{2} g_N q_\oplus \bar{\xi}_V (e^{-z/\lambda_V} - \alpha_1 e^{-z\zeta_1/\lambda_V}), \tag{3.93}$$

$$d_{5zz} = \frac{3}{2} g_N q_\oplus \frac{\bar{\xi}_V}{\lambda_V} (e^{-z/\lambda_V} - \alpha_1 \zeta_1 e^{-z\zeta_1/\lambda_V}). \tag{3.94}$$

The Eötvös parameters in the EPF and E-W experiments are then

$$\begin{aligned} \frac{\eta_{EPF}}{\frac{3}{2}\Delta q q_{\oplus} \bar{\xi}_V} &= \bar{\eta}_{EPF} = -s_{\beta} \left[e^{-z_{EPF}/\lambda_V} - \alpha_1 e^{-z_{EPF}\zeta_1/\lambda_V} \right] \\ &\quad + s_{\beta} \frac{h}{\lambda_V} \left[e^{-z_{EPF}/\lambda_V} - \alpha_1 \zeta_1 e^{-z_{EPF}\zeta_1/\lambda_V} \right], \end{aligned} \quad (3.95)$$

$$\begin{aligned} \frac{\eta_{EW}}{\frac{3}{2}\Delta q q_{\oplus} \bar{\xi}_V} &= \bar{\eta}_{EW} = \sqrt{2} \left| - \left(e^{-x_{EW}/\lambda_V} - \alpha_1 e^{-x_{EW}\zeta_1/\lambda_V} \right) \right. \\ &\quad \left. - s_{\beta} \left(e^{-z_{EW}/\lambda_V} - \alpha_1 e^{-z_{EW}\zeta_1/\lambda_V} \right) \right|. \end{aligned} \quad (3.96)$$

We note that $\bar{\xi}_V$ simply scales the effect and so we move it to the left side of the equation. Now we only have three parameters in which to search: λ_V , α_1 , and ζ_1 .

We can plot Eq. (3.95) and (3.96) for various values of α_1 , ζ_1 , and λ_V . In our calculations, we used $s_{\beta} = 1.73 \times 10^{-3}$, $h = 21.2$ cm [2], $x_{EW} = 10$ m, $z_{EPF} = z_{EW} = 1$ m. The plots are shown in Figure 3.95 for EPF and Figure 3.7 for E-W. We note that in Figure 3.95, the results are negative for small α_1 values and eventually become positive as α_1 increases. As α_1 measures the relative strengths of the two Yukawas, we would expect α_1 to have a large effect on the sign of the response. Figure 3.96 starts positive and would eventually go negative if not for the absolute value in Eq. (3.96); instead it grows positive. The zeros of η_{EW} occur at higher λ_V for increasing α_1 and fixed ζ_1 and occur at lower λ_V for increasing ζ_1 at fixed α_1 .

We notice in Figure 3.96 that for every α_1 and ζ_1 , there exists a λ_V value where the signal is zero, which was one of the requirements for this force (see discussion at the beginning of Section 3.3). In fact, we can find these values analytically. By setting $\bar{\eta}_{EW} = 0$ in Eq. (3.96), we solve for α_1 as a function of λ_V and ζ_1

$$\alpha_1 = \frac{e^{-x_{EW}/\lambda_V} + s_{\beta} e^{-z_{EW}/\lambda_V}}{e^{-x_{EW}\zeta_1/\lambda_V} + s_{\beta} e^{-z_{EW}\zeta_1/\lambda_V}} \quad (3.97)$$

The top plot of Figure 3.8 shows the values of α_1 which give $\bar{\eta}_{EW} = 0$ for various values of ζ_1 and λ_V . Interestingly, α_1 remains less than or equal to one, as required but our initial definition. The bottom plot shows the value of $\bar{\eta}_{EPF}$ for each triplet $(\lambda_V, \zeta_1, \alpha_1)$. As before the answer is negative, and its magnitude peaks around $\lambda_V \approx (2 - 3)$ m for the whole range of ζ_1 , with the actual value decreasing as ζ_1 increases.

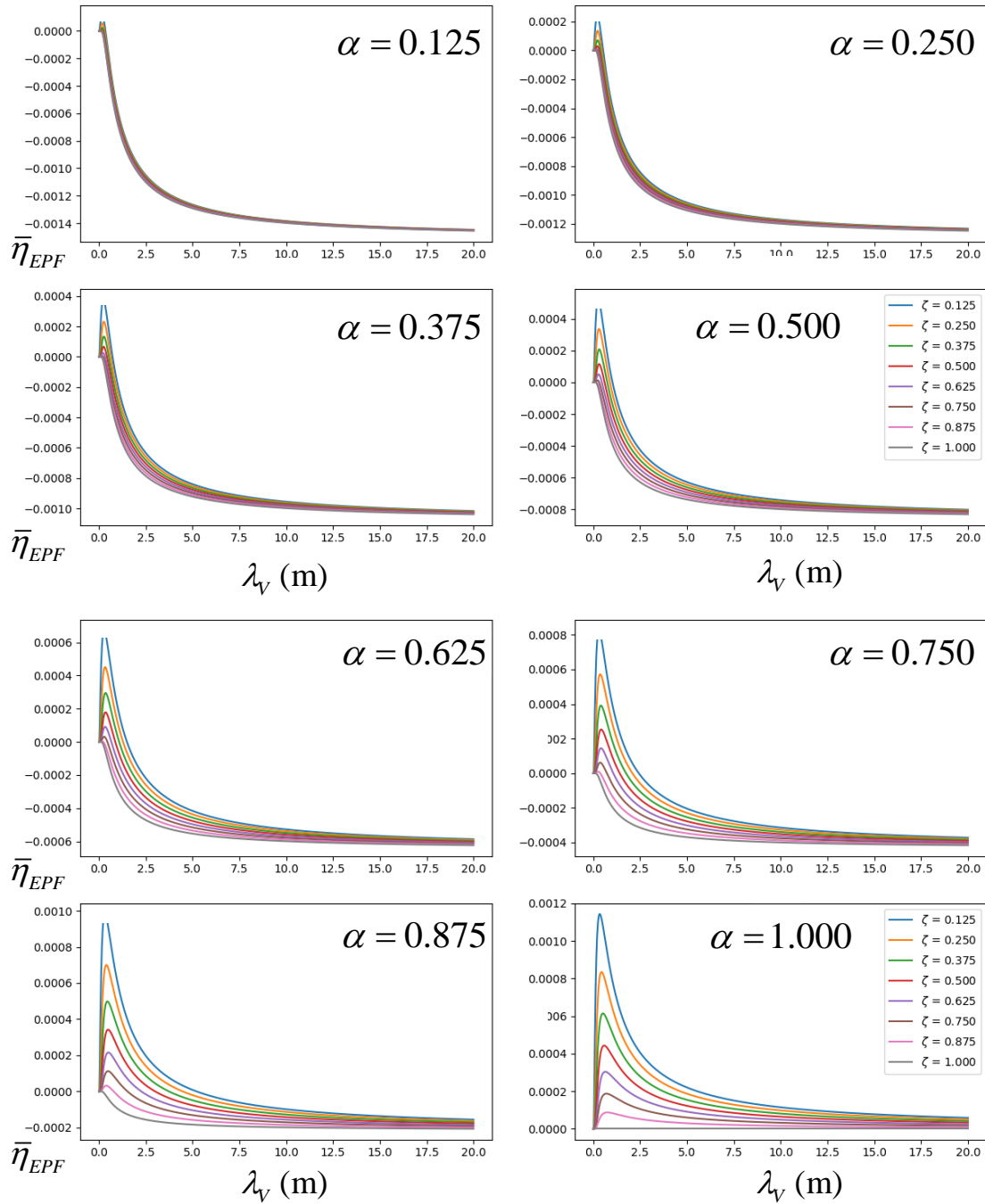


Fig. 3.6. Reduced Eötvös parameter for the Eötvös experiment for various values of α_1 , ζ_1 , and λ_V .

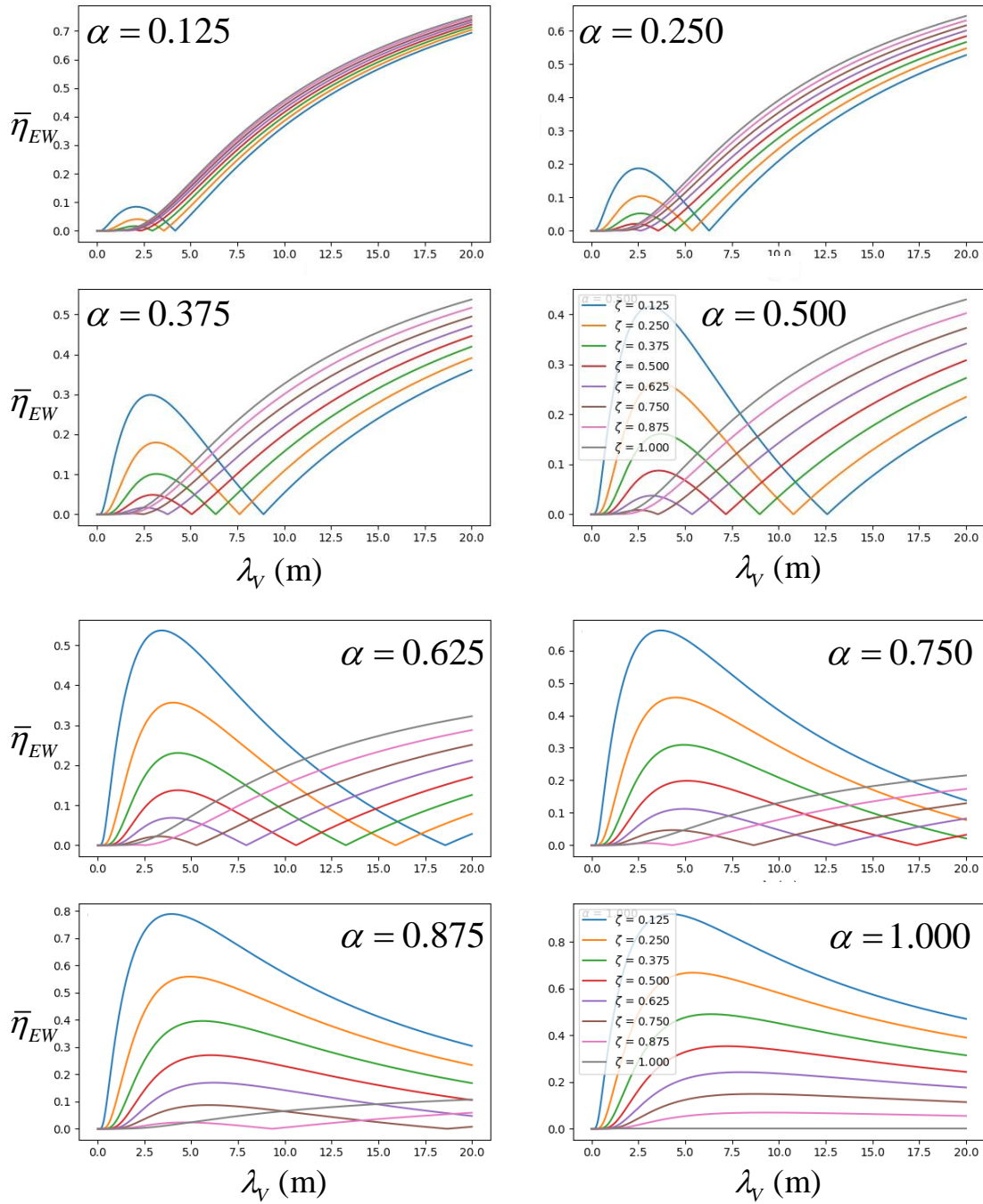


Fig. 3.7. Reduced Eöt-Wash parameter for the Eöt-Wash experiment for various values of α_1 , ζ_1 , and λ_V .

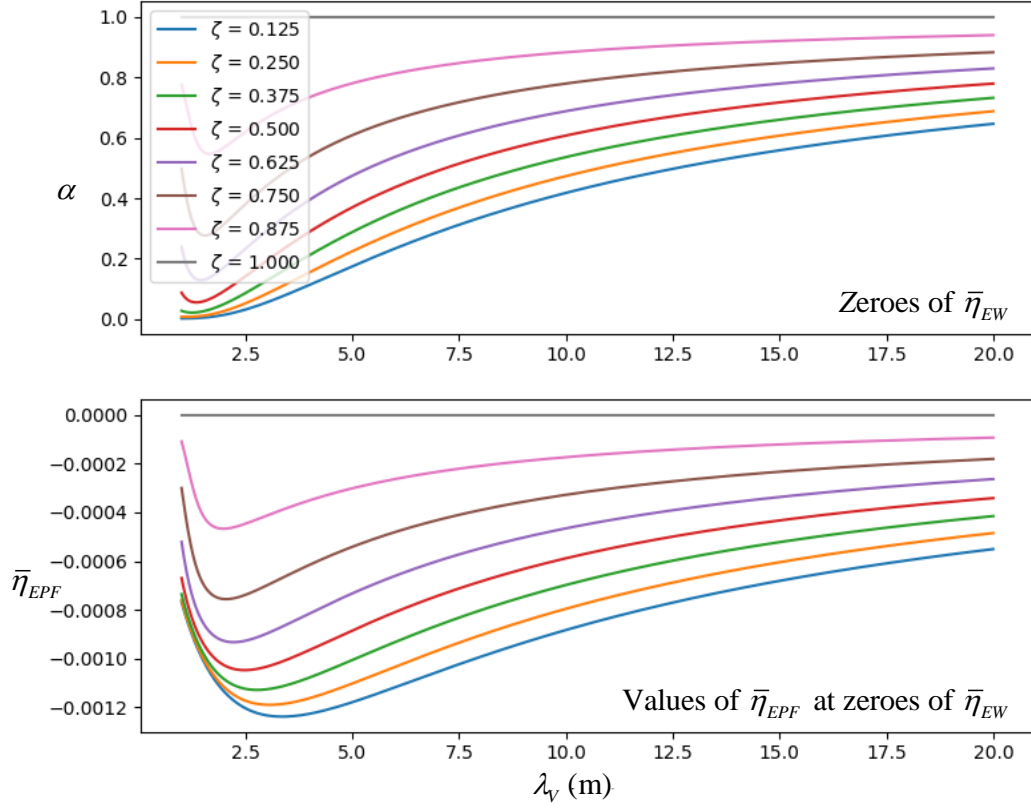


Fig. 3.8. The top plot shows zeros of $\bar{\eta}_{EW}$. The bottom plot shows the values of $\bar{\eta}_{EPF}$ at the zeros of $\bar{\eta}_{EW}$.

3.3.2 Case 2: $\bar{\xi}_S > \bar{\xi}_V$, $\lambda_V > \lambda_S$

We now write the positivity conditions as

$$\frac{\bar{\xi}_V}{\bar{\xi}_S} \leq 1, \quad (3.98)$$

$$\frac{\lambda_S}{\lambda_V} \leq 1_{text}. \quad (3.99)$$

We introduce parameters $\alpha_2 = \bar{\xi}_V/\bar{\xi}_S$ and $\zeta_s = \lambda_S\lambda_V$ which are bounded between zero and unity.

We can then write the relevant phenomenological coefficients from Eq. (3.1) as

$$f_{5x} = -\frac{3}{2}g_N q_{\oplus} \bar{\xi}_S (\alpha_2 e^{-x\zeta_2/\lambda_S} - e^{-x/\lambda_S}), \quad (3.100)$$

$$f_{5z} = -\frac{3}{2}g_N q_{\oplus} \bar{\xi}_S (\alpha_2 e^{-z\zeta_2/\lambda_S} - e^{-z/\lambda_S}), \quad (3.101)$$

$$d_{5zz} = \frac{3}{2}g_N q_{\oplus} \frac{\bar{\xi}_S}{\lambda_S} (\alpha_2 \zeta_2 e^{-z\zeta_2/\lambda_S} - e^{-z/\lambda_S}). \quad (3.102)$$

The Eötvös parameters in the EPF and E-W experiments are then given by

$$\begin{aligned} \frac{\eta_{EPF}}{\frac{3}{2}\Delta q q_{\oplus} \bar{\xi}_S} &= \bar{\eta}_{EPF} = -s_{\beta} [\alpha_2 e^{-z_{EPF}\zeta_2/\lambda_S} - e^{-z_{EPF}/\lambda_S}] \\ &\quad + s_{\beta} \frac{h}{\lambda_S} [\alpha_2 \zeta_2 e^{-z_{EPF}\zeta_2/\lambda_S} - e^{-z_{EPF}/\lambda_S}], \end{aligned} \quad (3.103)$$

$$\begin{aligned} \frac{\eta_{EW}}{\frac{3}{2}\Delta q q_{\oplus} \bar{\xi}_S} &= \bar{\eta}_{EW} = \sqrt{2} \left| -(\alpha_2 e^{-x_{EW}\zeta_2/\lambda_S} - e^{-x_{EW}/\lambda_S}) \right. \\ &\quad \left. - s_{\beta} (\alpha_2 e^{-z_{EW}\zeta_2/\lambda_S} - e^{-z_{EW}/\lambda_S}) \right|. \end{aligned} \quad (3.104)$$

We notice that $\bar{\eta}_{EW}$ will be unchanged due to the absolute value, while $\bar{\eta}_{EPF}$ will change sign. These conclusions are supported by Figures 3.9 and 3.10.

We once again search for the zeros of $\bar{\eta}_{EW}$, given by Eq. (3.105). The results are shown in Figure 3.11 and we obtain the same result, but with $\bar{\eta}_{EPF}$ having the opposite sign

$$\alpha_2 = \frac{e^{-x_{EW}/\lambda_S} + s_{\beta} e^{-z_{EW}/\lambda_S}}{e^{-x_{EW}\zeta_2/\lambda_S} + s_{\beta} e^{-z_{EW}\zeta_2/\lambda_S}}. \quad (3.105)$$

3.4 Discussion

We conclude this chapter with an estimate of ξ_S . We choose Case 2 since that will give us the positive $\bar{\eta}_{EW}$. From Figure 3.11, we select, $\zeta_2 = 0.5$, $\lambda_S = 2.5\text{m}$, which gives $\alpha_2 = 0.2$ and $\bar{\eta}_{EPF} = 10^{-3}$. We also note that $\eta_{EPF} = \Delta\kappa s_{\beta} \approx 10^{-9}$ [7]. Then we can write ξ_S as

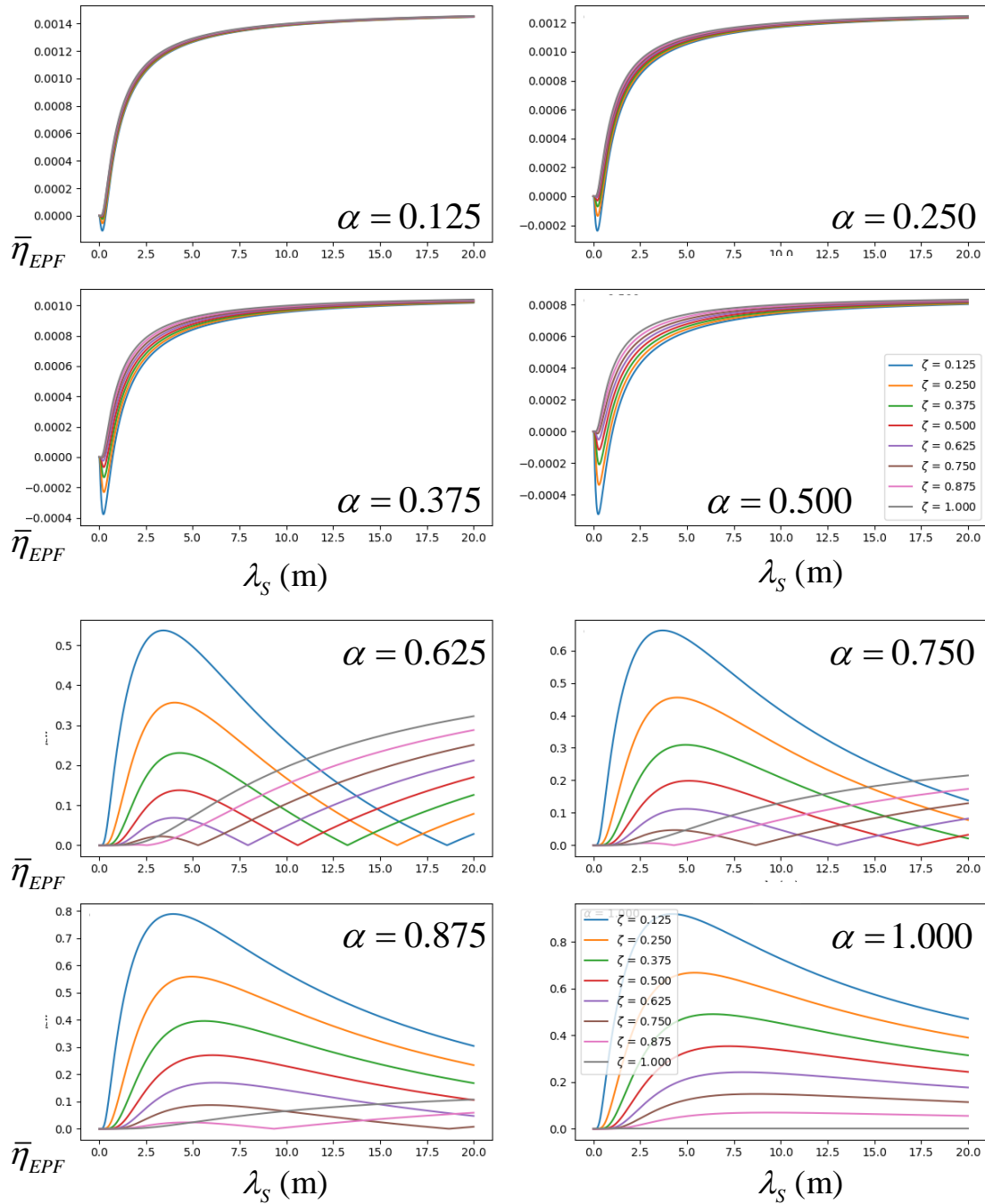


Fig. 3.9. Reduced Eötvös parameter for the Eötvös experiment for various values of α_2 , ζ_2 , and λ_S .

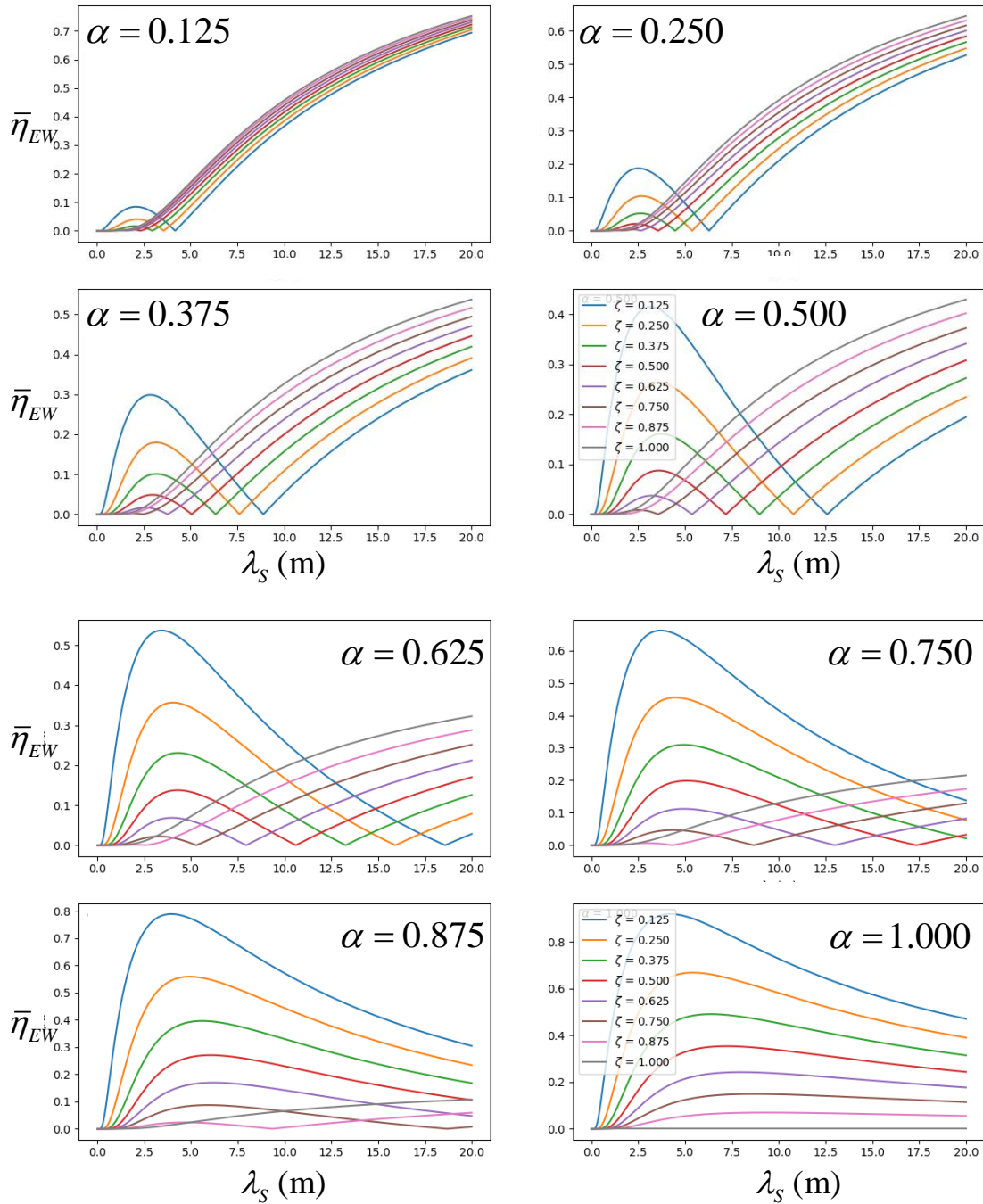


Fig. 3.10. Reduced Eötvös parameter for the Eöt-Wash experiment for various values of α_2 , ζ_2 , and λ_S .

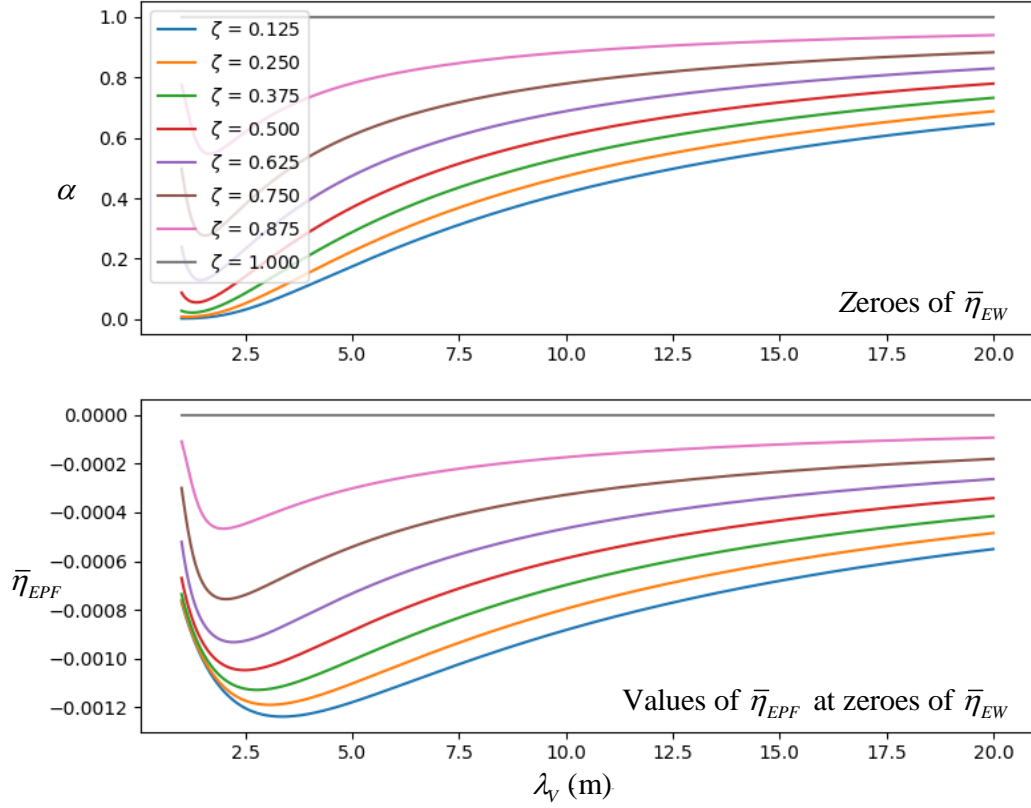


Fig. 3.11. The top plot shows zeros of η_{EW} for Case 2. The bottom plot shows value of $\bar{\eta}_{EPF}$ at the zeros of $\bar{\eta}_{EW}$.

$$\xi_S = \frac{R_{\oplus}}{\lambda_S} \bar{\xi}_S = \frac{\eta_{EPF}}{\frac{3}{2} \Delta q q_{\oplus} \bar{\eta}_{EPF}} \frac{R_{\oplus}}{\lambda_S} \quad (3.106)$$

$$\begin{aligned} \xi_V &= \frac{R_{\oplus}}{\lambda_V} \bar{\xi}_V = \frac{R_{\oplus}}{\lambda_V} \alpha_2 \bar{\xi}_S = \frac{\lambda_S}{\lambda_V} \alpha_2 \xi_S = \alpha_2 \zeta_2 \xi_S \\ &= \alpha_2 \zeta_2 \frac{\eta_{EPF}}{\frac{3}{2} \Delta q q_{\oplus} \bar{\eta}_{EPF}} \frac{R_{\oplus}}{\lambda_S} \end{aligned} \quad (3.107)$$

From [7], $\Delta q \approx 10^{-3}$ and $q_{\oplus} \approx 1$. We also note $R_{\oplus} = 6 \times 10^6$ m. Then we find

$$\xi_S = 1600$$
$$\xi_V = 160$$

Solving for the coupling constant $f_{S,V}^2 = \xi_{S,V} G m_H^2$

$$f_S^2 = 2.98 \times 10^{-55} \text{ Jm} = 9.42 \times 10^{-30} \hbar c$$
$$f_V^2 = 2.98 \times 10^{-56} \text{ Jm} = 9.42 \times 10^{-31} \hbar c$$

4. FIFTH FORCES IN THE MICROSCOPE EXPERIMENT

4.1 The MICROSCOPE Satellite

The MICROSCOPE spacecraft is a special type of spacecraft known as a "drag-free" spacecraft. Normally, spacecraft are subject to a variety of nongravitational perturbations, include residual atmospheric drag, solar radiation pressure, and pressure due to solar wind. Certain applications require a satellite to follow a purely gravitational path, so the perturbations must be canceled out.

A second special feature of the MICROSCOPE satellite it's special orbit known as a sun synchronous orbit. A sun synchronous orbit is one that passes over a specific part of the planet at the same time every day. Normally, a spacecraft orbit about the Earth remains fixed in space, so as the Earth orbits the Sun, the spacecraft's ground track moves. A sun-synchronous orbit is a near polar orbit that takes advantage of the Earth's oblateness to perturb the orbital plane. By tuning the altitude and inclination of the orbit, the perturbation can be set to $360^\circ/yr$. Thus, if the satellite orbital plane is initially perpendicular to the Earth-Sun vector, it will precess approximately one degree per day and remain perpendicular to the Earth-Sun vector. The sun synchronous orbit keeps the solar perturbation in a constant location and it ensures that the spacecraft is continuously illuminated by the Sun, eliminating heating effects from the experiment.

4.2 Dynamics of Drag-Free Satellites

A drag-free satellite contains a second mass called a test mass located inside the main spacecraft. This mass is ideally freely floating, but usually the test mass is

lightly coupled to eliminate electrostatic effects. The perturbations described above are all surface effects, so the test mass is shielded from these forces by the body of the main spacecraft. Thus the test mass will follow a purely gravitational path. Hence, it is simply a matter of keeping the spacecraft centered on top of test mass, and the satellite will follow a gravitational path as well. Centering the spacecraft is accomplished by measuring the position of the test mass relative to the spacecraft and using this measurement as feedback to control the spacecraft thrusters. A schematic of the drag-free satellite is shown in Fig. 4.1

The MICROSCOPE satellite differs from a typical drag-free satellite is that MICROSCOPE has two test masses, not one. Only one mass is necessary to compensate for drag; with two masses of different materials, we can not only compensate for drag, but also search for composition dependent effects.

The dynamics of the satellite (subscript sat) and the test masses (subscript i) are given by

$$m_{I,sat}\vec{a}_{sat} = m_{G,sat}\vec{g}_N[\vec{r}_{sat}] - \sum_i \vec{F}_{c,i} + \vec{F}_{drag} + \vec{F}_{con} + \xi m_{I,sat} q_{sat} q_0 \vec{\mathcal{F}}_5(\vec{r}_{sat}), \quad (4.1)$$

$$m_{I,i}\vec{a}_i = m_{I,i}(\vec{a}_{i,sat} + \vec{a}_{sat}) = m_{G,i}\vec{g}_N[\vec{r}_i] + \vec{F}_{c,i} + \xi m_{I,i} q_i q_0 \vec{\mathcal{F}}_5(\vec{r}_i), \quad (4.2)$$

where \vec{r}_k (\vec{a}_k), $k = sat, 1, 2$ is the position (acceleration) vector of the satellite or test mass, $\vec{a}_{i,sat}$ is the acceleration of mass i relative to the satellite, $\vec{F}_{c,i}$ are couplings between the satellite and the i th test mass, \vec{F}_{drag} is the drag force on the satellite, \vec{F}_{con} is the control (thruster) force, $\xi m_{I,k} q_k q_0 \vec{\mathcal{F}}_5$ is the fifth force acceleration acting on the k th object due to source q_0 , and $\vec{g}[\vec{r}]$ is the gravitational force acting at location \vec{r} . We can make $\vec{g}[\vec{r}]$ as precise as we desire by going beyond the point particle approximation by including higher harmonics of the Earth's field. At a minimum we need to include the J_2 term to reproduce the sun synchronous orbit of the MICROSCOPE spacecraft. The minimally precise gravitational field is then

$$\vec{g}(\vec{r}) = -\frac{GM}{r^3}\vec{r} + \vec{g}_{J_2}(\vec{r}), \quad (4.3)$$

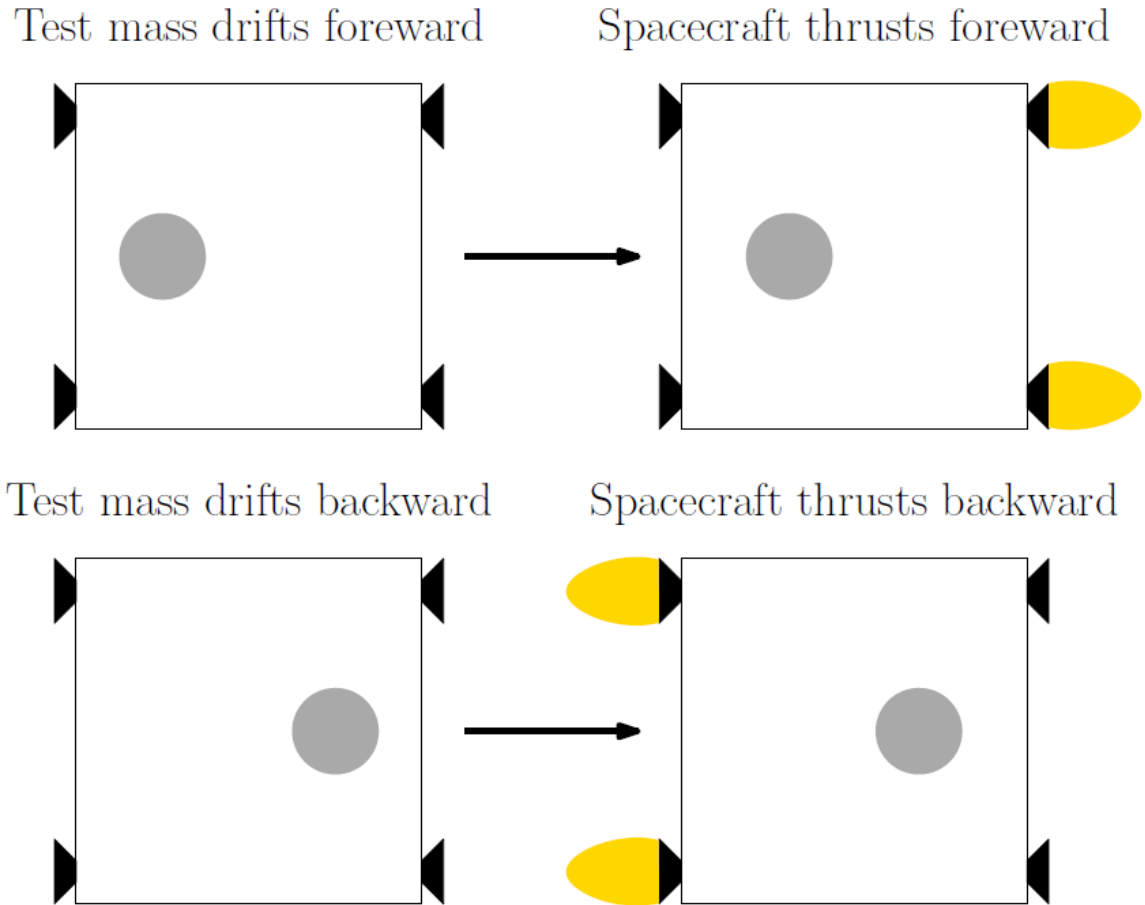


Fig. 4.1. A one-dimensional schematic of a drag free satellite. If the test mass moves forward relative to the spacecraft, the aft thrusters fire, accelerating the spacecraft. If the test mass moves after relative to the spacecraft, the froward thrusters fire, decelerating the spacecraft. This process generalizes to three dimensions

where, in inertial coordinates with $\vec{r} = x\hat{I} + y\hat{J} + z\hat{K}$,

$$\begin{aligned}
 g_{J_2,x} &= J_2 \frac{x}{r^7} \left[6z^2 - \frac{3}{2}(x^2 + y^2) \right], \\
 g_{J_2,y} &= J_2 \frac{y}{r^7} \left[6z^2 - \frac{3}{2}(x^2 + y^2) \right], \\
 g_{J_2,z} &= J_2 \frac{z}{r^7} \left[3z^2 - \frac{9}{2}(x^2 + y^2) \right].
 \end{aligned} \tag{4.4}$$

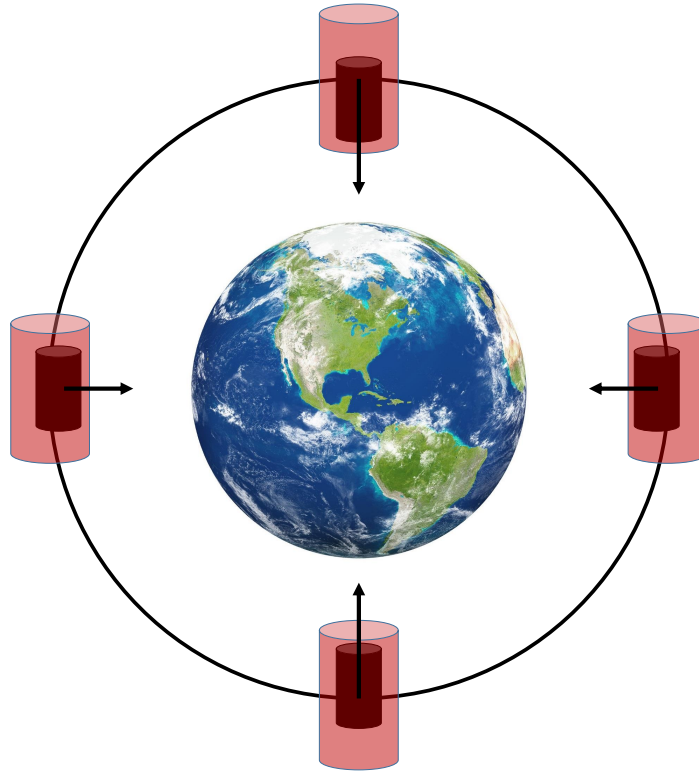


Fig. 4.2. The two test masses for the MICROSCOPE satellite with fixed orientation. The two masses drift due to a composition dependent force or a WEP violation.

The test masses on the MICROSCOPE satellite consist of two concentric cylinders of different radii. Each cylinder has a set of electrodes with corresponding electrodes on the accelerometer housing. As the spacecraft orbits the Earth, any composition dependent force (or gravity gradients) will cause the two cylinders to move relative to each other, as shown in Fig. 4.2. As the cylinders move, the electrodes measure a change in capacitance. This change is fed back into the electrodes to pull the mass back into place. The feedback signals for the two cylinders are then averaged and fed into the thruster controller for drag compensation, and the difference of the two signals may show composition dependent forces.

The force that is needed to reset the masses can be found by rearranging Eq. (4.2). Using body-fixed coordinates, the test mass acceleration can be written as

$$\vec{a}_{i,sat} = \ddot{\vec{r}}_{i,sat} + \dot{\vec{\omega}}_i \times \vec{r}_{i,sat} + 2\vec{\omega}_i \times \dot{\vec{r}}_{i,sat} + \vec{\omega}_i \times \vec{\omega}_i \times \vec{r}_{i,sat}, \quad (4.5)$$

where $\vec{\omega}_i$ is the angular velocity vector of the test mass relative to the inertial frame.

The coupling term, $\vec{F}_{c,i}$ is the coupling term and represents the electrodes that are used to measure the position of the test masses and drive them back to their zero positions. The amount of force exerted by the electrodes then represents the amount of force acting on the test mass at a given moment. Solving for the coupling term and dropping terms involving derivatives of $\vec{r}_{i,sat}$, we find

$$\begin{aligned} \vec{a}_{c,i} &= \frac{\vec{F}_{c,i}}{m_{I,i}} = \dot{\vec{\omega}}_i \times \vec{r}_{i,sat} + \vec{\omega}_i \times \vec{\omega}_i \times \vec{r}_{i,sat} + \vec{a}_{sat} \\ &\quad - \frac{m_{G,i}}{m_{I,i}} \vec{g}_N(\vec{r}_i) - \xi q_i q_0 \vec{\mathcal{F}}_5(\vec{r}_i). \end{aligned} \quad (4.6)$$

Finally, we can take the difference of $\vec{a}_{coup,i}$ in Eq. (4.6) for two different materials, leading to final signal

$$\begin{aligned} \vec{\Gamma}_{signal} &= \frac{\Delta \vec{a}_{c,i}}{2} = \frac{\kappa_2 - \kappa_1}{2} \vec{g}(\vec{r}_{sat}) + \frac{1}{2} (T(\Delta \vec{r}_{tm,sat}) - I(\Delta \vec{r}_{tm,sat})) \\ &\quad + \frac{q_2 - q_1}{2} \vec{a}_{dist}(\vec{r}_{sat}), \end{aligned} \quad (4.7)$$

$$T(\Delta \vec{r}_{tm,sat}) = \vec{g}(\vec{r}_{sat} + \vec{r}_{tm1,sat}) - \vec{g}(\vec{r}_{sat} + \vec{r}_{tm2,sat}), \quad (4.8)$$

where $I(\Delta \vec{r}_{tm,sat})$ is the inertial tensor made from the cross products of the angular velocities and accelerations of the test masses.

We can see that our signal contains three contributions: the first is the explicit equivalence principle violating term, the second is due to gravitational and inertial forces and a mismatch of the test mass positions, and the third is due to our assumed composition-dependent force acting on the test masses. If we drop the third term, our signal matches the signal obtained in Eq. (7) of Ref. [18].

4.3 Data Analysis

Now that we have characterized the signal that would be seen by the MICROSCOPE satellite due to an explicit WEP violation and a generic fifth force, we need to consider the data analysis. The satellite's orbit and spin produces a periodic signal, so it is natural to focus on the power spectrum density (PSD) of the signal. Then, the different frequencies present in the signal will appear as peaks in the PSD. Hence, we must first determine which frequencies are predicted in our models of the forces, and whether they are present in the MICROSCOPE data. As the WEP term is a gravitational monopole, it will appear at a frequency of $(f_{orbit} - f_{rot})$, while the gravity gradient term is a dipole term and will appear at $2(f_{orbit} - f_{rot})$.

Since the PSD is a linear process, any scalar multiplying our function will simply pass through the PSD,

$$\text{PSD}(\Delta\vec{a}) = \xi\Delta q q_0\text{PSD}(\vec{\mathcal{F}}_5). \quad (4.9)$$

Here, $\text{PSD}(\Delta\vec{a})$ are the data from the MICROSCOPE analysis (in units of $\text{m/s}^2/\text{Hz}^{1/2}$), $\text{PSD}(\vec{\mathcal{F}}_5)$ (in units of $\text{m/s}^2/\text{Hz}^{1/2}$) can be determined from prior analysis, Δq is a known property of the test masses, and q_0 can be estimated for the source. The unknown parameter, ξ can then be determined via a linear fit. We first consider the time dependence of \mathcal{F}_5 . Then, we take the PSD of \mathcal{F}_5 and note the frequency and the height of the peaks of the PSD. We then examine the same frequencies in the published MICROSCOPE data, noting the peak heights there as well. We now have a set of data points $(\text{PSD}(\Delta\vec{a})_1, \text{PSD}(\mathcal{F}_5)_1), (\text{PSD}(\Delta\vec{a})_2, \text{PSD}(\mathcal{F}_5)_2), \dots$ and can perform a linear fit $y = mx + b$ where $y_i = \text{PSD}(\Delta\vec{a})_i$, $x_i = \text{PSD}(\mathcal{F}_5)_i$, the slope, a , is $\xi\Delta q q_0$ and the intersection, b is nominally zero. As an example consider Fig. 4.3 from Ref. [37].

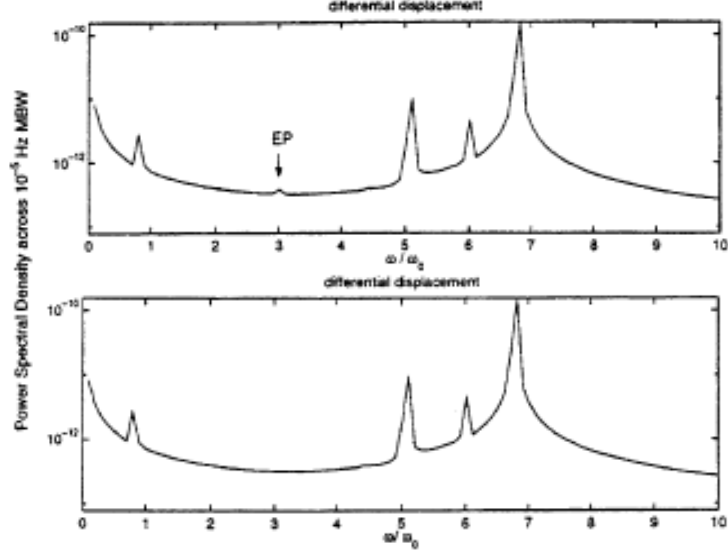


Fig. 4.3. Simulated result of the differential acceleration of the STEP Experiment [17]. The top plot shows the signal with the WEP violation due to $\Delta\kappa$ and the bottom plot lacks a WEP violation. The difference is the slight peak at $\omega/\omega_0 = 3$. The remaining peaks are due to the orbit, gravity gradients, and effective spring constants. [17]. To test for WEP violation, we would look for the peak at $3\omega_0$.

This method assumes a single scalar parameter multiplying $\mathcal{F}_5(\vec{r})$, but we can generalize to parameter dependent forces $\mathcal{F}_5(\vec{r}, \beta_i)$, such as Yukawa forces or power law forces,

$$\vec{\mathcal{F}}(\vec{r}; \beta) = \frac{\hat{r}}{r^2} \exp(-\beta r) (1 + \beta r), \quad (4.10)$$

$$\vec{\mathcal{F}}(\vec{r}; \beta) = r^\beta, \quad (4.11)$$

respectively. Here, we simply tabulate $\xi\Delta q q_0$ versus β .

4.4 Drag Due to Background Particles

We consider here a force arising from the passage of the MICROSCOPE spacecraft through background field. The test masses interact with the background field through a short range force with scattering cross section σ_{BB} . The force acting on the test

mass can be computed knowing the number of scattering events per unit time, Γ , multiplied the change in momentum per event, Δp ,

$$F_5 = \Gamma_{BB}\Delta p. \quad (4.12)$$

The number of events is given by the flux times the cross section ($\Gamma_{BB} = \Phi_{BB}\sigma$) and the flux is given by the number density times velocity ($\Phi_{BB} = n_{BB}v$). We assume maximum momentum transfer, so that $\Delta p = 2m_{BB}v$. The force is then given by (introducing the mass density $\rho_{BB} = n_{BB}m_{BB}$),

$$F_5 = 2\sigma_{BB}\rho_{BB}V^2. \quad (4.13)$$

This is the force on a single nucleon, and if we assume the coupling with the background field is identical for protons and neutrons, then the force on an atom introduces a factor of baryon number, B . This force also opposes the direction of motion, so the full, vector form of the force is

$$\begin{aligned} \vec{F}_{5,i} &= -2B_i\sigma_{BB}\rho_{BB}v_i\vec{v}_i \\ &= -2m_{I,i}q_i\sigma_{BB}\frac{\rho_{BB}}{m_H}v_i\vec{v}_i \\ &= -2m_{I,i}q_i\sigma_{BB}\frac{\rho_{BB}}{m_H}\ell^*\frac{v_i\vec{v}_i}{\ell^*} \\ &= -m_{I,i}q_iC_5\vec{\mathcal{F}}(\vec{r}, \vec{v}, t). \end{aligned} \quad (4.14)$$

In the last line, we have introduced a constant C_5 ,

$$C_5 = 2\sigma_{BB}\ell^*\rho_{BB}/m_H, \quad (4.15)$$

and the characteristic length, ℓ^* , to make C_5 dimensionless and give $\vec{\mathcal{F}}$ the units of acceleration. As expected, the force has the form of drag. The velocity, \vec{v}_i , is the velocity of the test mass relative to a background particle field. We consider a two possibilities: the background is stationary and non-rotating relative to the galaxy, and the background co-rotates with the galaxy. The velocity of the i th test mass relative to the sun or the galaxy can be broken up into multiple pieces

$$\vec{V}_{i,Sun} = \vec{V}_{i,sat} + \vec{V}_{sat,Earth} + \vec{V}_{Earth,Sun}, \quad (4.16)$$

$$\vec{V}_{i,gal} = \vec{V}_{i,Sun} + \vec{V}_{Sun,gal}. \quad (4.17)$$

The first term, $\vec{v}_{i,sat}$ is the velocity of the i th test mass relative to the satellite. This number is extremely small and will be neglected. The second term, $\vec{v}_{sat,Earth}$, is the velocity of the satellite relative to the Earth, i.e., the orbital velocity of the satellite. The third term, $\vec{v}_{Earth,Sun}$ is the orbital velocity of the Earth about the Sun. The final term, $\vec{v}_{Sun,gal}$, is the velocity of the Sun relative to the center of the galaxy. This term is needed if we are considering motion through a background that does not rotate relative to the galaxy, which we assume. (If the background does rotate with the galaxy, this term is unnecessary). The components of the velocity are derived in detail in Appendix B, and the total velocity is given in terms of orbital elements and angular velocities as shown in equation (B.14).

4.5 Comparison with MICROSCOPE

4.5.1 Orbital Elements

In Appendix B, we exhibit the functional form of the velocities, but we also need to find the actual values of the parameters. The velocity of the Sun through the galaxy can be taken as a constant in the Earth-Centered Inertial (ECI) frame. For the Earth, we have a set of orbital elements and their derivatives at the J2000 epoch. We can then update the orbital elements using the time since J2000, and we can then find the true anomaly using Kepler's Equation.

We need the orbital elements for the spacecraft. We know that the desired orbit is circular with a frequency of 0.16818×10^{-3} Hz [37]. Using this frequency, we compute the semimajor axis of the spacecraft to be 700 km. Since the eccentricity of the orbit is zero, the argument of periapsis is ill-defined, so we can simply set it to zero. Since we will be propagating the system over several orbits, the initial phase of the spacecraft is not important either, so we can set the initial true anomaly to zero. We are now left with determining the initial longitude of the ascending node and inclination, which we can estimate by using the fact that the spacecraft is in a Sun-synchronous orbit. To maintain consistent solar heating, we assume that we want the orbit to

be roughly perpendicular to the Earth-Sun line; this ensures that the spacecraft will never pass into the Earth's shadow. Therefore, we find the unit vector pointing from the Sun to the Earth. Rotating into the ECI frame, this vector becomes the angular momentum unit vector for the satellite orbit, allowing us to determine the longitude of the ascending node. To find the initial inclination, we note that including the J_2 term in the gravitational force causes a precession of the orbital plane (change in the longitude of the ascending node) equal which (for a circular orbit) is given by

$$\dot{\Omega} = -\frac{3J_2 \cos i}{2a^{7/2}(GM)^{1/2}}. \quad (4.18)$$

Hence, if we know both the semimajor axis ($a \approx 7000$ km), and also the desired rate of change of the ascending node (360deg/year), we can find the required inclination ($i \approx 98$ deg). With this, we have a full set of orbital elements; to update the position and velocity of the spacecraft, we update the true anomaly using Kepler's Equation and increase the longitude of the ascending node linearly.

4.5.2 Results and Discussion

The expected PSDs for our background particle field are shown in Figures 4.4 and 4.5. The spacecraft has an orbital frequency of 0.16818×10^{-3} Hz and the spacecraft rotational frequency was 2.0432×10^{-3} Hz and 0.5885×10^{-3} Hz, respectively, for the two tests.

In Figure 4.4, the background field is fixed to the center of the galaxy and non-rotation, so the velocity used in the PSD was given by Eq. (4.17). The left hand plot has rotation frequency 2.0432×10^{-3} Hz and the right has 0.5885×10^{-3} Hz. We have denoted the expected WEP violation as the red vertical line and the gravity gradient line (at twice the WEP violation). In the right-hand plot, we see a number of peaks about the central peak. The primary component of the velocity is the Sun relative to the galaxy, which is constant in the inertial frame I-J-K. Hence, the solar velocity enters at the satellite rotation rate, which we see. As our signal is proportional to v^2 , we obtain significant mixing among the frequencies of the various orbits. These

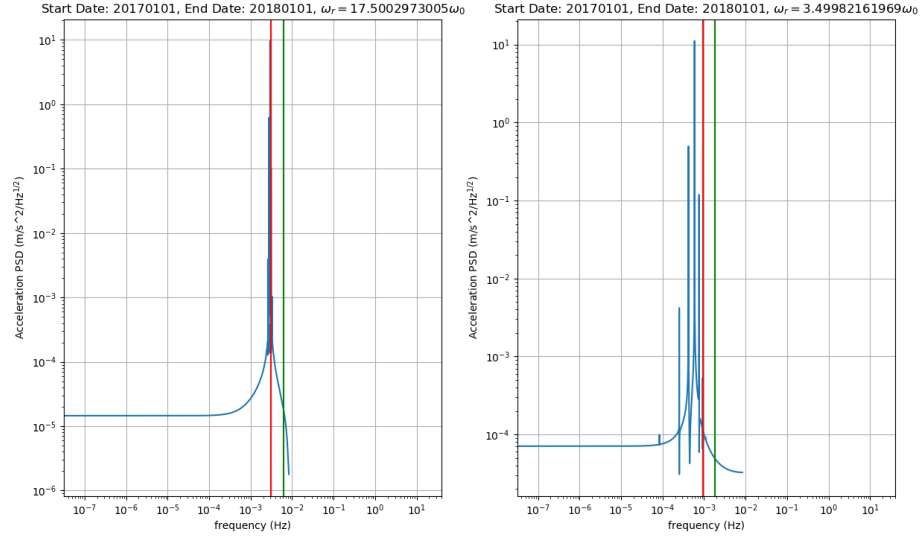


Fig. 4.4. The expected results for background particles fixed relative to the galaxy. The left plot has satellite spin rate of 2.0432×10^{-3} Hz and the plot on the right has a spin rate of 0.5885×10^{-3} Hz, as in Figure 4.6. The red and green lines show the locations of a WEP violation and gravity gradient, respectively.

frequencies (along with higher harmonics) are represented by peaks to either side of the central peak.

At first glance, it may seem that the left hand plot only contains one peak, but if we look more closely, we can make out the other peaks on either side of the central peak. The high rotation rate during this test drowns out most of the other frequencies involved. As we stated before, to find our constant C_5 we compare the amplitude of the peaks in our plot to the amplitude at the same frequency in Figure 4.6. However, we do not see any peak around at $\sim 2 \times 10^{-3}$ for the left and $(2 - 6) \times 10^{-4}$ for the right plot in Figure 4.6. We conclude that if our signal is present its amplitude must be less than the amplitude of the noise $\sim 10^{-10} \text{m/s}^2/\text{H}^{1/2}$ Comparing to the peak height in Figure 4.4 gives

$$\boxed{C_5 < 10^{-10}}. \quad (4.19)$$

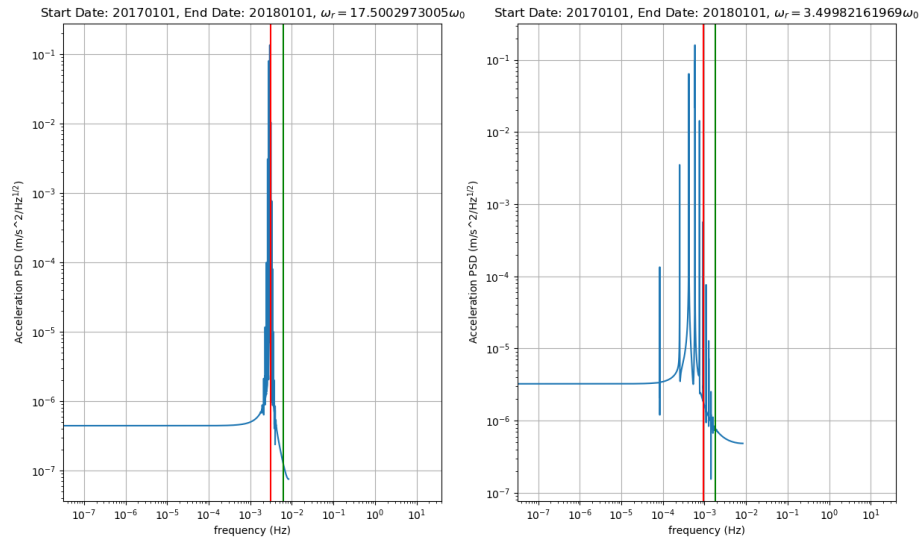


Fig. 4.5. The expected results for background particles that rotate with the galaxy. The left plot has satellite spin rate of 2.0432×10^{-3} Hz and the plot on the right has a spin rate of 0.5885×10^{-3} Hz, as in Figure 4.6. The red and green lines show the locations of a WEP violation and gravity gradient, respectively.

We repeat the analysis for Figure 4.5 where the background particle field co-rotates with the galaxy. We see similar results between Figure 4.5 and Figure 4.5 just with the peaks shifted because we no longer have the large, constant solar velocity in the PSD. Once again, we conclude that since our peaks do not exceed the level of the noise, it follows that

$$\boxed{C_5 < 10^{-9}}. \quad (4.20)$$

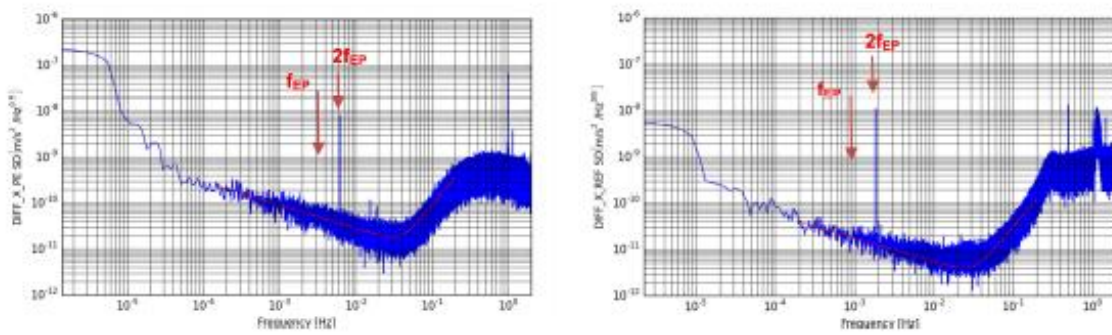


Fig. 4.6. The results from two different runs of the MICROSCOPE Experiment [37]. The left plot has satellite spin rate of 2.0432×10^{-3} Hz, the plot on the right has a spin rate of 0.5885×10^{-3} Hz, and both plots have an orbital frequency of 0.16818×10^{-3} Hz. The frequency of an expected WEP violation is f_{EP} . The gravity gradient signal is located at $2f_{EP}$. Note the lack of peak at f_{EP} , indicating no WEP violation (to the level of the noise).

5. TIME-VARYING NUCLEAR DECAY RATES: REVIEW OF PAST EXPERIMENTS

We begin by introducing some notation. We are interested in considering the possibility that some decay rates may oscillate with the distance from the Sun. To study this possibility parameterize the decay rate in the form

$$\Gamma(t) = \Gamma_0 \left\{ 1 + \xi \left[\frac{R_0}{R(t)} \right]^2 \right\}, \quad (5.1)$$

where $R(t)$ is the distance from the Sun, R_0 is the reference distance (usually taken to be 1 AU), ξ characterizes the time-dependence of the perturbation, and Γ_0 is the contribution to a β -decay rate from the weak interaction, and from time-independent perturbations. The standard value of the decay rates, defined when $R(t) = R_0$, is given by,

$$\Gamma_{ave} = \ln 2/t_{1/2} = \Gamma_0(1 + \xi), \quad (5.2)$$

where $t_{1/2}$ is the half-life. We can then write $\Gamma(t)$ (for small ξ) as

$$\Gamma(t) = \Gamma_{ave} \left\{ 1 + \xi \left[\left(\frac{R_0}{R(t)} \right)^2 - 1 \right] \right\}. \quad (5.3)$$

In the following sections, we will review the experimental evidence suggesting correlations between nuclear decay rates and the Earth-Sun distance, by compiling a list of ξ values. It is convenient to consider normalized decay rates, which refer to data where the exponential decay term has been removed. If the decay is purely exponential, the normalized decay rates should be randomly distributed about a normalized decay rate of unity. As we shall see in the discussion following discussion, normalized decay rates occasionally show clear oscillations.

5.1 Falkenberg ^3H

Perhaps the first of these experiments was that of Falkenberg [38]. Between Fall 1980 and Spring 1982, Falkenberg examined the decay of tritium by placing a phosphorescent vessel containing tritium inside a box along with light-sensing diodes. He measured a half-life consistent with the accepted value of 12.33 years, but he also noticed a surprising annual variation of 0.37% in the amplitude of the decay. Convinced that this was not a systematic effect, Falkenberg was the first to suggest that the decays may be influenced (or caused) by neutrinos from the Sun. The Falkenberg data are shown in Figure 5.1.

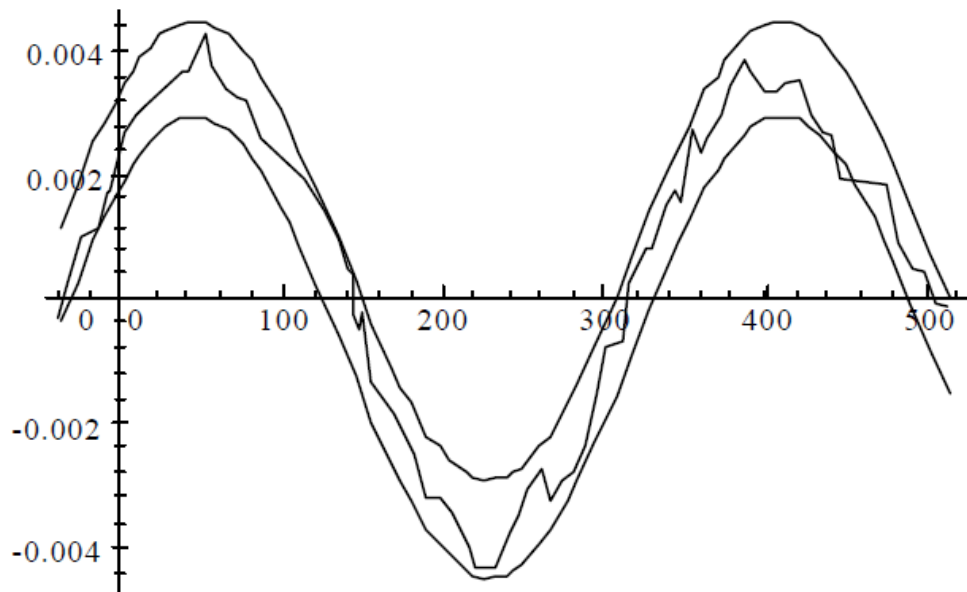


Fig. 5.1. Plot of the data from the Falkenberg experiment along with bounded curve, taken from [38]. The horizontal axis represents days since January 1, 1981. The vertical axis represents the detrended data (exponential removed).

5.2 PTB $^{226}\text{Ra}/^{152}\text{Eu}$

The second experiment was a long term study of the stability of detectors using the decay of ^{152}Eu and ^{154}Eu by Siegert et al. [31] of the Physikalisch-Technische Bundesanstalt (PTB). They measured the decay of the Eu isotopes in a 4π ionization chamber using ^{226}Ra as the comparison sample. The ^{152}Eu data are plotted in Figure 5.2. As the PTB experiment was meant to study the long-term stability of detectors, Siegert et al. attributed the oscillations to a periodic changes in detector efficiency. Jenkins et al. [32] were able to obtain the raw data from the PTB experiment and were able to compare the decay of ^{226}Ra to the Earth-Sun distance to find an amplitude of 3×10^{-3} , and a Pearson correlation coefficient 0.66. The data of Jenkins et al. are shown in Figure 5.3.

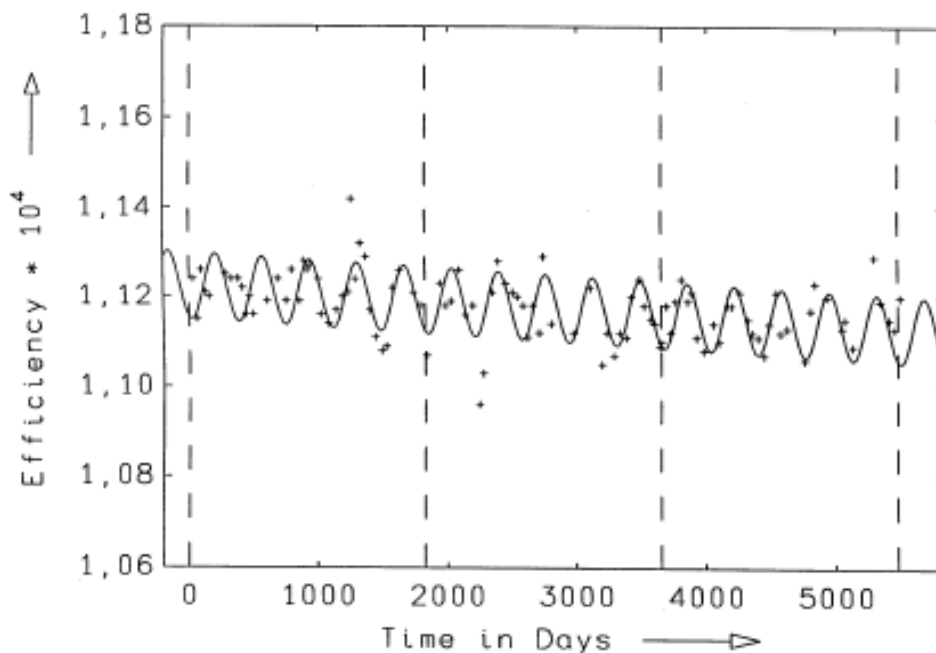


Fig. 5.2. Normalized decay rates of ^{152}Eu from [31]. The vertical dotted lines indicate January 1st every five years. The vertical axis measures the normalized decay rates, but it is presented as a change in the efficiency of the detector. The oscillations have a period of ~ 1 yr and an amplitude of $\sim 10^{-3}$.

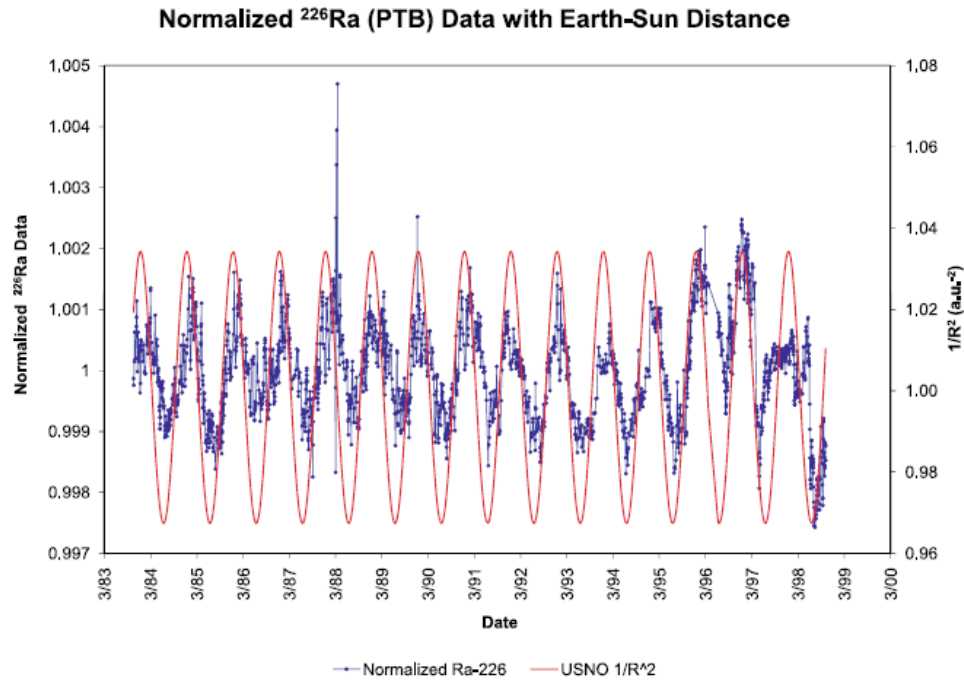


Fig. 5.3. Normalized decay rates of ^{226}Ra and $1/R^2$ plotted versus time. The decay rates are measured relative to the left axis and $1/R^2$ is measured relative to right axis.

5.3 BNL ^{32}Si

The Brookhaven National Laboratory (BNL) experiment was performed by Alburger et al. [30] between 1982 and 1986. The experiment consisted of a ^{32}Si sample and a ^{36}Cl calibration. The samples were measured alternately for 30 minutes apiece using a precision sample changer. Given the long half-life of ^{36}Cl ($t_{1/2} = 301,000$ yr), compared to the expected half-life of ^{32}Si (172 yr), the ^{36}Cl sample was used as a long lived comparison to eliminate systematic effects. Jenkins et al. [32] were able to obtain the raw data from BNL, and performed a fit of the ξ parameter. They found an amplitude of approximately $\xi = 3 \times 10^{-3}$ and a Pearson correlation coefficient between the BNL data and $1/R^2$ of 0.52. The plot of the $^{32}\text{Si}/^{36}\text{Cl}$ and $1/R^2$ data is shown in Figure 5.4.

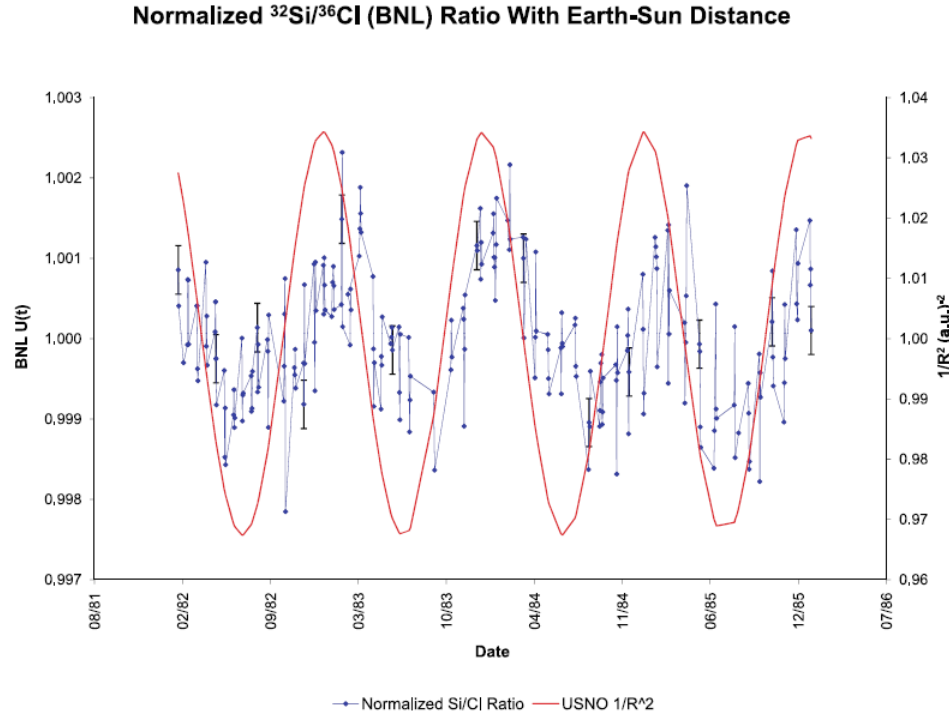


Fig. 5.4. The raw $^{32}\text{Si}/^{36}\text{Cl}$ data from BNL plotted with the $1/R^2$ data (from [32]). The scale for $^{32}\text{Si}/^{36}\text{Cl}$ is given on the left axis while the scale for $1/R^2$ is given on the right axis. We see good qualitative agreement between the two curves.

5.4 Parkhomov $^{60}\text{Co}/^{90}\text{Sr}/^{239}\text{Pu}$

Between 1999 and 2010, Parkhomov [39] measured the decay rates of ^{60}Co , ^{90}Sr , and ^{239}Pu using Geiger-Mueller detectors. The normalized data for the three isotopes are presented in Figure 5.5. Parkhomov found yearly oscillations in ^{60}Co of 2×10^{-3} and in ^{90}Sr of 1.3×10^{-3} . No discernible oscillations were found in the ^{239}Pu , using a silicon detector.

5.5 Purdue ^{54}Mn

Following the analysis of the $^{32}\text{Si}/^{36}\text{Cl}$ data, Purdue began an experiment studying the decay of ^{54}Mn measured by a NaI detector [40]. Data taken between 2008 and

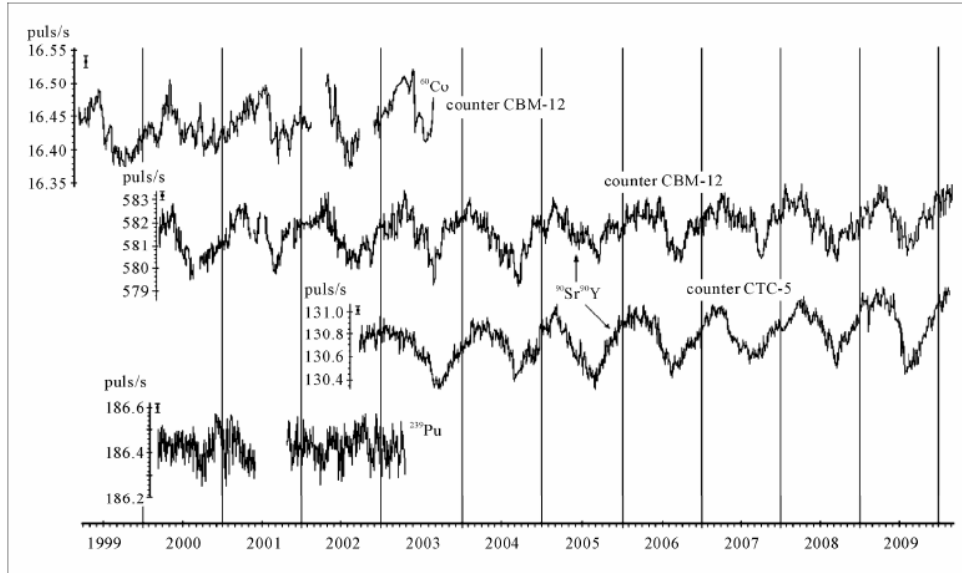


Fig. 5.5. From top to bottom, normalized decay rates of ^{60}Co , ^{90}Sr , and ^{239}Pu from Parkhomov [39].

2012 are shown in Figure 5.6 (unpublished, from [40]). The vertical lines in the plot indicate when the Earth passed through perihelion and aphelion respectively, during the experiment duration. We immediately notice an upward trend in the data which seems to correlate to the average number of sunspots, also shown in the Figure. In addition to the upward trend, we can also see oscillations in the data. These oscillations seem to correlate with the perihelion/aphelion lines, indicating a period of approximately 1 year. The amplitude of these oscillations appears to be approximately 10^{-3} .

5.6 Mercury MESSENGER

The position of a particle in an elliptical orbit is given by

$$r(t) = \frac{a(1 - e^2)}{1 + e \cos(\theta(t))}, \quad (5.4)$$

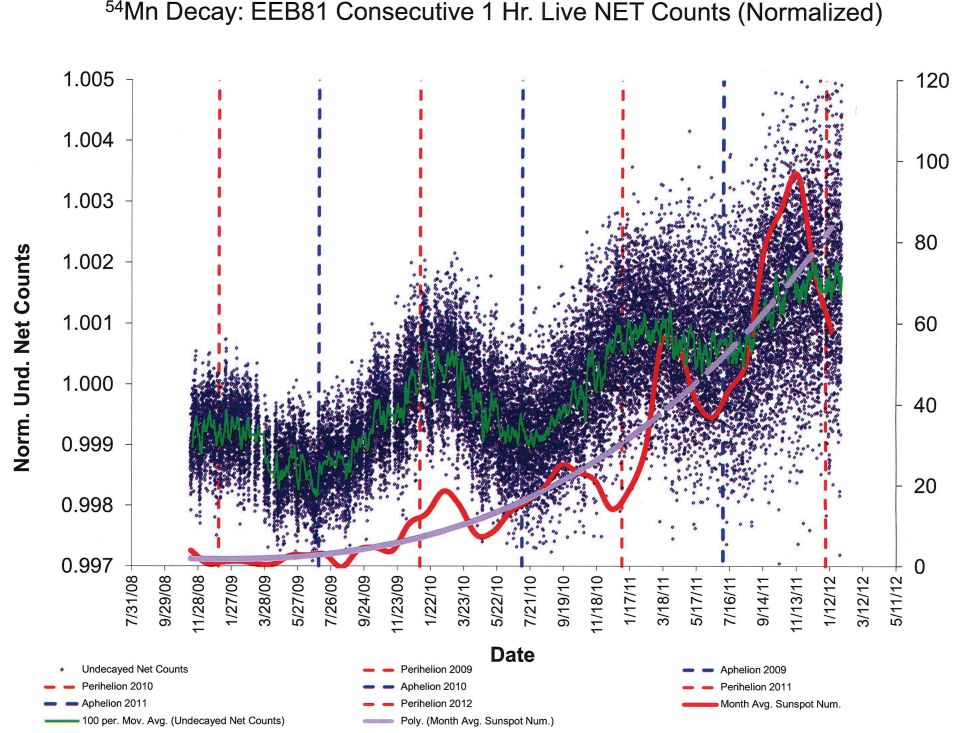


Fig. 5.6. Data from the Purdue ^{54}Mn experiment between 2008 and 2012 (unpublished, from [40]). The vertical lines represent locations of perihelion and aphelion. We see that the data have a general upward trend, which appears to correlate to the upward trend in the number of sunspots during the observation period. In addition to the upward trend, the data appear to oscillate with an estimated period of ~ 1 yr with an amplitude of $\sim 10^{-3}$.

where a is the semi-major axis, e is the eccentricity, and $\theta(t)$ is the true anomaly of the orbit. For small e , $a \approx R_0$ and $\theta(t) \approx 2\pi t/T$ where T is the orbit period. If we substitute Eq. (5.4) into Eq. (5.3) the decay rate becomes

$$\Gamma(t) \approx \Gamma_{ave} \left[1 + 2\xi e \cos\left(\frac{2\pi}{T}t\right) \right]. \quad (5.5)$$

The magnitudes of the oscillations of the decay rate are proportional to the eccentricity of the orbit. Hence, if we wish to improve the signal-to-noise ratio, we need to increase the eccentricity of the orbit as much as possible. This suggests radioactive decay experiments in space. While the MESSENGER spacecraft was en route from Earth to Mercury, tests of the gamma ray spectrometer revealed a previously

unknown quantity of ^{137}Cs on-board [41]. A total of five measurements of the ^{137}Cs decay rate were taken during the six years of cruise from Earth to Mercury. Fischbach et al. [41] analyzed the data, accounting for the time variation of $\Gamma(t)$. They found a ξ value of -3.1×10^{-3} . Problems with the gamma ray spectrometer precluded additional measurements taken after the MESSENGER spacecraft entered Mercury orbit.

5.7 Summary

A summary of the different experiments, the isotopes involved, and corresponding properties are shown in Table 5.1. In addition to the experiments shown above, we also consider the experiment of Ellis [42] [39].

We can see from the table that all isotopes show an oscillation amplitude, ξ , of similar magnitude. This is quite a remarkable result: the isotopes have a wide range of isotopic masses, decay rates, and decay Q -value, but still have similar amplitudes. ^{226}Ra is an α emitter, while ^{54}Mn is pure electron capture, but they have approximately the same ξ -values as isotopes that decay primarily via electron emission. There is no reason *a priori* to expect these isotopes to receive similar fractional decay contributions. The experiments were performed at different times, different locations, and with different types of detectors, so the possibility of an unknown systematic or environmental effect seems low. We therefore consider the possibility that this is a universal phenomenon potentially affecting all isotopes. It is this scenario that we will consider in the remaining sections.

The data in Table 5.1, along with the power spectrum analyses, suggest a solar influence, and the solar flare data seems to indicate that the solar influence is mediated by neutrinos. As we have not seen these oscillations in other parameters, we are led to conclude that the true origin of the phenomenon is a novel neutrino-neutrino interaction. This interaction is applicable to β^- decay and electron capture as they both contain final state neutrinos or antineutrinos that could interact with solar

Table 5.1.

Experiments showing changes to radioactive decay rates with distance from the Sun, along with properties of the isotopes, and the computed oscillation amplitude, ξ

Experiment	Source	Mode	Duration	$t_{1/2}$ (d)	Q (keV)	$10^3\xi$
Ellis [42] [39]	^{56}Mn	β^-	1978-87	1.1×10^{-1}	3695.5	3
Parkhomov [39]	^{60}Co	β^-	1999-03	1.9×10^2	2823.9	2
Purdue [40]	^{54}Mn	EC	2008-13	3.1×10^2	1377.1	~ 1
Norman [43] [44]	$^{22}\text{Na}/^{44}\text{Ti}$	β^+, EC	1994-96	–	–	0.34
	^{22}Na	β^+		9.5×10^2	2842.2	–
	^{44}Ti	EC		2.2×10^3	267.5	–
Schrader [45]	^{154}Eu	β^-	1990-96	3.1×10^3	1968.4	1
Schrader [45]	^{85}Kr	β^-	1990-96	3.6×10^3	687.1	1
Falkenberg [38]	^3H	β^-	1980-82	4.5×10^3	18.59	3.7
Schrader [45]	^{152}Eu	β, EC	1981-96	4.9×10^3	1874.3	1
MESSENGER [41]	^{137}Cs	β^-	2004-10	1.1×10^4	1175.6	-3.1
Parkhomov [39]	^{90}Sr	β^-	2000-10	1.1×10^4	546.0	1.3
BNL [30]	^{32}Si	β^-	1982-86	5.5×10^4	224.5	1.5
Schrader [45]	^{108m}Ag	β^+	1990-96	1.5×10^5	1918	1
PTB [31]	^{226}Ra	various	1981-96	5.8×10^5	4870.6	1.5
Matthews [46]	^{14}C	β^-	2016	2.2×10^6	156.4	2-4
BNL [30]	^{36}Cl	β^-	1982-86	1.1×10^8	708.6	1.5
Ohio State [47]	^{36}Cl	β^-	2005-2011	1.1×10^8	708.6	5.8

neutrinos. However, this mechanism would not affect α decay in an obvious way, since α decay is modeled as a quantum tunneling phenomenon and no neutrinos are involved. We can apply the mechanism to the daughter products of ^{226}Ra . The PTB group only measured the current produced by their detector, and not individual frequencies. Therefore, their results would be affected by the daughters of ^{226}Ra , which decay primarily via beta decay, and could be affected by a novel neutrino interaction.

6. PERTURBATIONS OF NUCLEAR DECAY RATES

6.1 Theory

We have seen that the fractional change in decay rate is, surprisingly, constant for a variety of isotopes with a large range of Q-values and nominal half lives. A few attempts have been made to describe this phenomenon theoretically [48] [49], but all have thus far been unsuccessful. We will consider a different method to describe this phenomenon inspired by the work of Fassio-Canuto [28] and Matese and O'Connell [27] on radioactive decays in extreme environments and the preliminary work by Fischbach et. al [29].

We begin by giving an introduction to beta decay and electron capture that will serve as a foundation for the work in this chapter and Chapter 7. It should be noted that when we refer to beta decay we mean electron emission. We should also consider positron emission, but the equations will be similar to those of electron emission with the electron replaced by an neutrino and the antineutrino replaced by a positron. The transition rate of a quantum system is given by Fermi's Golden Rule [50]

$$\Gamma = \frac{2\pi}{\hbar} |\langle f | H_{int} | i \rangle|^2 \delta(E_f - E_i) dn, \quad (6.1)$$

where H_{int} is the interaction Hamiltonian, $|i\rangle$ is the initial nuclear state vector, $\langle f|$ is the final nuclear state vector, dn are the final states over which we sum, and $\delta(E_f - E_i)$ is the energy-conserving delta function. Beta decay and electron capture are weak interaction processes which are described by an effective interaction Hamiltonian given by

$$H_{int} = \frac{G_F}{\sqrt{2}} \tau^+ \gamma^\mu (1 - \lambda \gamma^5) J_\mu^\ell, \quad (6.2)$$

where τ^+ is the isospin operator, G_F is the Fermi constant, λ is the ratio of the axial-vector and vector coupling constants, γ_μ , γ^5 are the 4×4 Dirac matrices [50]

(see also Appendix D), and J_α^ℓ is the lepton current. The lepton current will take on different forms based on the reaction.

6.1.1 β Decay

In a beta decay reaction, a neutron inside a nucleus is converted into a proton, an electron, and an electron anti-neutrino

$$I_P \rightarrow I_D + e^- + \bar{\nu}_e, \quad (6.3)$$

where I_P and I_D are the parent and daughter nuclei, e^- is the emitted electron and $\bar{\nu}_e$ is the electron antineutrino. The lepton current for this process is

$$J_\mu^\ell = \bar{\psi}_e \gamma_\mu (1 - \gamma^5) \psi_{\bar{\nu}}, \quad (6.4)$$

where ψ_e and $\psi_{\bar{\nu}}$ are the Dirac wave functions for the electron and antineutrino. We use a plane wave approximation,

$$\psi_e(\vec{r}) = \frac{1}{\sqrt{V}} e^{-i\vec{p}_e \cdot \vec{r}/\hbar}, \quad (6.5)$$

$$\psi_{\bar{\nu}}(\vec{r}) = \frac{1}{\sqrt{V}} e^{i\vec{p}_\nu \cdot \vec{r}/\hbar}, \quad (6.6)$$

where p_i is the momentum of the i th particle, the subscripts e and ν represent the electron and antineutrino, respectively, and we have normalized the wavefunctions in a periodic box of volume V . We can then write the unpolarized matrix element as (see Appendix C for the derivation for a neutron)

$$\langle f | H_{int} | i \rangle = \frac{4G_F |\mathcal{M}_{if}|^2}{V} \left(1 + a \frac{\vec{p}_e c}{E_e} \cdot \frac{\vec{p}_\nu c}{E_\nu} \right), \quad (6.7)$$

where $|\mathcal{M}_{if}|^2$ and a are defined in Appendix C. Equation (6.7) was computed for the neutron. For general nuclei, $|\mathcal{M}_{if}|^2$ and a will have different values, and there will be additional terms proportional to $\vec{p}_e \cdot \vec{p}_\nu$ (see [51]) which will drop out due to solid angle integrals.

The final piece needed to solve for the decay rate is the phase space factor. This is a sum of all phase space volumes that the final particles can occupy. The momentum

of the daughter nucleus is determined by conservation of linear momentum, and is typically small. If we assume in addition that the recoil velocity is low, $E_D \approx m_D c^2$, where E_D and m_D are the energy and mass, respectively, of the daughter nucleus. The phase space factor is then

$$dn = dn_e dn_\nu = \left(\frac{V d^3 \vec{p}_e}{(2\pi\hbar)^3} \right) \left(\frac{V d^3 \vec{p}_\nu}{(2\pi\hbar)^3} \right). \quad (6.8)$$

We can now substitute Eqs. (6.7) and (6.8) into Eq. (6.1) to obtain the full decay rate [50] [51]

$$\begin{aligned} d\Gamma &= \frac{4G_F^2 |\mathcal{M}_{if}|^2}{(2\pi)^5 \hbar^7} F(Z_D, E_e) d^3 p_e d^3 p_\nu \delta(M_p c^2 - M_D c^2 - E_e - E_\nu) \\ &\times \left(1 + a \frac{\vec{p}_e c}{E_e} \cdot \frac{\vec{p}_\nu c}{E_\nu} \right), \end{aligned} \quad (6.9)$$

where we have included the factor, $F(Z_D, E_e)$ which corrects for the fact that the outgoing electron wavefunction should be distorted by the charge of the daughter nucleus. Setting $Z_D = 0$ implies that $F(0, E_e) = 1$, a simplification we will use frequently. We can now integrate over the neutrino and electron solid angles (which eliminates $\vec{p}_e \cdot p_\nu$)

$$d\Gamma = \frac{2G_F^2 |\mathcal{M}_{if}|^2}{\pi^3 \hbar^7} F(Z_D, E_e) p_e^2 p_\nu^2 dp_e dp_\nu \delta(M_p c^2 - M_D c^2 - E_e - E_\nu). \quad (6.10)$$

Defining $E_0 \equiv M_p c^2 - M_D c^2$ (the energy released in the decay), and using the fact that $p dp = E dE/c^2$ along with the assumption that the neutrino is massless, allows us to integrate over the neutrino energy utilizing the delta function. Hence,

$$\frac{d\Gamma}{dE} = \frac{2G_F^2 |\mathcal{M}_{if}|^2}{\pi^3 \hbar^7 c^6} F(Z_D, E_e) E_e \sqrt{E_e^2 - m_e^2 c^4} (E_0 - E_e)^2. \quad (6.11)$$

This is the standard form of the differential beta decay rate [50]. We can finally integrate over the electron energy to find the decay rate Γ ,

$$\Gamma = \frac{2G_F^2 |\mathcal{M}_{if}|^2}{\pi^3 \hbar^7 c^6} (m_e c^2)^5 f(Z_D, E_0), \quad (6.12)$$

$$f(Z_D, E_0) = \frac{1}{(m_e c^2)^5} \int_{m_e c^2}^{E_0} F(Z_D, E_e) \sqrt{E_e^2 - m_e^2 c^4} E_e (E_0 - E_e)^2 dE_e. \quad (6.13)$$

We introduced the dimensionless function $f(Z, E_0)$ for simplicity. Positron emission will have the same form as Eq. (6.12) with $Z_D \rightarrow -Z_D$. If we set $Z_D = 0$ and neglect the daughter nucleus' charge, we can solve $f(0, E_e)$ analytically (see Appendix E).

$$f(0, E_e) = \frac{1}{4} \left[\frac{1}{15} (2a^4 - 9a^2 - 8) \sqrt{a^2 - 1} + a \ln \left(a + \sqrt{a^2 - 1} \right) \right], \quad (6.14)$$

with $a = E_0/m_e c^2$.

6.1.2 Electron Capture

In electron capture, an orbital electron is captured by the parent nucleus, I_P , converting a proton into a neutron to produce the daughter nucleus, I_D . and releasing an electron neutrino

$$I_P + e^- \rightarrow I_D + \nu_e. \quad (6.15)$$

Here, the lepton current is given by

$$J_\mu^\ell = \frac{g}{2\sqrt{2}} \bar{\psi}_\nu \gamma_\mu (1 - \gamma^5) \psi_e. \quad (6.16)$$

We can use the plane wave approximation for the neutrino, but the electron is initially in a bound state, so we cannot ignore the Coulomb effects as we do for beta decay. Hence, we use the first coulomb bound state as our electron wavefunction

$$\psi_e(\vec{r}) = \phi_{100}(r) = \frac{1}{\sqrt{\pi}} \left(\frac{Z_P}{a_0} \right)^{3/2} e^{-Z_P r/a_0} = \frac{1}{\sqrt{\pi}} \left(\frac{m_e c \alpha Z_P}{\hbar} \right)^{3/2} e^{-Z_P r/a_0}. \quad (6.17)$$

where Z_P is the charge of the parent nucleus, a_0 is the Bohr radius of the electron, and α is the fine structure constant. We evaluate the electron wavefunction at the location of the nucleus ($r = 0$) and the squared matrix element is

$$|\langle f | H_I | i \rangle|^2 = \frac{2G_F^2 (m_e c \alpha Z_P)^3}{V \pi \hbar^3} |\mathcal{M}_{if}|^2. \quad (6.18)$$

The number of final states is computed the same way as Eq. (6.8), now excluding the electron contribution. In the nuclear rest frame, the initial energy, E_i , is given by the sum of the rest masses of the parent nucleus and electron along with the atomic

binding energy, E_B , so that $E_i = M_P c^2 + M_e c^2 + E_B$. The final energy, E_F is the sum of the energies of the daughter nucleus and the neutrino, so that $E_f = m_D c^2 + E_\nu$, where we have again neglected the recoil. We must also multiply the total decay rate by two since there are two ground state electrons in the K-shell of the parent nucleus. Hence,

$$\begin{aligned}
d\Gamma &= 2 \times 4\pi \frac{G_F^2 (m_e c \alpha Z_P)^3}{V \pi \hbar^4} |\mathcal{M}_{if}|^2 \\
&\quad \times \delta(E_\nu + M_D c^2 - M_P c^2 - m_e c^2 - E_B) \frac{V}{(2\pi \hbar)^3} d^3 p_\nu \\
&= 4G_F^2 \frac{(m_e c \alpha Z_P)^3}{\pi^2 \hbar^7} |\mathcal{M}_{if}|^2 \\
&\quad \times \delta(E_\nu + M_D c^2 - M_P c^2 - m_e c^2 - E_B) p_\nu^2 dp_\nu.
\end{aligned} \tag{6.19}$$

In the last line of Eq. (6.19), we integrated over the neutrino solid angle. We can use the neutrino dispersion relations ($E = pc$) to convert the momenta to energies, and then perform the integral with the help of the delta function. Introducing the dimensionless neutrino energy,

$$q = (M_P + E_B + m_e - M_D)/m_e, \tag{6.20}$$

we find

$$\Gamma(q) = \frac{4G_F^2 (m_e c)^5 \alpha^3 Z_P^3}{\pi^2 \hbar^7 c^6} |\mathcal{M}_{if}|^2 q^2. \tag{6.21}$$

6.2 Modified Decay Energy

6.2.1 β decay

We see from Eq. (6.14) that the decay rate is given as a function of $a = (m_p - m_d)/m_e$, which is the total electron and antineutrino kinetic energy (the total phase space energy). Since the perturbing potential only affects the phase space factor, we can approximate its effect by perturbing a in Eq. (6.14). The simplest case would be a constant perturbation $a \rightarrow a' = a + V$, $|V| \ll a$. We can then expand the decay rate in terms of V and we find that

$$\frac{\delta\Gamma}{\Gamma} = V \frac{1}{\Gamma} \frac{d\Gamma}{da}. \tag{6.22}$$

This expression is not satisfactory, as $1/\Gamma$ has a pole at $a = 1$. To improve the analytical behavior of $\delta\Gamma/\Gamma$, we take the next simplest form of V , that is, V proportional to $a - 1$ to try to eliminate that pole. We find that this form of V results in a fractional change that is relatively constant over the desired range. To determine if this is the best choice for V , we first let V be proportional to a^n for several values of n , as shown in Figure 6.1. The curves for $n = 0$ and $n = 1$ flatten out as a gets larger, but all four curves diverge as a approaches one, which is the behavior we want to avoid.

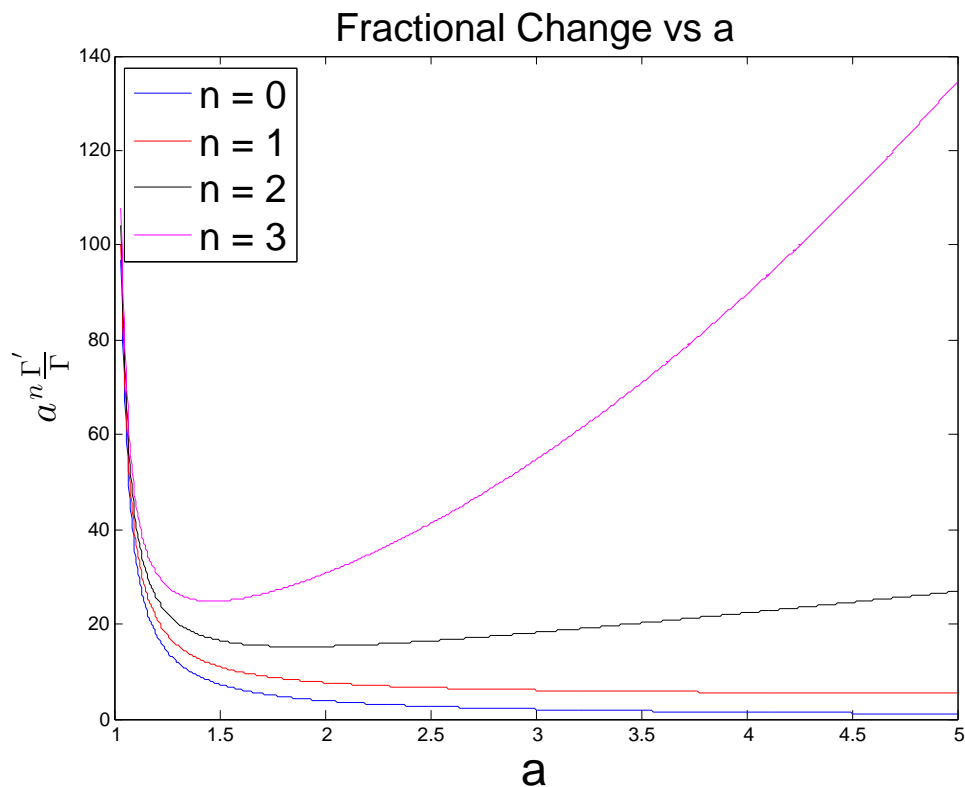


Fig. 6.1. The fractional change for the perturbation of the form $V \sim a^n$. We see that lower values of n are well behaved as a gets large, but the curves diverge as $a \rightarrow 1$, which is undesired.

Figure 6.2 shows the fractional change for a potential of the form $V \sim (a - 1)^n$ for several values of n . We see that $n = 2$ and $n = 3$ grow too much as a gets large, and $n = 0$ diverges as a approaches unity. hence, $n = 1$ appears to be the best choice

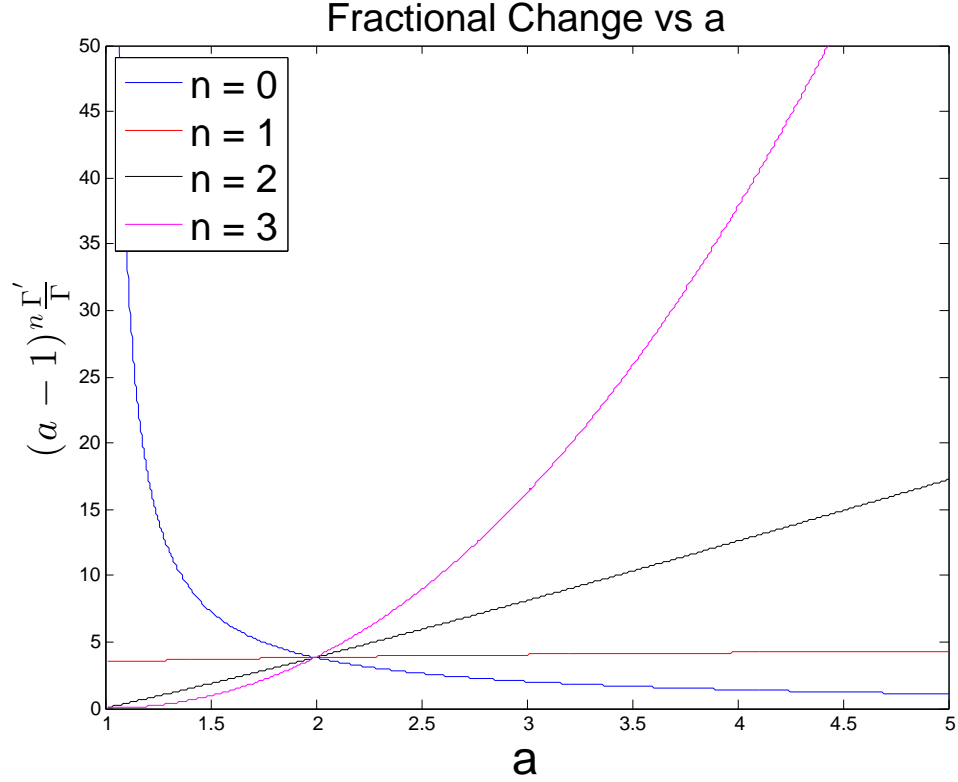


Fig. 6.2. The fractional change for the perturbation of the form $V \sim (a - 1)^n$. We see that $n = 0$ and $n = 1$ are well behaved as a gets large, but $n = 0$ diverges as $a \rightarrow 1$.

for the perturbation. We next consider what $(a - 1)$ means physically. a was the maximum total energy of the electron (in units of the electron mass), so $a - 1$ would be the maximum kinetic energy of the electron, since the sum of the kinetic energy of the electron and antineutrino is a constant, which we define as $q \equiv a - 1$.

The decay rate as a function of q is then given by

$$\Gamma(q) = \frac{G_F^2 m_e^5}{2\pi^3} \left[\frac{1}{15} (2q^4 + 8q^3 + 3q^2 - 10q - 15) \sqrt{q^2 + 2q} + (q + 1) \ln \left(q + 1 + \sqrt{q^2 + 2q} \right) \right]. \quad (6.23)$$

We now introduce a perturbation proportional to q , $q \rightarrow q' = q(1 + \epsilon)$, $|\epsilon| \ll 1$. We expand Γ in ϵ , $\Gamma(q') = \Gamma^{(0)}(q) + \epsilon\Gamma^{(1)}(q) + \epsilon^2\Gamma^{(2)}(q)$, where

$$\Gamma^{(0)}(q) = \frac{G_F^2}{2\pi^3} m_e^5 \left[(q+1) \ln \left(q+1 + \sqrt{q^2+2q} \right) + \frac{1}{15} (2q^4 + 8q^3 + 3q^2 - 10q - 15) \sqrt{q^2+2q} \right], \quad (6.24)$$

$$\Gamma^{(1)}(q) = q \frac{d\Gamma(q)}{dq} = \frac{G_F^2}{2\pi^3} m_e^5 \left[q \ln \left(q+1 + \sqrt{q^2+2q} \right) + \frac{q^2}{3\sqrt{q^2+2q}} (2q^4 + 10q^3 + 13q^2 - 6q - 6) \right], \quad (6.25)$$

$$\Gamma^{(2)}(q) = \frac{q^2}{2} \frac{d^2\Gamma(q)}{dq^2} = \frac{G_F^2}{2\pi^3} m_e^5 \frac{4}{3} q^2 [q^2 + 2q]^{3/2}. \quad (6.26)$$

We next examine the first- and second- order corrections (excluding ϵ) in Figure 6.3. We see that $\Gamma^{(1)}/\Gamma^{(0)}$ is fairly flat over the range of values considered, and significantly flatter than $\Gamma^{(2)}/\Gamma^{(0)}$. Since $\Gamma^{(2)}/\Gamma^{(0)}$ does not diverge, and is of a similar order of magnitude as $\Gamma^{(1)}/\Gamma^{(0)}$, it is safe to say that only the lowest order term is important, since the second order term is suppressed by an extra factor of ϵ . We can interpret these results to mean that if the neutrino-neutrino interaction shifts the phase space energy of a decay by $V = \epsilon q$, then the resulting fractional change in the decay rate will be relatively constant (same order of magnitude) for all isotopes (all q values). The factor of ϵ will contain the oscillatory component and the strength of the interaction.

6.2.2 Electron capture

To determine the perturbation of electron capture rates, we begin with Eq. (6.21). We see that the decay rate is simply proportional to q^2 . If we let $q \rightarrow q' = q(1 + \epsilon)$ and expand for small ϵ , we find that

$$\boxed{\frac{\delta\Gamma}{\Gamma} \approx 2\epsilon}, \quad (6.27)$$

which is a constant for all isotopes.

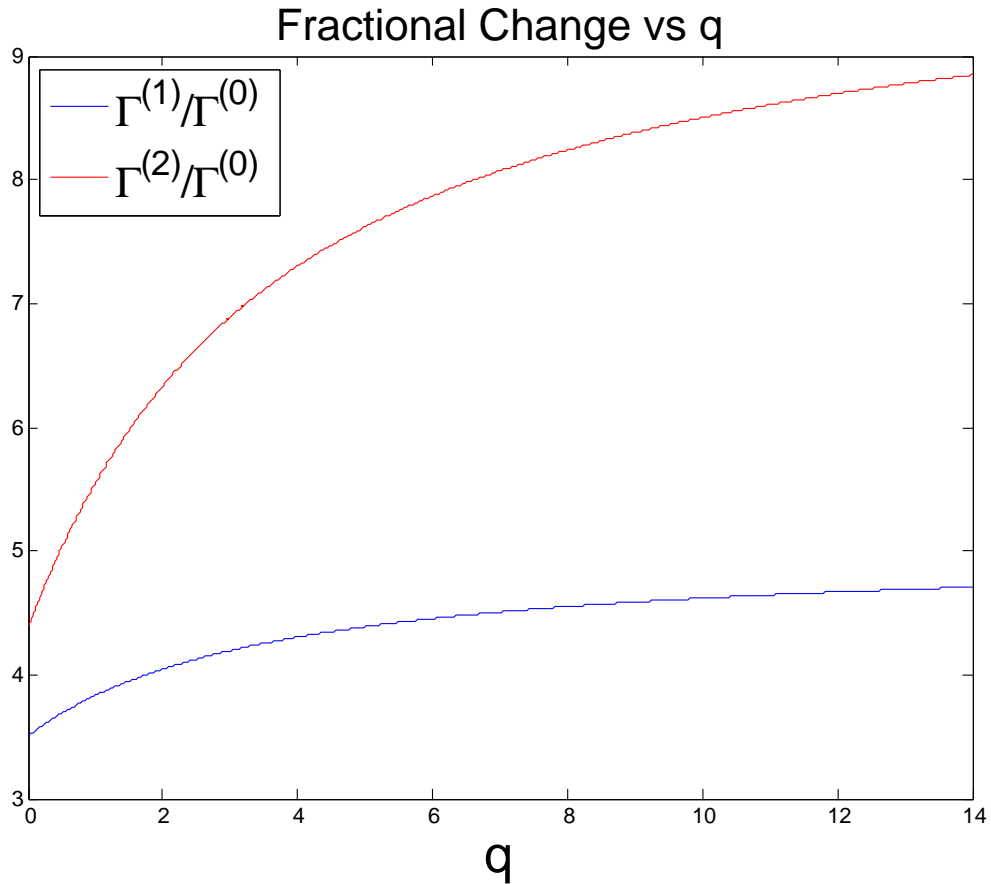


Fig. 6.3. The first- and second- order corrections from a perturbation of the form $V = \epsilon q$. We see that $\Gamma^{(1)}/\Gamma^{(0)}$ is fairly flat over the range of q values considered.

6.3 Modified Dispersion Relations

In the previous section, we showed how perturbing the total amount of phase space energy by an amount proportional to the phase space energy itself could lead to a fairly constant fractional change for all isotopes. In what follows, we assume that a neutrino-neutrino interaction modifies the phase space, but we do not speculate on a form of the interaction.

A somewhat surprising aspect of this picture is that the intermediary particle would appear to know about the entire available phase space energy, and hence

it would seem that this particle would “know” too much. With this in mind and inspired by our previous result, we assume that a potential exists which is proportional to the total energy of only the neutrino (or anti-neutrino). We presume this is due to a neutrino-neutrino interaction with solar neutrinos, but the exact details are not necessary at this stage. This new potential will modify the neutrino dispersion relation and we will investigate the effect on the decay rate.

We consider a neutrino moving through a potential field given by V . We treat this neutrino as being nearly free and we can assume that the wavefunction is given by a plane wave. The energy of the neutrino is then

$$E_\nu = \langle H \rangle = \langle H_0 \rangle + \langle H \rangle = p_\nu c + \langle V \rangle, \quad (6.28)$$

where H_0 is the free particle Hamiltonian whose expectation value is $p_\nu c$ for a massless neutrino. Now, we use the results from the previous section and we assume that the expectation value of the potential is proportional to the momentum (or free particle energy), $\langle V \rangle \approx -\epsilon p_\nu c$. Then

$$E_\nu = p_\nu c - \epsilon p_\nu c = (1 - \epsilon) p_\nu c. \quad (6.29)$$

6.3.1 β decay

To compute the new decay rate for beta emission, we combine Eqs. (6.12) and (6.14). As before, we integrate over the two solid angles. We now convert the electron and neutrino momenta to energy; the electron dispersion relation is unchanged, while we use Eq. (6.29) for the neutrino. The decay rate is then

$$\Gamma = \frac{2G_F^2}{\pi^3} (1 - \epsilon)^{-3} \int_{m_e}^{m_P - m_D} |\mathcal{M}_{if}|^2 E_e \sqrt{E_e^2 - m_e^2} (m_P - m_D - E_e)^2 dE_e. \quad (6.30)$$

We define the unperturbed decay rate as

$$\Gamma_0 = 2G_F^2 \pi^{-3} \int_{m_e}^{m_P - m_D} |\mathcal{M}_{if}|^2 E_e \sqrt{E_e^2 - m_e^2} (m_P - m_D - E_e)^2 dE_e, \quad (6.31)$$

(whose solution is given by Eq. (6.12)) and Taylor expand in ϵ we find

$$\Gamma \approx \Gamma_0 (1 + 3\epsilon), \quad (6.32)$$

and have

$$\boxed{\frac{\delta\Gamma}{\Gamma_0} = 3\epsilon}, \quad (6.33)$$

which is constant (to lowest order) for all isotopes.

6.3.2 Electron capture

For electron capture, we return to Eq. (6.19) and use our modified dispersion relations to convert the momenta to energies. Then,

$$\begin{aligned} \Gamma &= \frac{4G_F^2}{\pi^2} (m_e \alpha Z_P)^3 (1 - \epsilon)^{-3} \int |\mathcal{M}_{if}|^2 \delta(E_\nu - qm_E) E_\nu^2 dE_\nu \\ &= \frac{4G_F^2}{\pi^2} m_e^5 \alpha^3 Z_P^3 (1 - \epsilon)^{-3} |\mathcal{M}_{if}|^2 q^2 \\ &\approx \Gamma_0 (1 + 3\epsilon), \end{aligned} \quad (6.34)$$

where

$$\Gamma_0 = 4G_F^2 \pi^{-2} m_e^5 \alpha^3 Z_P^3 |\mathcal{M}_{if}|^2 q^2. \quad (6.35)$$

We see that, as in β decay,

$$\boxed{\frac{\delta\Gamma}{\Gamma_0} = 3\epsilon}, \quad (6.36)$$

which is, again, constant for all isotopes.

We see that β decay and electron capture have the same perturbation in this model, which emerges from the fact that the perturbation arises when evaluating the neutrino contribution to the number of final states. This would appear to be general: each neutrino or antineutrino phase space integral contributes a perturbation of $\pm 3\epsilon$, with the sign depending on the type of fundamental interaction (scalar, vector, etc.).

6.4 Time Dependence of the Perturbations

The periodic time dependence of the fractional decay rate can be written as

$$\frac{\Delta\Gamma(t)}{\Gamma} \approx \xi \cos\left(\frac{2\pi}{T}t + \phi\right), \quad (6.37)$$

where T is the period of one year, ϕ is the and ξ is the amplitude of oscillation which appears to be independent of isotope. Since the oscillation has a period of one year, it is natural to assume that the time-dependence is related to either the Earth-Sun distance or to the velocity of the Earth about the Sun, both of which have a period of one year.

6.4.1 Earth-Sun Distance

We begin with the Earth-Sun distance. We choose an inverse square law for the spatial variation, since any effect emanating from the Sun (such as solar neutrino field density) falls off as the inverse square. The assumed perturbation then has the form

$$\epsilon(r) = \zeta \left(\frac{\bar{r}_\oplus}{r(t)} \right)^2, \quad (6.38)$$

where ζ is the new dimensionless constant, and \bar{r}_\oplus is the average Earth-Sun distance (1 a.u.). The radius for a conic section is given by

$$r_\oplus = \frac{p}{1 + e \cos \nu} \approx \bar{r}_\oplus \left[1 - e \cos \left(\frac{2\pi t}{T_\oplus} + \phi_\oplus \right) \right]. \quad (6.39)$$

We have used the fact that the eccentricity is small to replace the semilatus rectum, p , with the average orbital distance, \bar{r}_\oplus , and the true anomaly ν , with the time and phase angle. The perturbation then becomes,

$$\begin{aligned} \epsilon(t) &= \zeta \left(\frac{\bar{r}_\oplus}{\bar{r}_\oplus} \right)^2 \left[1 - e \cos \left(\frac{2\pi t}{T_\oplus} + \phi_\oplus \right) \right]^{-2} \\ &\approx \zeta \left[1 + 2e \cos \left(\frac{2\pi t}{T_\oplus} + \phi_\oplus \right) \right]. \end{aligned} \quad (6.40)$$

We substitute Eq. (6.40) into Eq. (6.32) to find the time dependence of the decay rate

$$\begin{aligned} \Gamma(t) &\approx \Gamma_{vac} \left[1 + 3\zeta + 6\zeta e \cos \left(\frac{2\pi t}{T_\oplus} + \phi_\oplus \right) \right], \\ &\approx \Gamma_\oplus \left[1 + 6\zeta e \cos \left(\frac{2\pi t}{T_\oplus} + \phi_\oplus \right) \right], \end{aligned} \quad (6.41)$$

where we have identified the decay rate on the Earth as $\Gamma_{\oplus} = (1 + 3\zeta)\Gamma_{vac}$. The fractional decay rate is then

$$\frac{\Delta\Gamma}{\Gamma_{\oplus}} = 6\zeta e \cos\left(\frac{2\pi t}{T_{\oplus}} + \phi_{\oplus}\right). \quad (6.42)$$

We can then use the observed value of ξ to write

$$\xi = 6e\zeta \rightarrow \boxed{\zeta = \frac{\xi}{6e} \sim \frac{\xi}{6(0.0167)} \sim 10^{-2}}. \quad (6.43)$$

6.4.2 Earth Orbital Velocity

We now consider the Earth orbital velocity. We assume a perturbation linear in the velocity

$$\epsilon(v) = \kappa \left(\frac{v_t}{\bar{v}_{\oplus}} \right), \quad (6.44)$$

where κ is our new dimensionless parameter and \bar{v}_{\oplus} is our reference (average) velocity of the Earth.

The orbital velocity is given by Eq. (B.11)

$$\vec{v}_{PQW} = \sqrt{\frac{GM}{p}} \begin{bmatrix} -\sin \nu \\ e + \cos \nu \\ 0 \end{bmatrix}. \quad (6.45)$$

The magnitude of the velocity is then,

$$\begin{aligned} v^2 &= \frac{GM}{p} (\sin^2 \nu + e^2 + 2e \cos \nu) \\ &\approx \frac{GM}{a} \left[1 + 2e \cos\left(\frac{2\pi t}{T_{\oplus}}\right) \right], \end{aligned} \quad (6.46)$$

$$v \approx \sqrt{\frac{GM}{a}} \left[1 + e \cos\left(\frac{2\pi t}{T_{\oplus}}\right) \right]. \quad (6.47)$$

The perturbation is then,

$$\begin{aligned} \epsilon(t) &= \kappa \left(\frac{\frac{GM}{a}}{\bar{v}_{\oplus}} \right) \left[1 + e \cos\left(\frac{2\pi t}{T_{\oplus}} + \phi_{\oplus}\right) \right] \\ &= \kappa \left[1 + e \cos\left(\frac{2\pi t}{T_{\oplus}} + \phi_{\oplus}\right) \right], \end{aligned} \quad (6.48)$$

where we have identified \bar{v}_\oplus with GM/a . We see the velocity perturbation has the same phase as the inverse square perturbation. The position and velocity of an object in orbit are out of phase by π (periapsis has closest distance and highest velocity), hence taking the inverse squared distance would shift the phase by π . Comparing Eq. (6.48) to Eq. (6.40) we can compare κ to ζ

$$\boxed{\kappa = 2\zeta \sim 2 \times 10^{-2}}. \quad (6.49)$$

We note in passing that for a general v^n force we have $\kappa = 2\zeta/n$.

6.5 Neutrino Index of Refraction

The form of Eq. (6.29) is familiar from electromagnetism; it is the energy momentum relationship for a photon in a medium with an index of refraction. Since the index of refraction is the speed of light divided by the velocity of the particle in a medium, v_ν ,

$$n_\nu = \frac{c}{v_\nu}, \quad (6.50)$$

n_ν is by definition greater than one. We can rederive Eq. (6.29) by starting from the wave equation for massless particles (which also applies to fermions),

$$\frac{1}{v_\nu} \frac{\partial^2 \psi}{\partial t^2} = \frac{n^2}{c^2} \frac{\partial^2 \psi}{\partial t^2} = \nabla^2 \psi. \quad (6.51)$$

If we substitute in the plane wave solution $e^{i(\vec{p}_\nu \cdot \vec{r} - E_\nu t)}$, then

$$\frac{n^2}{c^2} \frac{E^2}{\hbar^2} = \frac{p^2}{\hbar^2} \rightarrow E = \frac{pc}{n}, \quad (6.52)$$

where we have taken the positive energy solution. Since n must be greater than unity, we let $n = (1 + \epsilon)$ where ϵ once again a small parameter. Substituting into Eq. (6.52) we have

$$E = \frac{pc}{n} = \frac{pc}{(1 + \epsilon)} \approx (1 - \epsilon)pc. \quad (6.53)$$

We can also use the index of refraction to relate the frequency to the wavenumber using $E = \hbar\omega$ and $p = \hbar k$

$$E = \frac{pc}{n} \rightarrow \omega = \frac{kc}{n}. \quad (6.54)$$

Since the frequency in the medium is not affected by the index of refraction, we can relate it (and the wave number in the medium) to the wave number in vacuum, k_0 ,

$$\omega = \frac{kc}{n} = k_0c \rightarrow k = k_0n. \quad (6.55)$$

We can use this result to consider the decay rate from a different point of view. Decay rates have the functional form (matrix element) \times (phase space factor). As we saw in Eq. (6.8), the phase space contains an integral over all neutrino momenta, d^3p , which is proportional to the integral over all wavenumbers d^3k . Therefore, in a medium, the decay rate will be proportional to $d^3k = n_\nu^3 d^3k_0$, instead of being proportional to the vacuum value d^3k_0 . If we assume that the matrix element is independent of n_ν (which is contrary to electromagnetism, where the electric and magnetic fields are also proportional to index of refraction), the decay rate in a medium is

$$\Gamma = n_\nu^3 \Gamma_0 = (1 + \epsilon)^3 \Gamma_0 \approx (1 + 3\epsilon) \Gamma_0, \quad (6.56)$$

which matches our result from Eqs. (6.32) and (6.34). Thus our modified dispersion relation, Eq. (6.29) is equivalent to a medium description.

6.5.1 Dispersionless Models

Using the definition of the index of refraction, and the fact that $\epsilon = \zeta \sim 10^{-2}$, we find

$$\frac{v}{c} \approx 1 - \epsilon \approx 0.99, \quad (6.57)$$

or the deviation from the speed of light is given by

$$1 - \frac{v}{c} \sim 10^2. \quad (6.58)$$

The deviation of v from c has been measured or estimated from a number of experiments (see Table 6.1). These differ significantly from our value of 10^{-2} . The most precise limits from Earth-based experiments give $1 - v/c \lesssim 10^{-6}$ obtained from neutrino pulse timing experiments using 3 GeV neutrinos. It seems that an energy-independent perturbation amplitude will not work.

Table 6.1.
Measurements of neutrino (and anti-neutrino) speeds from various experiments.

System/Experiment	Neutrino Type	Neutrino Energy	$ v/c - 1 $	
Fermilab NuMi Beam (MINOS) [52]	ν and $\bar{\nu}$	3 GeV	$(5.1 \pm 2.1) \times 10^{-5}$	
Fermilab [53]		30-200 GeV	$< 4 \times 10^{-5}$	
CERN CNGS Beam (LVD) [54]		ν_μ	17 GeV	$\lesssim 3.8 \times 10^{-6}$
CERN CNGS Beam (OPERA) [55]		ν_μ	17 GeV	$[2.7 \pm 3.1(\text{stat})_{-3.3}^{+3.4}(\text{sys.})] \times 10^{-8}$
CERN CNGS Beam (Borexino) [56]		ν_μ	17 GeV	$\lesssim 2.1 \times 10^{-6}$
Fermilab (MINOS) [57]		ν_μ	3 GeV	$(1.0 \pm 1.1) \times 10^{-6}$
SN1987A [58]	$\bar{\nu}_e$	10-40 MeV	$\lesssim 10^{-8}$	
SN1987A [59]	$\bar{\nu}_e$	10-40 MeV	$\lesssim 2 \times 10^{-9}$	
Cosmic Neutrinos (ICECUBE) [60]		PeV	$< 1.0 \times 10^{-20}(v/c > 1)$	

6.5.2 Dispersive Models

A purely constant (or dispersionless) index of refraction predicts a neutrino speed that is inconsistent with results obtained from a number of experiments. We once again look to optics for inspiration [61]. In optics we know that real indexes of refraction are complex and energy-dependent. In fact, the optical theorem, which is relatively simple to derive using only conservation of energy (optics), or conservation of probability (quantum mechanics), states that a particle interacting with background particles of density \mathcal{N} , has an index of refraction (let $\hbar = c = 1$),

$$n = 1 + \frac{2\pi\mathcal{N}f(0,p)}{p^2} \simeq 1 + \frac{2\pi\mathcal{N}f(0,E)}{E^2}, \quad (6.59)$$

where $f(0,E)$ is the forward scattering amplitude. The optical theorem assumes that $|n - 1| \ll 1$, and we assume that the neutrino mass is small, $m \ll E$.

We seem to be in similar situation here, as we were with the fifth force, where we have different experiments yielding different results: Specifically, we need ϵ to be larger and roughly constant ($\zeta \sim 10^{-2}$) for beta decay, while we need it to be smaller ($\lesssim 10^{-6}$) to satisfy the neutrino speed experiments at large energies.

A type of function that could fit this requirement is a resonance, well known from optics and mechanics. For the scattering length, we use the relativistic Breit-Wigner distribution, which is similar to optical resonances

$$\begin{aligned} f(0, E) &= \frac{f_\infty E^2}{M_0^2 - E^2 - i\gamma E} \\ &= f_\infty \left[\frac{E^2(M_0^2 - E^2)^2}{(M_0^2 - E^2)^2 + \gamma^2 E^2} + i \frac{\gamma E^3}{(M_0^2 - E^2)^2 + \gamma^2 E^2} \right], \end{aligned} \quad (6.60)$$

where $f_\infty = |f(0, \infty)|$ is the magnitude of the forward scattering length, M_0 is the mass scale of the resonance, and γ is the width of the resonance.

We can write our now complex index of refraction in the form

$$\tilde{n} = 1 + \frac{\epsilon_0 M_0^2}{M_0^2 - E^2 - i\gamma E} \quad (6.61)$$

$$\begin{aligned} &= 1 + \epsilon_0 \left[\frac{M_0^2(M_0^2 - E^2)^2}{(M_0^2 - E^2)^2 + \gamma^2 E^2} + i \frac{\gamma M_0^2 E}{(M_0^2 - E^2)^2 + \gamma^2 E^2} \right], \\ \epsilon_0 &= 2\pi \mathcal{N} \frac{f_\infty}{M_0^2}. \end{aligned} \quad (6.62)$$

The real and imaginary parts are then,

$$\boxed{n(E) \equiv \text{Re}[\tilde{n}(E)] = 1 + \frac{\epsilon_0 M_0^2 (M_0^2 - E^2)^2}{(M_0^2 - E^2)^2 + \gamma^2 E^2},} \quad (6.63)$$

$$\boxed{\kappa(E) \equiv \text{Im}[\tilde{n}(E)] = \frac{\epsilon_0 \gamma M_0^2 E}{(M_0^2 - E^2)^2 + \gamma^2 E^2}.} \quad (6.64)$$

We can take the limit of $n(E)$ and $\kappa(E)$ as E is much larger than (or much smaller than) M_0 , giving

$$n(E) \rightarrow \begin{cases} 1 + \epsilon_0 & E \ll M_0, \\ 1 - \epsilon_0 M_0^2 / E^2 & E \gg M_0, \end{cases} \quad (6.65)$$

$$\kappa(E) \rightarrow \begin{cases} 0 & E \ll M_0, \\ 0 & E \gg M_0. \end{cases} \quad (6.66)$$

The real and imaginary parts of the index of refraction are plotted in Figure 6.4.

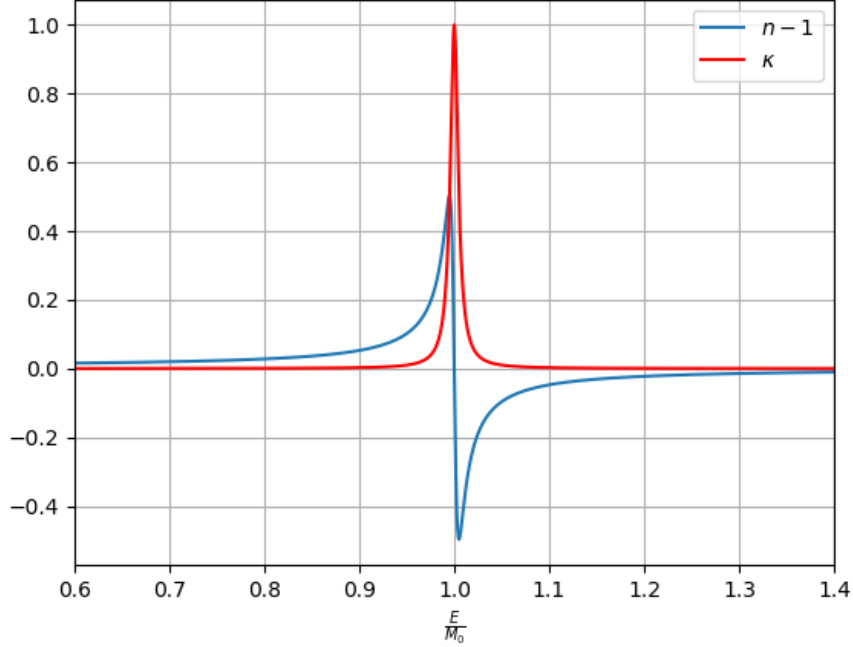


Fig. 6.4. The real and imaginary parts of the index of refraction, $n(E)$ and $\kappa(E)$ assuming $\epsilon = 0.01$ and $\gamma/M_0 = 0.01$.

We can also compute the total scattering cross section, σ_{tot} , [62]

$$\begin{aligned}\sigma_{tot} &= \frac{4\pi}{E} \text{Im}[f(0, E)] \\ &= \frac{4\pi f_{\infty} \gamma E^2}{(M_0^2 - E^2)^2 + \gamma^2 E^2} = \frac{2E}{N} \kappa(E).\end{aligned}\quad (6.67)$$

Our choice of the relativistic Breit-Wigner distribution leads to the desired behavior in the limiting cases. For $M_0 \sim 1$ MeV, beta decay probes the region $E_{\nu} \ll M_0$, where the index of refraction is roughly constant, whereas neutrino speed experiments probe $E_{\nu} \gg M_0$, where the index of refraction approaches unity. However, near $E_{\nu} \sim M_0$, there is a resonance in the distribution. Since the intensity of the beam falls off as $e^{-\kappa x}$ in the medium, this would remove neutrinos from the beam. Interestingly, the RENO [63], Double Chooz [64], and Daya Bay [65] experiments have observed a “bump” at $M_0 \sim 5$ MeV in their measured reactor antineutrino flux. If we let our factor γ become negative, the real part of the index of refraction

is unchanged, while the imaginary part becomes negative, and the neutrino beam would gain particles rather than lose. Physically, this could be due to sterile antineutrinos not measurable in the RENO experiment being converted to standard model antineutrinos.

If we take the $M_0 \sim 5$ MeV from the reactor experiments, $\epsilon_0 \sim 0.01$ from our preceding analysis, and assume $\gamma = 0.01M_0 = 0.05$ MeV, we find the numerical values given in Table 6.2.

Table 6.2.
Computed values for the real and imaginary parts of the index of refraction for $M_0 = 5$ MeV and $\gamma = 0.05$ MeV.

E (MeV)	$n - 1$	κ
0	0.0100	0.00000
1	0.0104	0.00002
2	0.0119	0.00006
3	0.0156	0.00015
4	0.0278	0.00062
5	0.0000	1.00000
6	-0.0227	0.00062
7	-0.0104	0.00015
8	-0.0064	0.00007
9	-0.0045	0.00004
10	-0.0033	0.00002

6.5.3 Anomalous Dispersion

We note from Figure 6.4 that if $E > M_0$ for small γ we can have a negative refractive index, leading to a negative phase velocity. However, the actual speed is determined by the group velocity

$$v_{gr} = \frac{d\omega}{dk} = \left(\frac{dp}{dE} \right)^{-1} = \left\{ \frac{d}{dE} [En(E)] \right\}^{-1} = \left\{ n(E) + E \frac{d}{dE} n(E) \right\}^{-1}. \quad (6.68)$$

At the high energy limit $E \gg M_0$, we have

$$n(E) + E \frac{d}{dE} n(E) \simeq 1 - \frac{\epsilon_0 M_0^2}{E^2} + E \left(-\frac{\epsilon_0 M_0^2}{E^3} \right) = 1. \quad (6.69)$$

Hence, for high energies, the group velocity approaches c as expected from the velocity experiments. However, near the resonance, $E = M_0$ we find anomalous dispersion ($v_{gr} > c$ or $v_{gr} < 0$, Figure 6.5). This is not as bad as it sounds, since the anomalous dispersion when occurs when $n(E) \sim \kappa(E)$ (Figure 6.5a), so our initial assumption that the neutrino is a plane wave with definite momentum breaks down. We can compare this to the case in optics where a photon is absorbed by an atom before being re-emitted. It is possible that something similar happens to neutrinos when they scatter with $E \simeq M_0$.

6.6 Future Experiments

We can gain more information on the perturbation and the index of refraction by consider the effects on some other experiments.

6.6.1 Multiple Neutrino Emission

Our results show the final state neutrino (or antineutrino) contributes 3ϵ to the fractional decay rate. This generalizes to decays with multiple final state neutrinos such as muon decay to electrons, two neutrino double beta decay, and two neutrino double electron capture. In muon decay, the final state includes a muon neutrino and an electron antineutrino, giving a fractional decay rate of $3(\epsilon_\mu + \epsilon_{\bar{e}})$. Two neutrino

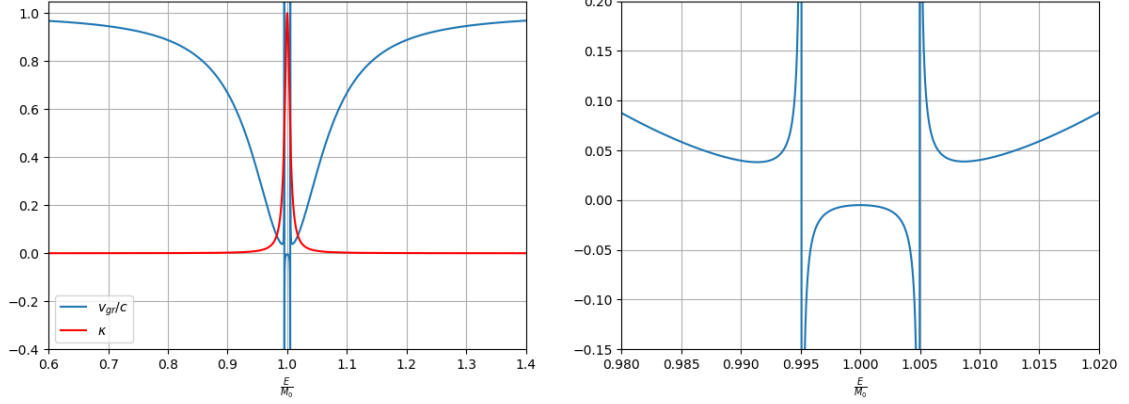


Fig. 6.5. The neutrino group velocity (blue) for $\epsilon_0 = \gamma/M_0 = 0.01$. (a), and zooming in on the region of anomalous dispersion (b). The red line in (a) is the the imaginary part of the refractive index which shows absorption is largest in the region of anomalous dispersion.

double beta decay emits two electron antineutrinos which would yield a fractional decay rate of $6\epsilon_{\bar{e}}$. Two neutrino double electron capture produces two electron neutrinos and a fractional change of $6\epsilon_e$

6.6.2 Neutrinoless Double Beta Decay

At first glance it would appear that neutrinoless double beta decay would be immune to the medium influence since there are no emitted neutrinos. However, there are internal neutrino lines in the Feynman diagram, contributing a propagator to the scattering amplitude. If the neutrino wave function is evaluated in the presence of the index of refraction, the propagator will be modified such that

$$\frac{1}{\not{p} - m} \rightarrow \frac{1}{\gamma^0 p_0 - (1 - \epsilon)\gamma^i p_i - m} \simeq \frac{1}{\not{p} - m} (-\epsilon\gamma^i p_i) \frac{1}{\not{p} - m}, \quad (6.70)$$

Hence, an index of refraction is equivalent to adding an interaction vertex $-\epsilon\gamma^i p_i$. If neutrinoless double beta decay exists and is observed, the index of refraction would result in an oscillation in the decay rate. Since neutrinoless double beta decay is

already extremely rare and difficult to observe, observing oscillations in the decay rate would be unlikely for some time.

6.6.3 Torsion Balance Experiments

Like neutrinoless double beta decay, it would seem that the index of refraction would affect torsion balance experiments. However it must be noted that since the decay rates are being changed by the background, some transfer of energy is occurring and this transfer of energy should also be observable as a force. On a more microscopic level, a portion of the self energy of a nucleus is due to neutrino-antineutrino exchanges between nucleons. We can have three types of interactions: proton-proton, which will have a statistical weight of $Z(Z - 1)/2$, neutron-neutron, with a statistical weight of $N(N - 1)/2$, and proton-neutron with a weight of NZ . If we assume that these three interactions have the same strength, we can sum the three effects, giving

$$\begin{aligned} \frac{1}{2}N^2 - \frac{1}{2}N + \frac{1}{2}Z^2 - \frac{1}{2}Z + NZ &\rightarrow \frac{1}{2}(N^2 + 2NZ + Z^2) + \frac{1}{2}(N + Z) \\ &\rightarrow \frac{(N + Z)[(N + Z) + 1]}{2} = \frac{B(B + 1)}{2}. \end{aligned} \quad (6.71)$$

So the total interaction would appear as a baryon-baryon interaction. Since the neutrino exchange forces are expected to be around 10^{-15} g, observing a time dependence will be unlikely in the near future.

6.6.4 Mass Problem

Finally, we note that the index of refraction model could also shed some light on attempts to determine the mass of the neutrino, such as KATRIN, an experiment using ^3H , which Falkenberg [38] found to exhibit the annual periodicity. The most recent experiments have found the neutrino mass squared to have negative values [66].

Consider the kinematics of the beta decay spectrum in the presence of a medium (written in terms of the neutrino energy, E_ν)

$$\begin{aligned}
d\Gamma &\sim (E_0 - E_\nu)\sqrt{(E_0 - E_\nu)^2 - m_e^2 c^4} E_\nu^2 n^3 \\
&\sim (E_0 - E_\nu)\sqrt{(E_0 - E_\nu)^2 - m_e^2 c^4} E_\nu^2 \left[1 + \frac{2\pi\mathcal{N}\hbar^2 c^2 f(0, E_\nu)}{E_\nu^2}\right]^3 \\
&\sim (E_0 - E_\nu)\sqrt{(E_0 - E_\nu)^2 - m_e^2 c^4} E_\nu^2 [E_\nu^2 + 6\pi\hbar^2 c^2 \mathcal{N} f(0, E_\nu)]. \quad (6.72)
\end{aligned}$$

The analogous expression for the case with a massive neutrino is given by

$$\begin{aligned}
d\Gamma &\sim (E_0 - E_\nu)\sqrt{(E_0 - E_\nu)^2 - m_e^2 c^4} E_\nu \sqrt{E_\nu^2 - m_\nu^2 c^4} \\
&\sim (E_0 - E_\nu)\sqrt{(E_0 - E_\nu)^2 - m_e^2 c^4} E_\nu^2 \sqrt{1 - \frac{m_\nu^2 c^4}{E_\nu^2}} \\
&\sim (E_0 - E_\nu)\sqrt{(E_0 - E_\nu)^2 - m_e^2 c^4} \left(E_\nu^2 - \frac{1}{2}m_\nu^2 c^4\right). \quad (6.73)
\end{aligned}$$

Comparing Eqs. (6.72) and (6.73), we can find that a medium can simulate a decay where the neutrino mass squared is negative: $m_\nu^2 c^4 = -12\pi\hbar^2 c^2 \mathcal{N} f(0, E)$. Interestingly, a number of recent determinations of $(m_\nu c^2)^2$ give negative values [67].

We can also consider modified dispersion relations which give

$$\begin{aligned}
E_\nu^2 &\simeq (1 - \epsilon)^2 c^2 p_\nu^2 + m_\nu c^4 \equiv p_\nu^2 c^2 + M_{\nu,eff}^2 c^4 \\
&\rightarrow M_{\nu,eff}^2 c^4 \simeq m_\nu^2 c^4 - 2\epsilon p_\nu^2 c^2 \simeq m_\nu^2 c^4 - 4\pi\hbar^2 c^2 \mathcal{N} f(0, p), \quad (6.74)
\end{aligned}$$

The effective mass, $m_{\nu,eff}^2$ can be positive, negative, or zero, and it is negative when the true mass $m_\nu^2 < 2\epsilon p_\nu^2/c^2$. Calculations of neutron star stability imply a lower bound on neutrino mass $m_\nu \gtrsim 0.4\text{eV}/c^2$ [68], so $M_{\nu,eff}$ is negative when $p_\nu c \gtrsim 10$ eV. We also note that in our Breit-Wigner model, $f(0, P) \rightarrow E^2$ as $E \rightarrow 0$. If the distribution was modified in such a way to approach a constant in this region, then the model could account for the neutrino mass problem as well. However, this leads to the question of the validity of the optical theorem at such low momentum.

7. DECAY RATE SUPPRESSION BY THE PAULI EXCLUSION PRINCIPLE

In Chapter 5, we described a number of methods that can affect nuclear decay rates. In Chapter 6, we found a novel method to generate the constant relative perturbation of beta decay and electron capture. Here we consider one of the methods supported by the current quantum mechanical/electroweak theory, namely the suppression of the decays due to the Pauli Exclusion Principle (PEP, not to be confused with the pep process in the Sun where two protons and an electron fuse together to produce deuterium and a neutrino). Any final state neutrino will be emitted into a background neutrino field consisting of cosmic background neutrinos and solar neutrinos. The cosmic background neutrinos are thermal in nature with a temperature of $k_B T = 1.68 \times 10^{-4} eV$ and a density of $\rho_\nu = 56/cm^3$ per flavor [69]. Note, we only consider electron neutrinos here. The solar neutrinos are created by a variety of process and we will consider the pp process later. Depending on the location of the experiment, the decaying sample may also be subject to a non-thermal background of reactor antineutrinos, but they can be treated the same as the solar neutrinos. We are interested on the effects of Pauli blocking on a full spectrum, so we neglect electron capture (which emits at a single energy) in favor of positron/electron emission. Technically, the cosmic neutrino background contains both neutrinos and antineutrinos, so the effects discussed below apply to both electron and positron emission, while the solar flux contains neutrinos, meaning it should only affect positron emission. So we shall consider positron emission below, but we note that the solar flux results may also apply to electron emission decay if the neutrino and antineutrino are the same particle (i.e., Majorana fermions).

The background neutrinos occupy positions in phase space, meaning there are fewer positions for the emitted neutrino to occupy, thus there is a suppression. We can

model this by multiplying the differential decay rate given Eq. (6.9) by a suppression factor $1 - K(\vec{p}_\nu)$

$$\begin{aligned} d\Gamma &= \frac{4G_F^2 |\mathcal{M}_{if}|^2}{(2\pi)^5 \hbar^7} F(Z, E_e) d^3 p_e d^3 p_\nu \delta(M_p c^2 - M_D c^2 - E_e - E_\nu) \\ &\times (1 - K(\vec{p}_\nu)) \left\{ 1 + a \frac{\vec{p}_\nu c}{E_\nu} \cdot \frac{\vec{p}_e c}{E_e} + \hat{I} \cdot \left[A \frac{\vec{p}_e c}{E_e} + B \frac{\vec{p}_\nu c}{E_\nu} \right] \right\} \end{aligned} \quad (7.1)$$

where, again, $|\mathcal{M}_{if}|^2$, a , A , and B are defined in Appendix C. As started in the last chapter, this equation is valid for neutrons. For general nuclei, $|\mathcal{M}_{if}|^2$, a , A , and B will depend on the nuclear matrix elements and a couple extra terms proportional to $\vec{p}_e \cdot \vec{p}_\nu$ appear. Since K depends on the neutrino momentum and not the electron momentum, we can integrate over the electron solid angle and get rid of the a and A terms.

$$\begin{aligned} d\Gamma &= \frac{16\pi G_F^2 |\mathcal{M}_{if}|^2}{(2\pi)^5 \hbar^7} F(Z, E_e) p_e^2 dp_e d^3 p_\nu \delta(M_p c^2 - M_D c^2 - E_e - E_\nu) \\ &\times (1 - K(\vec{p}_\nu)) \left\{ 1 + \hat{I} \cdot \frac{\vec{p}_\nu c}{E_\nu} \right\} \end{aligned} \quad (7.2)$$

7.1 Thermal Neutrinos

We treat the background cosmic neutrinos as a Fermi gas, whose energy distribution and blocking factor (for electron neutrinos) is [69]

$$K(\vec{p}_\nu) = \frac{1}{\exp[(u_\alpha p^\alpha c - \mu_e)/k_B T] + 1} \quad (7.3)$$

where $k_B T$ is the temperature of the background field (in units of energy, p_α is the four momentum of the neutrino in the lab frame, and u_α is the 4-velocity of the observer, namely, the velocity of the cosmic rest frame relative to the lab frame. Due to the comparatively slow speed of the Sun and the Earth relative to the speed of light, we can assume the lab frame and cosmic rest frame coincide, giving $u_\alpha = (1, 0, 0, 0)$ with metric signature $(+, -, -, -)$. The $u_\alpha p^\alpha c$ simplifies to the neutrino energy E_ν . The final unknown in Eq. (7.3) is the chemical potential μ_e of the background. In a Fermi gas at

zero temperature, the chemical potential separates occupied from unoccupied state. This is also given by the Fermi energy and is a function of the density of particles

$$\mu_e = E_F = \hbar c (3\pi^2 \rho_\nu)^{\frac{1}{3}} \quad (7.4)$$

We can now simplify Eq. (7.1). We can integrate over the electron solid angle. As $K(\vec{p}_\nu) = K(E_\nu)$ is isotropic we can also integrate over the neutrino solid angle. This eliminates every term but but the 1 in the curly brackets; the direction of the nuclear spin is irrelevant. The change in the decay rate is then given by

$$\delta\Gamma = \frac{g^2 |\mathcal{M}_{if}|^2}{2\pi^3 \hbar^7} \int F(Z, E_e) K(E_\nu) \delta(M_P c^2 - M_D c^2 - E_e - E_\nu) p_\nu^2 p_e^2 dp_e dp_\nu \quad (7.5)$$

$$(7.6)$$

Finally, we can use the definitions of the electron and neutrino energy to integrate the delta function over the electron energy ($E_0 = (M_P - M_D)c^2$)

$$\begin{aligned} \delta\Gamma &= \frac{g^2 \xi}{2\pi^3 \hbar^7 c^6} \int_0^{E_0 - m_e c^2} F(Z, E_0 - E_\nu) K(E_\nu) \\ &\times (E_0 - E_\nu) \sqrt{(E_0 - E_\nu)^2 - m_e^2 c^4} E_\nu^2 dE_\nu \end{aligned} \quad (7.7)$$

We further simplify by dropping the coulomb correction, $F(Z, E)$, and divide by the nominal decay rate to find the relative change in the decay rate

$$\frac{\delta\Gamma}{\Gamma} = \frac{1}{f(Z, am_e c^2)} \int_0^{a-1} [\exp(zx - \bar{\mu}_e) + 1]^{-1} x^2 (a-x) \sqrt{(a-x)^2 - 1} dx$$

where $x = E_\nu/m_e c^2$, $a = E_0/m_e c^2$, $z = m_e c^2/k_B T$ and $\bar{\mu}_e = \mu_e/k_B T$.

As example, we will consider a polarized neutron decaying in a bath of cosmic background neutrinos. As we noted before, the cosmic background neutrinos have a temperature $k_B T = 1.68 \times 10^{-10} \text{ MeV}$ and a density of $\rho_\nu = 56 \times 10^6 \text{ 1/m}^3$. Neutron decay has a q value $q = (a-1) = 0.782 \text{ MeV}/0.511 \text{ MeV} = 1.53$ [50], Then the fractional change in the decay rate is

$$\boxed{\frac{\delta\Gamma}{\Gamma} = -2.32 \times 10^{-28}} \quad (7.8)$$

7.2 Non-Thermal Neutrinos

7.2.1 PEP Suppression Factor

In addition to thermal neutrinos, non-thermal neutrinos can also suppress radioactive decays. Unfortunately, we do not have a simple distribution like Eq. (7.3), so we must derive it ourselves.

Consider an ensemble of nuclei undergoing decay. At the same time N solar neutrinos are passing near the nuclei. These particles occupy points in phase space, so these points must be removed from the sum over final states. We can rewrite decay rate from Eq. (6.9) as

$$\Gamma = \frac{4G_F^2 |\mathcal{M}_{if}|^2}{\pi\hbar^4 V} \sum_{k\nu=1}^{\infty} K_k \int p_e^2 dp_e \delta(E_0 - E_e - E_{\nu k}) \quad (7.9)$$

$$\times \left\{ 1 + \hat{I} \cdot B \frac{\vec{p}_{\nu,k} c}{E_{\nu}} \right\} \quad (7.10)$$

$$K_k = 1 - \sum_{i=1}^N \delta_{m_i \ell_k} \quad (7.11)$$

We have written the neutrino phase space as a discrete sum and introduced the PEP factor K_k . The emitted neutrinos are in the k th possible final state with the set of quantum numbers ℓ_k , while the background particles are in the k th quantum state with quantum numbers m_j . If ℓ_k represents m_i , that particular state is already filled and the decay cannot proceed. This is represented by the delta function. We can rewrite the suppression factor as an infinite sum by introducing parameters a_i

$$K_k = 1 - \sum_{i=1}^{\infty} a_i \delta_{m_i \ell_k} \quad (7.12)$$

$$\sum_{i=1}^{\infty} a_i = N \quad (7.13)$$

We estimate the a_i 's from the measured background neutrino flux. Let $\Phi(E_b)$ be the flux of neutrino per unit energy, which has a known spectrum from the standard solar model [70]. We can break the spectrum up into pieces of width ΔE_b with each piece having an energy E_{bi} corresponding to the quantum numbers m_i . The flux of particles with energies between E_{bi} and $E_{bi} + \Delta E_b$ is then $\Phi(E_{bi})\Delta E_b$. If we divide by the speed of the neutrino, we get the particle density. Finally, we multiply by the local volume V to get the total number of particles between E_{bi} and $E_{bi} + \Delta E_b$; if we sum over i , we get the total number of particles. The coefficients are then

$$a_i = \frac{\Phi(E_{bi})V}{c} \Delta E_b \quad (7.14)$$

Now we pass from discrete to continuous quantum. We note that the solar neutrinos are emitted radially away from the sun, so we orient the z-axis of the laboratory frame along this axis. Therefore, we can let

$$\begin{aligned} m_i &\rightarrow \left[0, 0, \frac{E_b L}{2\pi \hbar c} \right] \\ \ell_k &\rightarrow \frac{p_{\nu k} L}{2\pi \hbar} \\ \delta_{m_i, \ell_k} &\rightarrow \delta \left(\frac{p_{\nu x} L}{2\pi \hbar} \right) \delta \left(\frac{p_{\nu y} L}{2\pi \hbar} \right) \delta \left(\frac{p_{\nu z} L}{2\pi \hbar} - \frac{E_b L}{2\pi \hbar c} \right) \\ &= \frac{(2\pi \hbar)^3}{V} \delta(p_{\nu x}) \delta(p_{\nu y}) \delta \left(p_{\nu z} - \frac{E_b}{c} \right) \\ \sum_k &\rightarrow \int \left(\frac{V d^3 \vec{p}_\nu}{(2\pi \hbar)^3} \right) \\ \sum_j \Delta E_b &\rightarrow \int_0^{E_{b, max}} dE_b \end{aligned}$$

Then the decay rate and PEP suppression factor become

$$\begin{aligned} \Gamma &= \frac{4G_F^2 |\mathcal{M}_{if}|^2}{(2\pi)^5 \hbar^7} \int K(\vec{p}_\nu) \delta(E_0 - E_e - E_\nu) \\ &\quad \times \left(1 + B\hat{I} \frac{\vec{p}_\nu c}{E_\nu}\right) d^3 p_\nu d^3 p_e \end{aligned} \quad (7.15)$$

$$K(\vec{p}_\nu) = 1 - \frac{(2\pi\hbar)^3}{c} \int_0^{E_{b,max}} dE_b \Phi(E_b) \delta(p_{\nu x}) \delta(p_{\nu y}) \delta\left(p_{\nu z} - \frac{E_b}{c}\right) \quad (7.16)$$

The fractional decay rate is then (using the beta decay solution from Eqs. (6.12) and (6.14))

$$\begin{aligned} \frac{\delta\Gamma}{\Gamma} &= -\frac{c^6}{16\pi^2 f(0, E_0)} \frac{(2\pi\hbar)^3}{c} \frac{1}{(m_e c^2)^5} \int_0^{E_{b,max}} dE_b \Phi(E_b) \int \left(1 + B\hat{I} \frac{\vec{p}_\nu c}{E_\nu}\right) \\ &\quad \times \delta(E_0 - E_e - E_\nu) \delta(p_{\nu x}) \delta(p_{\nu y}) \delta\left(p_{\nu z} - \frac{E_b}{c}\right) d^3 p_\nu d^3 p_e \end{aligned} \quad (7.17)$$

The integral over the neutrino momenta removes three of the delta functions. Since $p_{\nu x}$ and $p_{\nu y}$ are set to zero, we have $E_\nu = p_{\nu z} c = E_b$. Then we have

$$\begin{aligned} \frac{\delta\Gamma}{\Gamma} &= -\frac{\pi\hbar^3 c^5}{2f(0, E_0)} \frac{1}{(m_e c^2)^5} \left(1 + B\hat{I}_z\right) \int_0^{E_{b,max}} dE_b \Phi(E_b) \\ &\quad \times \int \delta(E_0 - E_b - E_e) d^3 p_e \end{aligned} \quad (7.18)$$

We then perform the integral over the solid angle and switch to integrating over electron energy

$$\begin{aligned} \frac{\delta\Gamma}{\Gamma} &= -\frac{2\pi^2 \hbar^3 c^2}{f(0, E_0)} \frac{1}{(m_e c^2)^5} \left(1 + B\hat{I}_z\right) \int_0^{E_{b,max}} dE_b \Phi(E_b) \\ &\quad \times \int \delta(E_0 - E_b - E_e) E_e \sqrt{E_e^2 - m_e^2 c^4} dE_e \\ &= -\frac{2\pi^2 \hbar^3 c^2}{f(0, E_0)} \frac{1}{(m_e c^2)^5} \left(1 - \hat{I}_z\right) \\ &\quad \times \int_0^{E_{b,max}} \Phi(E_b) (E_0 - E_b) \sqrt{(E_0 - E_b)^2 - m_e^2 c^4} dE_b \end{aligned} \quad (7.19)$$

7.2.2 Simple Example

We consider a simple example where we are interested in the fractional decay rate a in the range ΔE_b about energy E_b . In Eq. (7.19), we set dE_b equal to ΔE_b and $f(0, E_b)$ becomes

$$f(0, E_0)|_{E_b} \rightarrow \frac{1}{(m_e c^2)^5} (E_0 - E_b) \sqrt{(E_0 - E_b)^2 - m_e^2 c^4} E_b^2 \Delta E_b \quad (7.20)$$

where we first shifted from integrating over electron energy to integrating over neutrino energy and then restricted it to ΔE_b about E_b . Then the fractional decay rate becomes

$$\frac{\delta\Gamma}{\Gamma}(E_b) = -2\pi^2 \hbar^3 c^2 \left(1 + B \hat{I}_z\right) \frac{\Phi(E_b)}{E_b^2} \quad (7.21)$$

Again we will consider neutron decay in the presence of solar pp neutrinos. The pp neutrino spectrum peaks at a value of $\sim 10^{15}$ $1/\text{m}^2\text{sMeV}$ as an energy E_b of 3 MeV [70]. The value of λ is 1.44 [50] and B is given by

$$B = -\frac{\frac{1}{2}(\lambda + \lambda^2)}{\frac{1}{4}(1 + 3\lambda^2)} - 0.97$$

To find the maximize the fractional change, we take $\hat{I}_z = 1$, then

$$\boxed{\frac{\delta\Gamma}{\Gamma} = -5.49 \times 10^{-29}} \quad (7.22)$$

7.2.3 A (Slightly) More Complicated Example

We now consider the influence of the background field over the entire spectrum. To accomplish this, we need to know the functional form of $\Phi(E_b)$. The neutrinos from the Sun come from a variety of sources. For simplicity, we will consider only the pp neutrinos. In the pp reaction, two protons collide to form a deuteron, a positron, and an electron neutrino.

$$p + p \rightarrow d + e^+ + \nu_e \quad (7.23)$$

The exact matrix element for this interaction quite complicated, but we do not actually need it. We note the decay involves three final state particles, just like beta decay, If we assume the matrix element is independent of energy, the only energy dependence will be from the phase space term, which is identical to beta decay. Using a max energy of E_1 and writing in terms of the neutrino energy, E_b , the energy dependence of $\Phi(E_b)$ is

$$\Phi(E_b) \sim \frac{1}{(m_e c^2)^5} (E_1 - E_b) \sqrt{(E_1 - E_b)^2 - m_e^2 c^4} E_b^2 \quad (7.24)$$

Introducing the total flux of pp neutrinos at Earth $I_{pp} = \int_0^{E_1 - m_e c^2} \phi(E_b) dE_b$, we can write $\Phi(E_b)$ as

$$\Phi(E_b) = \frac{I_{pp}}{f(0, E_1) (m_e c^2)^5} (E_1 - E_b) \sqrt{(E_1 - E_b)^2 - m_e^2 c^4} E_b^2 \quad (7.25)$$

$$\begin{aligned} \frac{\delta\Gamma}{\Gamma} &= - \frac{2\pi^2 \hbar^3 c^2}{(m_e c^2)^{10}} \frac{I_{pp}}{f(0, E_0) f(0, E_1)} \left(1 + B \hat{I}_z\right) \int_0^{E_{max}} \sqrt{(E_0 - E_b)^2 - m_e^2 c^4} \\ &\quad \times (E_0 - E_b) (E_1 - E_b) \sqrt{(E_1 - E_b)^2 - m_e^2 c^4} E_b^2 dE_b \end{aligned} \quad (7.26)$$

where $E_{max} = \min(E_0, E_1) - m_e c^2$. We introduce $a_0 = E_0/m_e c^2$, $a_1 = E_1/m_e c^2$, $x = E_b/m_e c^2$, $q_{max} = \min(E_0, E_1)/m_e c^2 - 1$

$$\frac{\delta\Gamma}{\Gamma} = - \frac{2\pi^2 \hbar^3 c^2}{(m_e c^2)^3} \frac{I_{pp}}{f(0, E_0) f(0, E_1)} \left(1 + B \hat{I}_z\right) J(a_0, a_1) \quad (7.27)$$

$$\begin{aligned} J(a_0, a_1) &= \int_0^{q_{max}} \sqrt{(a_0 - x)^2 - 1} \\ &\quad \times (a_0 - x) (a_1 - x) \sqrt{(a_1 - x)^2 - 1} x^2 dx \end{aligned} \quad (7.28)$$

Consider a polarized neutron once again decaying in the presence of solar neutrinos The pp neutrinos have a total flux at Earth is about $I_{pp} \sim 10^{15} 1/\text{m}^2\text{s}$ and a q-value

$q_1 = (a_1 - 1) = 0.42\text{MeV}/0.511\text{MeV} = 0.822$ [70]. Neutron decay has a $q_0 = (a_0 - 1) = 0.782\text{MeV}/0.511\text{MeV} = 1.53$ [50]. Since $q_1 < q_0$, the integral (7.28) is cut off at q_1 . Again, we take $\hat{I}_z = -1$. Then the total perturbation is

$$\boxed{\frac{\delta\Gamma}{\Gamma} = -8.01 \times 10^{-27}} \quad (7.29)$$

7.3 Discussion

We have seen that the fractional change in the decay rate of a neutron is negligible for both a thermal cosmic background and a non-thermal, solar background. Interestingly, the effect was of similar magnitude for both even though the non-thermal PEP factor was suppressed by three powers of Planck's constant, while the thermal PEP factor was suppressed by the low temperature. The only neutrinos that were blocked in the thermal case were the lowest energy ones, which had a low probability of occurring even before the PEP effects.

We should also note the time dependence of these affects. The non thermal flux falls off with distance from the sun with an inverse square power, so the PEP factor will vary with the Earth's orbit. At first glance it does not appear that nonthermal PEP effect has a time dependence, but we assume our nucleus could be modeled as stationary in the cosmic rest frame. In reality, we could include velocity affects, in which case we would have perturbation that depends on the Earth's velocity [69], which will also vary around the orbit;

8. CONCLUSIONS AND FUTURE WORK

8.1 Overview of Major Results

In this thesis, we considered two very different problems, the search for fifth forces/non-Newtonian gravity, especially in the Eötvös Experiment, and time-variation of nuclear decay rates. (Although as we pointed out, the parts are connected by a tiny thread, as a neutrino interaction that affects beta decay could also produce non-Newtonian gravity, albeit slight.)

8.1.1 Fifth Force/Non-Newtonian Gravity

Our goal in this section of the thesis was an attempt to explain how the Eötvös Experiment, seemingly primitive in comparison to modern experiments, could detect a baryon-number dependent effect while the more recent experiments performed by groups such as the Eötvash group continue to detect nothing.

We introduced a Taylor series expansion of an arbitrary force to determine how the different coefficients affect the Eötvös parameters for both the EPF and EW experiments. We found that the EPF parameter depends on both the monopole and dipole terms while the EW parameter only depends on the monopoles.

Ideally, we would like a force that is a dipole (i.e. couples to the moment of inertia) without the monopole term, as that would contribute to EPF but not EW. Unfortunate, there does not seem to be an obvious way to generate such a force from quantum mechanical interactions. Instead, we consider the possibility that the monopole term has a minimum around where the EW experiment was performed and a nonzero dipole term where the EPF experiment was performed. We took the simplest case of the combination of the Yukawa potentials due to exchange of vector and

scalar fields. We found that for different values of the Yukawa length scales, we could find suitable strengths to make the η_{EW} parameter equal zero. Unfortunately, this does appear to be more coincidence than general result. Implicit in our computations were assumptions on the distance from the experimental apparatus and the sources of the potentials. This would imply that the EW experiment happened to pick the worst location to perform the test and would have gotten non-zero results if they had simply moved the apparatus slightly closer or further away from the mountain. As this situation seems unlikely, we conclude that our results do not apply generally.

We also investigated whether the MICROSCOPE experiment could detect forces due to a wind of background particles. We computed the time dependence of force due to dark matter stationary with respect to the center of the galaxy and dark matter co-rotating with the galaxy. We then computed the power spectrum density of the signal and compared that to the measured power spectrum of the MICROSCOPE spacecraft. Unfortunately, we could not see that pattern of our forces in the noise of the measured results.

8.1.2 Time-variation in Nuclear Decay Rates

The goal of this chapter was to find the function form of a beta decay rate perturbation that would give a constant fractional decay rate regardless of isotope. Our first attempt perturbed the final energy of the spectrum, a , by an amount proportional to a itself. While this perturbation yielded a roughly constant fractional decay rate for beta decay, it was exact, and the perturbation "knew" about the energy of both the electron and the neutrino. We have been working under the basic assumption that the perturbation was due to the neutrino sector due to insights from the solar flare events and the assumption that a modification to the electron sector would have been discovered already.

Our second attempt assumed a perturbation proportional to the energy or momentum of the neutrino. While this perturbation could explain the decay rates, it was inconsistent with neutrino speed experiments.

Modeling our perturbation as an index of refraction let us introduce a scattering amplitude based on the relativistic Breit-Wigner distribution, and we were able to reconcile the low energy beta neutrinos with high energy speed experiments.

There are still questions to be answered, though. Our index of refraction necessarily had an imaginary component, which leads to neutrino attenuation. It is possible that by changing a sign we could gain neutrinos instead, which might explain the bump seen in reactor experiments, but as γ is related to a lifetime in the relativistic Breit-Wigner distribution, it seems hard to justify a negative value.

We applied the optical theorem to write the index of refraction in terms of the Breit-Wigner distribution. While the optical theorem can be derived very generally, we do not really know if it is applicable to the neutrinos. We have also used ideas from optics and atomic physics to guide our analysis, but we cannot take the comparison too seriously. The optical index of refraction arises from photons scattering off of electrons due to long range electromagnetic forces. We assume that the decay neutrinos are interacting with some sort of background, but the interaction is likely due to a short range, not a long range, force. Perhaps a better comparison is the bouncing of cold neutrons off a surface. The forces on the neutrons are short range and the index of refraction arises from the spreading of the neutron wavefunction to interact with many background particles simultaneously, it is hard to imagine the the decay neutrinos would spread like that. Perhaps it is the background particles that have spread out and overlapped enough for the neutrino to interact with multiple particles at the same time. This makes the background sound like a Bose Einstein Condensate, but this consideration is beyond the scope of this work.

Finally, we derived the suppression of beta decays due to thermal and nonthermal background fields and we found that their contribution to the annual variation in decay rates is negligible.

8.2 Future Work

8.2.1 Fifth Force/Non-Newtonian Gravity

Since our simple force model did not work out, we could consider more complicated forces. We could build these forces by combining additional Yukawa potentials; however, the likelihood that there are several vector and scalar fields all coupling to Baryon number seems unlikely.

As mentioned before, it is the second-order, or dipole, terms that appear in EPF but not EW, and it would be ideal if we could create a force that has no monopole and only the dipole. This would imply a force that couples to the shape of the apparatus at lowest order. Return to the example of the cold neutrons from before, perhaps the fifth force is due to a cold background where the wavefunctions have spread enough to couple to the entire apparatus simultaneously.

One avenue of particular interest takes its inspiration from measurements of weak transition moments in quantum optics. Here, there is a weak-electromagnetic cross term in the Hamiltonian, so the presence of the weak interaction allows certain optical transitions to occur that would not have with out the weak interaction. This allows scientists to probe the weak interaction using certain optical techniques. We can imagine a similar situation arising in the Eötvös experiment. A cross term between the new fifth force and the gravity gradients allow the fifth force to survive Eötvös' software program, while being excluded from the Eötwash experiment due to the symmetry toward the gravitational field.

Most likely, the best information regarding the validity of the results of the Eötvös Experiment will come from a repeat of the original experiment using one of the original torsion balances. While the experiment has been updated in some ways (automatic reading of the beam deflection), this is the first time anyone is actually replicated the experiment. We look forward to their results.

Since we were unable to see our desired signals over the noise of the MICROSOFT experiment, we must wait for additional data collection that can improve the accuracy

of the data. It may be possible to reorient the spacecraft such that the sensitive axis of it's dual accelerometer points in the same direction as our drag force, increasing the accuracy of the measurements. In the absence of further data from MICROSCOFT, we must wait for the next-generation experiments to look for those forces.

8.2.2 Time-variation in Nuclear Decay Rates

We currently have a model that seems to describe the constant fractional decay rates while still being consistent with neutrino speed measurements. There are still some lingering questions about the behavior around the resonance at M_0 , but those do not seem to model-breaking.

The best suggestion for future work is simply more experiments. We need more data, from a variety of isotopes. We can then compare the reactions of neutrinos and antineutrinos. Experiments with pions muons would also allow us to compare electron and muon antineutrinos.

Space-based experiments would be exceptionally useful as we can achieve large variations in the Sun-sample distance depending the the particular trajectory. Recent advances in measuring decay rates using betavoltaics [71] seem promising as several samples as well as the measuring circuitry could be placed on a single standardized PCB that could easily be incorporated in cubesats or full-sized spacecraft.

REFERENCES

REFERENCES

- [1] I. Newton, *Principia*. Book 3, Proposition 6, Theorem 6, p. 411: University of California Press, Cajori Edition, 1960.
- [2] L. Eötvös, D. Pekár, and E. Fekete, “Contributions to the law of proportionality of inertia and gravity,” *Annals of Physics (Liepzig)*, vol. 68, no. 11, 1922.
- [3] T. Lee and C. Yang, “Conservation of heavy particles and generalized gauge transformations,” *Physical Review*, vol. 98, p. 1501, 1955.
- [4] P. Roll, R. Krotkov, and R. Dicke, “The equivalence of inertial and passive gravitational mass,” *Annals of Physics*, vol. 26, pp. 442–517, 1964.
- [5] V. Braginskii and V. Panov, “Verification of the equivalence of inertial and gravitational mass,” *Sov. Phys. JETP*, vol. 34, pp. 463–466, 1972.
- [6] G. Keiser and J. Faller, “Eötvös experiment with a fluid fiber,” in *Proceedings of the Second Marcel Grossmann Meeting on General Relativity*, R. Ruffini, Ed. Amsterdam: North-Holland, 1982, pp. 969–967.
- [7] E. Fischbach, D. Sudarsky, A. Szafer, C. Talmadge, and S. Aronson, “Reanalysis of the eötvös experiment,” *Physical Review Letters*, vol. 56, no. 1, pp. 3–6, 1986.
- [8] C. Stubbs *et al.*, “Search for an intermediate-range interaction,” *Phys. Rev. Lett.*, vol. 58, pp. 1070–1073, 1987.
- [9] C. Stubbs, E. Adelberger, and E. Gregory, “Constraints of proposed spin-0 and spin-1 partners of the graviton,” *Phys. Rev. Lett.*, vol. 61, pp. 2409–2411, 1988.
- [10] C. Stubbs *et al.*, “Limits on composition-dependent interactions using a laboratory source: Is there a ‘fifth force’ coupled to isospin?” *Phys. Rev. Lett.*, vol. 62, pp. 609–612, 1989.
- [11] T. Niebauer, M. McHugh, and J. Faller, “Galilean test for the fifth force,” *Phys. Rev. Lett.*, vol. 59, pp. 609–612, 1987.
- [12] K. Kuroda and N. Mio, “Test of a composition-dependent force by a free-fall interferometer,” *Phys. Rev. Lett.*, vol. 62, pp. 1941–1944, 1989.
- [13] —, “Limits on a possible composition-dependent force by a galilean experiment,” *Phys. Rev. D*, vol. 42, pp. 3903–3907, 1990.
- [14] S. Carusotto *et al.*, “Test of 9 universality with a galileo type experiment,” *Phys. Rev. Lett.*, vol. 69, pp. 1722–1725, 1992.
- [15] P. Thieberger, “Search for a substance-dependent force with a new differential accelerometer,” *Phys. Rev. Lett.*, vol. 58, pp. 1066–1069, 1987.

- [16] P. G. Bizzeti *et al.*, “Search for a composition-dependent fifth force,” *Phys. Rev. Lett.*, vol. 62, pp. 2901–2904, 1989.
- [17] M. Wiegand, S. Scheithauer, and S. Thiel, “Step proof mass dynamics,” *Acta Astronautica*, vol. 54, pp. 631–638, 2004.
- [18] V. Josselin, P. Toubol, M. Rodrigues, and F. Liorzou, “Microscope on-ground and in-orbit calibration.” *Space Science Review*, vol. 151, pp. 25–38, 2010.
- [19] H. Becquerel, “On the invisible rays emitted by phosphorescent bodies,” *Comptes Rendus*, vol. 122, pp. 501–503, 1896.
- [20] E. Rutherford, J. Chadwick, and C. Ellis, *Radiations from Radioactive Substances*. Cambridge: Cambridge University Press, 1930.
- [21] E. Fermi, “Tentativo di una teoria dei raggi β ,” *La Ricerca Scientifica*, vol. 2, no. 12, 1934.
- [22] H. Irnich *et al.*, “Half-Life Measurements of Bare, Mass-Resolved Isomers in a Storage-Cooler Ring,” *Physical Review Letters*, vol. 75, no. 23, p. 4182, 1995.
- [23] A. Litvinov *et al.*, “Measurement of the β^+ and orbital electron-capture decay rates in fully-ionized, hydrogen-like, and helium-like ^{140}Pr ions,” *Physical Review Letters*, vol. 99, no. 26, p. 262501, 2007.
- [24] M. Jung *et al.*, “First observation of bound-state β^- decay,” *Physical Review Letters*, vol. 69, no. 15, p. 2164, 1992.
- [25] G. T. Emery, “Perturbation of Nuclear Decay Rates,” *Annual Reviews of Nuclear Science*, vol. 22, p. 165, 1972.
- [26] L. I. Bodine, D. S. Parno, and R. G. H. Robertson, “Assessment of molecular effects on neutrino mass measurements from tritium decay,” *Physical Review C*, vol. 91, no. 3, p. 035505, 2015.
- [27] J. J. Matese and R. F. O’Connell, “Neutron Beta Decay in a Uniform Constant Magnetic Field,” *Physical Review*, vol. 180, no. 5, p. 1289, 1969.
- [28] L. Fassio-Canuto, “Neutron beta decay in a strong magnetic field,” *Physics Review B*, vol. 187, no. 26, p. 2141, 1969.
- [29] E. Fischbach, J. B. Buncher, J. T. Gruenwald, J. H. Jenkins, D. E. Kraus, J. J. Mattes, and J. Newport, “Time-dependent nuclear decay parameters: New evidence for new forces?” *Space Science Reviews*, vol. 145, no. 3, pp. 285–335, 2009.
- [30] D. E. Alburger and G. Harbottle and E. F. Norton, “Half-life of ^{32}Si ,” *Earth and Planetary Science Letters*, vol. 78, no. 2-3, pp. 168–176, 1986.
- [31] H. Siegert, H. Schrader, and U. Schötzig, “Half-life measurements of europium radionuclides and the long-term stability of detectors,” *Applied Radiation and Isotopes*, vol. 49, no. 9-11, pp. 1397–1401, 1998.
- [32] J. H. Jenkins and others, “Evidence for Correlations Between Nuclear Decay Rates and Earth-Sun Distance,” *Astroparticle Physics*, vol. 32, no. 1, pp. 42–46, 2009.

- [33] J. H. Jenkins and E. Fischbach, “Perturbation of Nuclear Decay Rates During the Solar Flare of 13 December 2006,” *Astroparticle Physics*, vol. 31, pp. 407–411, 2009.
- [34] E. Fischbach, D. Sudarsky, A. Szafer, C. Talmadge, and S. Aronson, “Long-range forces the eötvös experiment,” *Annals of Physics*, vol. 182, pp. 1–89, 1999.
- [35] E. Fischbach and C. Talmadge, *The Search for Non-Newtonian Gravity*. New York: Springer-Verlag, 1999.
- [36] L. Bod, E. Fischbach, G. Marx, and M. Náray-Ziegler, “One hundred years of the eötvös experiment,” *Acta Physica Hungarica*, vol. 69, no. 2-3, pp. 335–355, 1991.
- [37] P. Touboul *et al.*, “MICROSCOPE Mission: First Results of a Space Test of the Equivalence Principle,” *Phys. Rev. Lett.*, vol. 119, no. 23, p. 231101, 2017.
- [38] E. D. Falkenberg, “Radioactive Decay Caused by Neutrinos?” *Apeiron*, vol. 8, no. 2, pp. 32–45, 2001.
- [39] A. G. Parkmahov, “Deviations from Beta Radioactivity Exponential Drop,” *Journal of Modern Physics*, vol. 2, pp. 1310–1317, 2011.
- [40] E. Fischbach, personal communication.
- [41] E. Fischbach *et al.*, “Solar Influence on Nuclear Decay Rates: Constraints from the MESSENGER Mission,” *Astrophysics and Space Science*, vol. 337, no. 1, pp. 39–45, 2012.
- [42] K. J. Ellis, “The effective half-life of a broad beam $^{238}\text{PuBe}$ total body neutron irradiator,” *Physics in Medicine and Biology*, vol. 35, no. 8, pp. 1079–1088, 1990.
- [43] D. O’Keefe, B. L. Morreale, R. H. Lee, J. B. Buncher, J. H. Jenkins, E. Fischbach, T. Gruenwald, D. Javorsek, and P. A. Sturrock, “Spectral content of $^{22}\text{Na}/^{44}\text{Ti}$ decay data: implications for a solar influence,” *Astrophysics and Space Science*, vol. 344, no. 2, 2013.
- [44] E. B. Norman, E. Browne, H. A. Shugart, T. H. Joshi, and R. B. Firestone, “Evidence against correlations between nuclear decay rates and earthsun distance,” *Astroparticle Physics*, vol. 31, no. 2, pp. 135 – 137, 2009.
- [45] H. Schrader, “Half-life measurements of long-lived radionuclides new data analysis and systematic effects,” *Applied Radiation and Isotopes*, vol. 68, no. 7, pp. 1583 – 1590, 2010.
- [46] S. Mathews, personal communication.
- [47] J. H. Jenkins, K. R. Herminghuysen, T. E. Blue, E. Fischbach, D. Javorsek, A. C. Kauffman, D. W. Mundy, P. A. Sturrock, and J. W. Talmagi, “Additional experimental evidence for a solar influence on nuclear decay rates,” *Astropart. Phys.*, vol. 37, pp. 81–88, 2012.
- [48] J. B. Buncher, “Phenomenology of time-varying nuclear decay parameters,” Ph.D. dissertation, Purdue University, 2010.

- [49] J. M. Nistor, “Direct and indirect searches for anomalous beta decay,” Ph.D. dissertation, Purdue University, 2015.
- [50] D. Griffiths, *Introduction to Elementary Particles*. Weinheim: Wiley-VCH, 2004.
- [51] J. Jackson, Treiman, and H. Wyld Jr, “Possible tests of time reversal invariance in beta decay,” *Physical Review*, vol. 106, no. 1, pp. 517–521, 1957.
- [52] P. Adamson *et al.*, “Measurement of neutrino velocity with the minos detectors and numi neutrino beam,” *Phys. Rev. D*, vol. 76, p. 072005, 2007.
- [53] G. Kalbfleisch, N. Baggett, E. Fowler, and J. Alspector, “Experimental comparison of neutrino, antineutrino, and muon velocities,” *Physical Review Letters*, vol. 43, pp. 1361–1364, 1979.
- [54] N. Yu. Agafonova *et al.*, “Measurement of the velocity of neutrinos from the CNGS beam with the Large Volume Detector,” *Phys. Rev. Lett.*, vol. 109, p. 070801, 2012.
- [55] T. Adam *et al.*, “Measurement of the neutrino velocity with the OPERA detector in the CNGS beam,” *JHEP*, vol. 10, p. 093, 2012.
- [56] P. Alvarez Sanchez *et al.*, “Measurement of CNGS muon neutrino speed with Borexino,” *Phys. Lett.*, vol. B716, pp. 401–405, 2012.
- [57] P. Adamson *et al.*, “Precision Measurement of the Speed of Propagation of Neutrinos using the MINOS Detectors,” *Phys. Rev.*, vol. D92, no. 5, p. 052005, 2015.
- [58] L. Stodolsky, “The speed of light and the speed of neutrinos,” *Physics Letters B*, vol. 201, no. 3, pp. 353 – 354, 1988.
- [59] M. J. Longo, “Tests of relativity from sn1987a,” *Phys. Rev. D*, vol. 36, pp. 3276–3277, 1987.
- [60] F. W. Stecker and S. T. Scully, “Propagation of superluminal pev icecube neutrinos: A high energy spectral cutoff or new constraints on lorentz invariance violation,” *Phys. Rev. D*, vol. 90, 2014.
- [61] D. J. Griffiths, *Introduction to Electrodynamics*, 4th ed. Cambridge: Cambridge University Press, 2017.
- [62] M. Goldberger and K. Watson, *Collision Theory*. Mineola, NY: Dover Publications, 2004.
- [63] S.-H. Seo, “New Results from RENO and The 5 MeV Excess,” *AIP Conf. Proc.*, vol. 1666, no. 1, p. 080002, 2015.
- [64] Y. Abe *et al.*, “Improved measurements of the neutrino mixing angle θ_{13} with the Double Chooz detector,” *JHEP*, vol. 10, p. 086, 2014.
- [65] F. P. An *et al.*, “Measurement of the reactor antineutrino flux and spectrum at daya bay,” *Phys. Rev. Lett.*, vol. 116, p. 061801, Feb 2016.
- [66] K. Olive, “Review of particle physics,” *Chinese Physics C*, vol. 38, no. 9, p. 090001, 2014.

- [67] M. Tanabashi *et al.*, “Review of particle physics,” *Phys. Rev. D*, vol. 98, p. 030001, Aug 2018. [Online]. Available: <https://link.aps.org/doi/10.1103/PhysRevD.98.030001>
- [68] E. Fischbach, “A lower bound on neutrino mass,” *Ann. Phys. (NY)*, vol. 247, p. 214, 1998.
- [69] B. McElrath, “Laboratory tests for the cosmic neutrino background using beta-decaying nuclei,” in *Particles and nuclei. Proceedings, 18th International Conference, PANIC08, Eilat, Israel, November 9-14, 2008*, 2009, pp. 806–809.
- [70] J. N. Bahcall and R. K. Ulrich, “Solar models, neutrino experiments, and helioseismology,” *Rev. Mod. Phys.*, vol. 60, pp. 297–372, Apr 1988.
- [71] M. Kay, “New methodologies for measuring and monitoring nuclear decay parameters for time dependent behavior,” Ph.D. dissertation, Purdue University, 2018.
- [72] D. A. Vallado, *Fundamentals of Astrodynamics and Applications*. El Segundo, California: Microcosm Press, 2007.
- [73] E. J. Konopinski, *The Theory of Beta Radioactivity*. Ely House, London: Oxford University Press, 1966.
- [74] T. Lee and C. Yang, “Question of parity conservation in weak interactions,” *Physical Review*, vol. 104, no. 1, pp. 254–258, 1956.

APPENDICES

A. ALTERNATE PARAMETERIZATION OF ARBITRARY FORCES IN TORSION BALANCE EXPERIMENTS

Here we introduce an alternative parameterization for arbitrary forces in the Eötvös experiment. We begin by writing the fifth force with arbitrary position and velocity dependence

$$\vec{F}_5 = m q_5 \vec{\mathcal{F}}_5(\vec{X}, \vec{v}), \quad (\text{A.1})$$

where $\vec{X} = [X, Y, Z]^T$, $\vec{v} = [v_X, v_Y, v_Z]^T$, and \vec{F}_5 are the position, velocity, and fifth force as measured in the N-E-D frame. The position and velocity can be decomposed into

$$\vec{X} = \vec{X}_0 + \vec{X}'(\vec{r}, \phi), \quad (\text{A.2})$$

$$\vec{v} = \vec{v}_0 + \vec{v}'(\vec{r}, \phi), \quad (\text{A.3})$$

where \vec{X}_0 and \vec{v}_0 are the position and velocity of the pivot point, \vec{X}' and \vec{v}' are the position and velocity of the test masses relative to the pivot point, \vec{r} is the position of the test masses in the balance frame, and ϕ is the twist angle of the balance.

We use the fact that $|\vec{X}'| \ll |\vec{X}_0|$ and $|\vec{v}'| \ll |\vec{v}_0|$ to Taylor expand the force

$$\vec{\mathcal{F}} = \vec{\mathcal{F}}_0 + \vec{X}' \cdot \nabla_{\vec{X}} \vec{\mathcal{F}} + \vec{v}' \cdot \nabla_{\vec{v}} \vec{\mathcal{F}}. \quad (\text{A.4})$$

We neglect the motion of the torsion balance itself, so the velocity is only due to the rotation of the Earth. Writing the position of the the test mass as

$$\vec{X} = X' \hat{N} + Y' \hat{E} + (Z' - R) \hat{D}, \quad (\text{A.5})$$

where R is the radius of the Earth. The velocity of the test mass can be written as

$$\begin{aligned}
\vec{v} &= \Omega Y' s_\zeta \hat{N} - \Omega [X' s_\zeta + (Z' - R) c_\zeta] \hat{E} + \Omega Y' c_\zeta \hat{D} \\
&= \Omega R c_\zeta \hat{E} + \left[\Omega Y' s_\zeta \hat{N} - \Omega (X' s_\zeta + Z' c_\zeta) \hat{E} + \Omega Y' c_\zeta \hat{D} \right] \\
&= \vec{v}_0 + \vec{v}'.
\end{aligned} \tag{A.6}$$

Since \vec{v}' is linear in \vec{X}' , we can then write v' as

$$\vec{v}' = \vec{X}' \cdot \nabla_{\vec{X}'} \vec{v}', \tag{A.7}$$

where

$$\nabla_{\vec{X}'} \vec{V}' = \begin{bmatrix} 0 & \Omega s_\zeta & 0 \\ -\Omega s_\zeta & 0 & -\Omega c_\zeta \\ 0 & \Omega c_\zeta & 0 \end{bmatrix}. \tag{A.8}$$

We can then write the specific force as

$$\vec{\mathcal{F}} = \vec{\mathcal{F}}_0 + \vec{X}' \cdot \left(\nabla_{\vec{X}'} \vec{\mathcal{F}} + \nabla_{\vec{X}'} \vec{V}' \cdot \nabla_{\vec{V}'} \vec{\mathcal{F}} \right). \tag{A.9}$$

We can compare this to the equation used in Chapter 3. We can now apply Eötvös' “software method” to compute the force on the torsion balance. The difference in fifth force charges for the Eötvös experiment

$$\begin{aligned}
&(\kappa - \kappa') G \sin \beta \\
&= (q_1 - q'_1) \left\{ F_{X_0} + \frac{\nu}{m} F_{Y_0} + \sin \beta F_{Z_0} \right. \\
&\quad - \frac{K}{M\ell} \frac{m}{4L} (\partial_{Y_0} F_{Y_0} - \partial_{X_0} F_{X_0}) \frac{\nu}{m} + h \left(\partial_{Z_0} F_{X_0} + \frac{\nu}{m} \partial_{Z_0} F_{Y_0} \right) \\
&\quad - h \sin \beta \left(\partial_{X_0} F_{X_0} + \frac{\nu}{m} \partial_{X_0} F_{Y_0} - \partial_{Z_0} F_{Z_0} \right) \\
&\quad - h \sin \beta \Omega \cos \zeta \left(\partial_{V_{Y_0}} F_{Z_0} - \frac{\nu}{m} \partial_{V_{Y_0}} F_{Y_0} - \tan \zeta \partial_{V_{Y_0}} F_{X_0} \right) \\
&\quad - h \Omega \cos \zeta \left(\partial_{V_{Y_0}} F_{X_0} + \frac{\nu}{m} \partial_{V_{Y_0}} F_{Y_0} \right) \\
&\quad - \frac{K}{M\ell} \frac{m}{4L} \frac{\nu}{m} \Omega \sin \zeta \left(\partial_{V_{Y_0}} F_{X_0} + \frac{1}{2} \partial_{V_{X_0}} F_{X_0} + \frac{1}{2} \partial_{V_{X_0}} F_{Y_0} \right. \\
&\quad \left. + \cot \zeta \partial_{V_{Z_0}} F_{Y_0} \right) \left. \right\}. \tag{A.10}
\end{aligned}$$

The fifth force signal for the Adelberger experiment is

$$\begin{aligned}
T = & - (q_1 - q_2) M \ell \sin \phi (F_{X_0} + F_{Y_0} + \sin \beta F_{Z_0}) \\
& - (q_1 - q_2) M \ell \cos \phi (F_{X_0} - F_{Y_0} + \sin \beta F_{Z_0}) \\
& + (q_1 + q_2) \frac{K}{2} (\partial_{X_0} F_{Y_0} - \partial_{Y_0} F_{X_0}) \\
& - (q_1 + q_2) \frac{K}{2} \sin \beta (\partial_{Y_0} F_{Z_0} - \partial_{Z_0} F_{Y_0}) \\
& - (q_1 + q_2) \frac{K}{2} \Omega \sin \zeta (\partial_{V_{X_0}} F_{X_0} + \partial_{V_{Y_0}} F_{Y_0} + \sin \beta \partial_{V_{X_0}} F_{Z_0}) \\
& - (q_1 + q_2) \frac{K}{2} \Omega \cos \zeta (\partial_{V_{Z_0}} F_{X_0} + \partial_{V_{Y_0}} F_{Y_0} + \sin \beta \partial_{V_{Z_0}} F_{Z_0}) . \quad (\text{A.11})
\end{aligned}$$

B. REFERENCE FRAMES AND FRAME ROTATIONS

B.1 Reference Frames and Conversions

B.1.1 Space-Based Reference Frames

We will use a number of reference frames in our analysis, which we define here. We will borrow heavily the notation of Vallado [72]. The **Heliocentric** (or **ecliptic**) Frame, $\{\hat{X}, \hat{Y}, \hat{Z}\}$, is an inertial frame fixed to the Sun with the ecliptic frame as the fundamental plane. The axes are defined such that \hat{X} points toward the vernal equinox, \hat{Z} is perpendicular to the ecliptic plane, and \hat{Y} completes the triplet

$$\hat{Y} = \hat{Z} \times \hat{X}. \quad (\text{B.1})$$

For an orbiting object, we can define a **perifocal** frame, $\{\hat{P}, \hat{Q}, \hat{W}\}$. The \hat{P} vector points toward periapsis of the orbit, \hat{W} points along the angular momentum vector and \hat{Q} completes the set. The relationship between the inertial perifocal frames are shown in Figure B.1. The angles relating the the perifocal frame to the inertial frame are the longitude of the ascending node, Ω , the inclination, i , and the argument of periapsis, θ^* .

B.1.2 Earth-Based Reference Frame

The **Earth Centered Inertial (ECI)** frame, $\{\hat{I}, \hat{J}, \hat{K}\}$ is fixed at the center of the Earth with \hat{I} pointing toward the vernal equinox, \hat{K} pointing along the Earth's rotation axis, and the \hat{J} completing the triplet

$$\hat{J} = \hat{K} \times \hat{I}. \quad (\text{B.2})$$

The ECI and heliocentric frames are related by a rotation about the common $\hat{X} - \hat{I}$ axis through the angle, ϵ , known as the obliquity of the ecliptic.

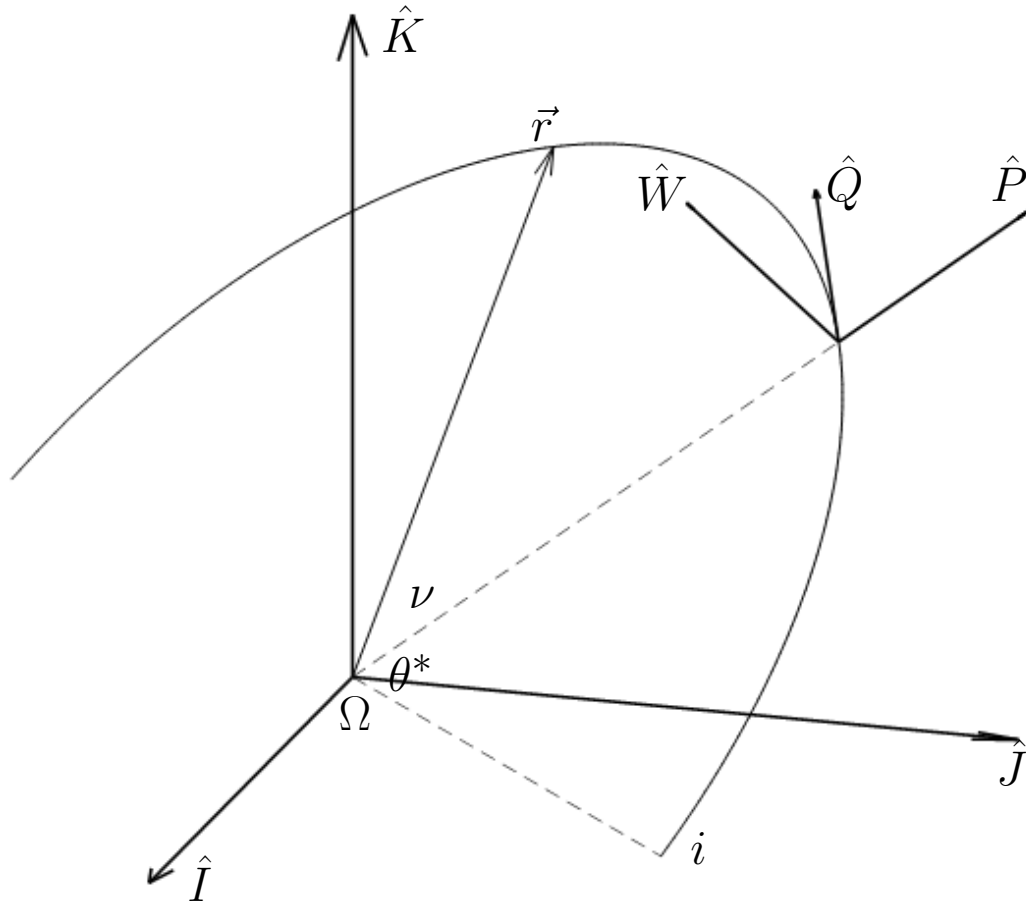


Fig. B.1. The relationship between the inertial frame and the perifocal frame. Ω is the longitude of the ascending node, i is the inclination and θ^* is the argument of periapsis. The perifocal frame is related to the local orbital frame by the true anomaly, ν .

B.1.3 Body Reference Frames

The final frame needed is the **body** frame denoted by $\{\hat{b}_1, \hat{b}_2, \hat{b}_3\}$. We will assume that \hat{b}_1 is along the sensitive axis of the test mass and \hat{b}_3 is along the rotation axis of the MICROSCOPE spacecraft. The body frame is related to an inertial frame by a sequence of three simple rotations, which will be discussed later.

B.1.4 Frame Conversions

We now need relationships between reference frames. Again, we will borrow heavily from Vallado. A general rotation from one reference frame to another requires an axis of rotation and an angle of rotation. We can define fundamental rotations as those about the x , y , and z -axes. These rotations are given by,

$$\text{Rot1}(\theta) = \begin{bmatrix} 1 & 0 & 0 \\ 0 & c_\theta & s_\theta \\ 0 & -s_\theta & c_\theta \end{bmatrix}, \quad (\text{B.3})$$

$$\text{Rot2}(\theta) = \begin{bmatrix} c_\theta & 0 & -s_\theta \\ 0 & 1 & 0 \\ s_\theta & 0 & c_\theta \end{bmatrix}, \quad (\text{B.4})$$

$$\text{Rot3}(\theta) = \begin{bmatrix} c_\theta & s_\theta & 0 \\ -s_\theta & c_\theta & 0 \\ 0 & 0 & 1 \end{bmatrix}. \quad (\text{B.5})$$

Any generic 3-dimensional rotation can be represented in terms of a sequence of fundamental rotations, such as 3-1-3 or 3-2-1.

Vectors in the heliocentric and ECI frames are related by the obliquity of the ecliptic

$$\vec{r}_{IJK}, \vec{v}_{IJK} = \text{Rot1}(-\epsilon) \vec{r}_{XYZ}, \vec{v}_{XYZ}, \quad (\text{B.6})$$

where $\epsilon = 23.44 \text{ deg}$ is the obliquity of the ecliptic, more commonly known as the axial tilt of the Earth.

The transformation from a perifocal frame to the heliocentric frame is given by a 3-1-3 rotation sequence,

$$\begin{aligned}\vec{r}_{inertial}, \vec{v}_{inertial} &= \text{Rot3}(-\Omega) \text{Rot1}(-i) \text{Rot3}(-\theta^*) \vec{r}_{PQW}, \vec{v}_{PQW}, \\ \vec{r}_{PQW}, \vec{v}_{PQW} &= \text{Rot3}(\theta^*) \text{Rot1}(i) \text{Rot3}(\Omega) \vec{r}_{inertial}, \vec{v}_{inertial}.\end{aligned}\tag{B.7}$$

The final coordinate transformation we need is to relate the body frame to ECI frame. As we stated before, the general transformation from one frame to another can be written in terms of the three Euler angles, three rotations about body-fixed x , y , and z axes. The order of rotations matters; a different order will yield a different set of Euler angles. Normally one order proves to be advantageous for a given problem, which is the case here. Since we want the spin (\hat{b}_3) axis perpendicular to the orbit (since the MICROSCOPE spacecraft is in a sun-synchronous orbit), we use a 3-1-3 order as we do for the perifocal frame. The first two angles are simply the satellite longitude of the ascending node, Ω_s , and the satellite inclination, i_s . The third angle is then the satellite spin rate times time, $\omega_{spin}t$, and the transformation is given by,

$$\vec{r}_{bod}, \vec{v}_{bod} = \text{Rot3}(\omega_{sat}t) \text{Rot1}(i_s) \text{Rot3}(\Omega_s) \vec{r}_{IJK}, \vec{v}_{IJK}.\tag{B.8}$$

B.2 Velocity of the MICROSCOPE Test Mass

B.2.1 Velocity of the Sun through the galaxy

The velocity of the sun relative to the galaxy is measured from Earth and can be written directly in the ECI frame

$$\vec{v}_{sun,gal} = 227.7 \text{ km/s} \begin{bmatrix} 0.464 \\ -0.489 \\ 0.739 \end{bmatrix}.\tag{B.9}$$

B.2.2 Orbital Velocity

The position vector of an orbiting body can be written in terms of the orbital elements in the perifocal coordinate frame as

$$\vec{r}_{PQW} = \begin{bmatrix} \frac{p \cos \nu}{1 + e \cos \nu} \\ \frac{p \sin \nu}{1 + e \cos \nu} \\ 0 \end{bmatrix}, \quad (\text{B.10})$$

where $p = a(1 - e^2)$ is the semilatus rectum, a is the semimajor axis, e is the eccentricity, and ν is the true anomaly of the orbit. Here ν is the only component that depends on time. We can take the derivative to find the velocity

$$\vec{v}_{PQW} = \sqrt{\frac{GM}{p}} \begin{bmatrix} -\sin \nu \\ e + \cos \nu \\ 0 \end{bmatrix}, \quad (\text{B.11})$$

where we have used definitions of the specific angular momentum, $h = r^2 \dot{\nu} = \sqrt{GMp}$.

We can now simply use our rotations to convert the orbital velocities to central body inertial frames. The satellite velocity is naturally in the ECI frame, and the Earth velocity is naturally in the heliocentric frame, so we will need an additional rotation of ϵ to write the velocity of the Earth in the ECI frame,

$$\begin{aligned} \vec{v}_{sat,IJK} &= \text{Rot3}(-\Omega_s) \text{Rot1}(-i_s) \text{Rot3}(-\theta_s^*) \sqrt{\frac{GM_{Earth}}{p_s}} \begin{bmatrix} -\sin \nu_s \\ e_s + \cos \nu_s \\ 0 \end{bmatrix}, \quad (\text{B.12}) \\ \vec{v}_{Earth,IJK} &= \text{Rot1}(-\epsilon) \text{Rot3}(-\Omega_e) \text{Rot1}(-i_e) \text{Rot3}(-\theta_e^*) \sqrt{\frac{GM_{Sun}}{p_e}} \begin{bmatrix} -\sin \nu_e \\ e_e + \cos \nu_e \\ 0 \end{bmatrix}, \quad (\text{B.13}) \end{aligned}$$

where the s and e subscripts on the orbital elements denote Earth and spacecraft.

B.2.3 Total Velocity

We now have the components of the velocity in the ECI, so we must convert to the body frame to analyze in the MICROSCOPE experiment. The total velocity in the body frame is then given by,

$$\begin{aligned}
\vec{v}_{tot,bod} &= \vec{v}_{sun,gal} + \vec{v}_{earth,sun} + \vec{v}_{sc,Earth} \\
&= \text{Rot3}(\omega_{sat}t) \text{Rot1}(i_s) \text{Rot3}(\Omega_s) \\
&\quad \times \left\{ 227.7 \text{ km/s} \begin{bmatrix} 0.464 \\ -0.489 \\ 0.739 \end{bmatrix} \right. \\
&\quad + \text{Rot3}(-\Omega_s) \text{Rot1}(-i_s) \text{Rot3}(-\theta_s^*) \sqrt{\frac{GM_{Earth}}{p_s}} \begin{bmatrix} -\sin \nu_s \\ e_s + \cos \nu_s \\ 0 \end{bmatrix} \\
&\quad \left. + \text{Rot1}(-\epsilon) \text{Rot3}(-\Omega_e) \text{Rot1}(-i_e) \text{Rot3}(-\theta_e^*) \sqrt{\frac{GM_{Sun}}{p_e}} \begin{bmatrix} -\sin \nu_e \\ e_e + \cos \nu_e \\ 0 \end{bmatrix} \right\}.
\end{aligned} \tag{B.14}$$

C. DERIVATION OF THE MATRIX ELEMENT FOR BETA DECAY OF A POLARIZED NEUTRON

We wish to evaluate the matrix element for nuclear beta decay

$$\mathcal{M} = \langle f | H_{int} | i \rangle, \quad (\text{C.1})$$

where H_i is the interaction Hamiltonian and J_μ^ℓ is the lepton current for this decay

$$H_{int} = \frac{G_F}{\sqrt{2}} \tau^+ \gamma^\mu (1 - \lambda \gamma^5) J_\mu^\ell, \quad (\text{C.2})$$

$$J_\mu^\ell = \bar{\psi}_e \gamma_\mu (1 - \gamma^5) \psi_{\bar{\nu}}, \quad (\text{C.3})$$

where G_F is the Fermi constant, λ is the relative strenght of the vector and axial-vector couplings, τ^+ is the isospin raising operator, γ_μ and γ_5 are the 4×4 Dirac matrices [50], and ϕ_i , $i = \{e, \bar{n}u\}$ are the electron and antineutrino wavefunctions. In position representation, the full matrix element becomes

$$\mathcal{M} = \frac{G_F}{\sqrt{2}} \int \bar{\psi}_p \gamma^\mu (1 - \lambda \gamma^5) \psi_n \bar{\psi}_e \gamma^\mu (1 - \gamma^5) \psi_{\bar{\nu}} d^3r. \quad (\text{C.4})$$

The proton, electron, and antineutrino are represented by standard wave functions

$$\psi_n(\vec{r}) = \sqrt{\frac{c}{2E_1V}} u^{s_1}(p_1) e^{i\vec{p}_1 \cdot \vec{r}/\hbar}, \quad (\text{C.5})$$

$$\psi_{\bar{\nu}}(\vec{r}) = \sqrt{\frac{c}{2E_2V}} u^{s_2}(p_2) e^{-i\vec{p}_2 \cdot \vec{r}/\hbar}, \quad (\text{C.6})$$

$$\psi_p(\vec{r}) = \sqrt{\frac{c}{2E_3V}} u^{s_3}(p_3) e^{i\vec{p}_3 \cdot \vec{r}/\hbar}, \quad (\text{C.7})$$

$$\psi_e(\vec{r}) = \sqrt{\frac{c}{2E_4V}} v^{u_4}(p_4) e^{i\vec{p}_4 \cdot \vec{r}/\hbar}, \quad (\text{C.8})$$

where V is the normalization volume, $p_i(E_i)$ is the momentum(energy) of the i th particle. We have followed the momentum prescription of Griffiths [50]. The spinors u and v are normalized as

$$u^{\dagger r} u^s = -v^{\dagger r} v^s = 2 \frac{E}{c} \delta_{rs}. \quad (\text{C.9})$$

Substituting the wavefunctions into Eq. (C.4), we obtain

$$\begin{aligned} \mathcal{M} = & \frac{G_F c^2}{4V^2 \sqrt{2E_1 E_2 E_3 E_4}} \bar{u}(p_3) \gamma^\mu (1 - \lambda \gamma^5) u(p_1) \\ & \times \bar{u}(p_4) \gamma_\mu (1 - \gamma^5) v(p_4) \int e^{i(\vec{p}_1 - \vec{p}_2 - \vec{p}_3 - \vec{p}_4) \cdot \vec{r} / \hbar} d^3 r, \end{aligned} \quad (\text{C.10})$$

where we have suppressed the spin indices. We now take the modulus squared of \mathcal{M} and sum over the proton, electron, and antineutrino spins

$$\begin{aligned} \langle |\mathcal{M}^2| \rangle = & \sum_{s_2, s_3, s_4} |\mathcal{M}|^2 = \frac{G_F^2 c^4}{32V^3 E_1 E_2 E_3 E_4} N^{\mu\nu} L_{\mu\nu} \\ & \times (2\pi\hbar)^3 \delta^3(\vec{p}_1 - \vec{p}_2 - \vec{p}_3 - \vec{p}_4), \end{aligned} \quad (\text{C.11})$$

where

$$\left[\int e^{i(\vec{p}_1 - \vec{p}_2 - \vec{p}_3 - \vec{p}_4) \cdot \vec{r} / \hbar} d^3 r \right]^2 = V (2\pi\hbar)^3 \delta^3(\vec{p}_1 - \vec{p}_2 - \vec{p}_3 - \vec{p}_4). \quad (\text{C.12})$$

The lepton tensor, $L_{\mu\nu}$, is a trace over gamma matrices

$$L_{\mu\nu} = \text{Tr} \left[\gamma_\mu (1 - \gamma^5) \not{p}_2 \gamma_\nu (1 - \gamma^5) (\not{p}_4 + m_4 c) \right]. \quad (\text{C.13})$$

The traces are straightforward to evaluate (see Appendix D or any text on particle physics, e.g. [50])

$$L_{\mu\nu} = 8 [p_{2\mu} p_{4\nu} + p_{2\nu} p_{4\mu} - \eta_{\mu\nu} (p_2 \cdot p_4) - i \epsilon_{\mu\nu\kappa\tau} p_2^\kappa p_4^\tau], \quad (\text{C.14})$$

where $\eta^{\mu\nu}$ is the Minkowski metric with signature $(+, -, -, -)$ and $\epsilon_{\mu\nu\kappa\tau}$ is the totally antisymmetric operator with $\epsilon_{0123} = -1$.

The nuclear tensor, $N^{\mu\nu}$ is

$$N^{\mu\nu} = u^\dagger(p_1) \gamma^0 \gamma^\nu (1 - \gamma^5) (\not{p}_3 + m_3 c) \gamma^\mu (1 - \gamma^5) u(p_1). \quad (\text{C.15})$$

We assume that the neutron is at rest. As we are considering a polarized neutron, we take the spin up state, given by

$$u(p_1) = \sqrt{2m_1 c} \begin{bmatrix} 1 \\ 0 \\ 0 \\ 0 \end{bmatrix}. \quad (\text{C.16})$$

To simplify calculations, we will neglect the recoil of the proton. We introduce the integral over the proton phase space $(Vd^3p_3) / (2\pi\hbar)^3$ which eliminates the delta function over momentum in Eq. (C.11). Then we neglect the proton's recoil momentum relative to it's mass, so we let $E_3 \rightarrow m_3c^2$. Then we have the following simplification

$$\not{p}_3 + m_3c = 2m_3c \begin{bmatrix} 1 & 0 & 0 & 0 \\ 0 & 1 & 0 & 0 \\ 0 & 0 & 0 & 0 \\ 0 & 0 & 0 & 0 \end{bmatrix}. \quad (\text{C.17})$$

We now compute the matrix elements for four cases.

$$\mu = 0, \nu = 0$$

$$N^{00} = 4m_1m_3c^2, \quad (\text{C.18})$$

$$N^{00}L_{00} = 32m_1m_3c^2 \left(\frac{E_2E_4}{c^2} + \vec{p}_2 \cdot \vec{p}_4 \right). \quad (\text{C.19})$$

$$\mu = 0, \nu = i$$

$$N^{0i} = -4m_1m_3c^2\delta_{i3}, \quad (\text{C.20})$$

$$N^{0i}L_{0i} = -32m_1m_3c^2\lambda \left(\frac{E_2}{c}p_{4z} + \frac{E_4}{c}p_{2z} - i\epsilon_{03\kappa\tau}P^{2\kappa}P^{4\tau} \right). \quad (\text{C.21})$$

$$\mu = i, \nu = 0$$

$$N^{i0} = -4m_1m_3c^2\delta_{i3}, \quad (\text{C.22})$$

$$N^{i0}L_{i0} = -32m_1m_3c^2\lambda \left(\frac{E_4}{c}p_{2z} + \frac{E_2}{c}p_{4z} + i\epsilon_{03\kappa\tau}P^{2\kappa}P^{4\tau} \right). \quad (\text{C.23})$$

$$\mu = i, \nu = j$$

$$N^{ij} = 4m_1m_3c^2\lambda^2(\delta_{ij} - i\epsilon_{ij3}), \quad (\text{C.24})$$

$$\begin{aligned} N^{ij}L_{ij} &= 32m_1m_3c^2\lambda^2\left(\frac{3E_2E_4}{c^2} + \vec{p}_2 \cdot \vec{p}_4\right) \\ &\quad - 64m_1m_3c^2\lambda^2\left(\frac{E_4}{c}p_{2z} - \frac{E_2}{c}p_{4z}\right). \end{aligned} \quad (\text{C.25})$$

Full Results

$$\begin{aligned} N^{\mu\nu}L_{\mu\nu} &= 32m_1m_3E_2E_4(1 + 3\lambda^2) + 32m_1m_3(1 - \lambda^2)\vec{p}_2c \cdot \vec{p}_4c \\ &\quad - 64m_1m_3E_4(\lambda + \lambda^2)p_{2z}c - 64m_1m_3E_2(\lambda - \lambda^2)p_{4z}c. \end{aligned} \quad (\text{C.26})$$

The p_{2z} and p_{4z} appear because we assumed that the neutron is polarized in the z-direction. To allow for arbitrary polarization, we let $p_z \rightarrow \hat{I} \cdot \vec{p}$ where \hat{I} is the neutron spin direction. We can then write

$$\begin{aligned} N^{\mu\nu}L_{\mu\nu} &= 128m_1m_3E_2E_4|\mathcal{M}_{if}|^2 \\ &\quad \times \left(1 + a\frac{\vec{p}_2c \cdot \vec{p}_4c}{E_2E_4} + A\hat{I} \cdot \frac{\vec{p}_4c}{E_4} + B\hat{I} \cdot \frac{\vec{p}_2c}{E_2}\right), \end{aligned} \quad (\text{C.27})$$

$$|\mathcal{M}_{if}|^2 = \frac{1}{4}(1 + 3\lambda^2), \quad (\text{C.28})$$

$$|\mathcal{M}_{if}|^2a = \frac{1}{4}(1 - \lambda^2), \quad (\text{C.29})$$

$$|\mathcal{M}_{if}|^2A = -\frac{1}{2}(\lambda - \lambda^2), \quad (\text{C.30})$$

$$|\mathcal{M}_{if}|^2B = -\frac{1}{2}(\lambda + \lambda^2). \quad (\text{C.31})$$

We have introduced fairly standard symbols for the anisotropies (see, for example, [73], [74], and [51]). For decays other than the neutron, ξ , A and B will differ based on the Fermi and Gamow-Teller matrix elements and spin of the parent and daughter nuclei. (Note: in a notable departure, we have used $|\mathcal{M}_{if}|^2$, instead of ξ , which is

common in the literature. We have done this to make it even more apparent that this term will depend on the nucleus decaying.)

The matrix element is then (recalling we got rid of the delta function and one factor of volume with the proton phase state factor).

$$\langle |\mathcal{M}^2| \rangle = \frac{4G_F^2 |\mathcal{M}_{if}|^2}{V^2} \left(1 + a \frac{\vec{p}_2 c}{E_2} \cdot \frac{\vec{p}_4 c}{E_4} + A \hat{I} \cdot \frac{\vec{p}_4 c}{E_4} + B \hat{I} \cdot \frac{\vec{p}_2 c}{E_2} \right). \quad (\text{C.32})$$

D. SOLUTION TO THE LEPTON TENSOR TRACES

We wish to solve for the traces in the lepton tensor, $L^{\mu\nu}$,

$$L^{\mu\nu} = \text{Tr} \left[\gamma^\mu (1 - \gamma^5) \not{p}_2 \gamma^\nu (1 - \gamma^5) (\not{p}_4 + m_4 c) \right]. \quad (\text{D.1})$$

There are eight total traces, but we can eliminate some right away. Any trace containing $m_4 c$ will have three γ^σ and zero, one, or two γ^5 's. The trace of an odd number of γ^σ 's or an odd number of γ^σ 's and a γ^5 is zero and the case with the two γ^5 's will eventually simplify to three γ^σ 's and will also be zero. Thus our $L^{\mu\nu}$ simplifies and we only have four traces to solve.

$$\begin{aligned} L^{\mu\nu} &= \text{Tr} \left[\gamma^\mu (1 - \gamma^5) \not{p}_2 \gamma^\nu (1 - \gamma^5) \not{p}_4 \right] \\ &= p_{2\kappa} p_{4\tau} \text{Tr} \left[\gamma^\mu (1 - \gamma^5) \gamma^\kappa \gamma^\nu (1 - \gamma^5) \gamma^\tau \right]. \end{aligned} \quad (\text{D.2})$$

D.1 $\text{Tr} (\gamma^\mu \gamma^\kappa \gamma^\nu \gamma^\tau)$

By definition (see any textbook on particle physics or quantum field theory [50])

$$\text{Tr} [\gamma^\mu \gamma^\kappa \gamma^\nu \gamma^\tau] = 4 (\eta^{\mu\kappa} \eta^{\nu\tau} - \eta^{\mu\nu} \eta^{\kappa\tau} + \eta^{\mu\tau} \eta^{\nu\kappa}). \quad (\text{D.3})$$

D.2 $-\text{Tr} (\gamma^\mu \gamma^\kappa \gamma^\nu \gamma^5 \gamma^\tau)$

Using the fact that γ^5 commutes with the γ^μ ($\{\gamma^5, \gamma^\mu\} = \gamma^5 \gamma^\mu + \gamma^\mu \gamma^5 = 0$) and the cyclicity of the trace,

$$\begin{aligned} -\text{Tr} (\gamma^\mu \gamma^\kappa \gamma^\nu \gamma^5 \gamma^\tau) &= \text{Tr} (\gamma^\mu \gamma^\kappa \gamma^\nu \gamma^\tau \gamma^5) \\ &= \text{Tr} (\gamma^5 \gamma^\mu \gamma^\kappa \gamma^\nu \gamma^\tau) \\ &= 4i \epsilon^{\mu\kappa\nu\tau} = -4i \epsilon^{\mu\nu\kappa\tau}. \end{aligned} \quad (\text{D.4})$$

D.3 $-Tr(\gamma^\mu \gamma^5 \gamma^\kappa \gamma^\nu \gamma^\tau)$

$$\begin{aligned} -Tr(\gamma^\mu \gamma^5 \gamma^\kappa \gamma^\nu \gamma^\tau) &= Tr(\gamma^5 \gamma^\mu \gamma^\kappa \gamma^\nu \gamma^\tau) \\ &= 4i\epsilon^{\mu\kappa\nu\tau} = -4i\epsilon^{\mu\nu\kappa\tau}. \end{aligned} \quad (\text{D.5})$$

D.4 $Tr(\gamma^\mu \gamma^5 \gamma^\kappa \gamma^\nu \gamma^5 \gamma^\tau)$

Since $(\gamma^5)^2 = 1$,

$$\begin{aligned} Tr(\gamma^\mu \gamma^5 \gamma^\kappa \gamma^\nu \gamma^5 \gamma^\tau) &= -Tr(\gamma^\mu \gamma^\kappa \gamma^5 \gamma^\nu \gamma^5 \gamma^\tau) \\ &= Tr(\gamma^\mu \gamma^\kappa \gamma^\nu \gamma^5 \gamma^5 \gamma^\tau) \\ &= Tr(\gamma^\mu \gamma^\kappa \gamma^\nu \gamma^\tau) \\ &= 4(\eta^{\mu\kappa} \eta^{\nu\tau} - \eta^{\mu\nu} \eta^{\kappa\tau} + \eta^{\mu\tau} \eta^{\nu\kappa}). \end{aligned} \quad (\text{D.6})$$

D.5 Full Solution

Combining the four solutions, we find

$$\boxed{L^{\mu\nu} = 8 [p_2^\mu p_4^\nu + p_2^\nu p_4^\mu - \eta^{\mu\nu} (p_2 \cdot p_4) - i\epsilon^{\mu\nu\kappa\tau} p_{2\kappa} p_{4\tau}]} \quad (\text{D.7})$$

E. COMPUTATION OF THE BETA DECAY INTEGRAL

In this appendix, we wish to evaluate the beta decay integral Eq. (6.13)

$$f(Z, E_0) = \frac{1}{(m_e c^2)^5} \int_{m_e c^2}^{E_0} F(Z, E_e) \sqrt{E_e^2 - m_e^2 c^4} E_e (E_0 - E_e)^2 dE_e. \quad (\text{E.1})$$

Unfortunately, it is not possible to solve this equation analytically for arbitrary Z .

We set $Z = 0$, then $F(0, E) = 1$ and the integral becomes

$$f(0, E_0) = \frac{1}{(m_e c^2)^5} \int_{m_e c^2}^{E_0} \sqrt{E_e^2 - m_e^2 c^4} E_e (E_0 - E_e)^2 dE_e. \quad (\text{E.2})$$

This integral is solvable; we begin by nondimensionalizing. Let $x = E_e/(m_e c^2)$ and $a = E_0/(m_e c^2)$. Then the integral is

$$\begin{aligned} f(0, a) &= \int_1^a \sqrt{x^2 - 1} x (a - x)^2 dx \\ &= \int_1^a \sqrt{x^2 - 1} (a^2 x - 2ax^2 + x^3) dx. \end{aligned} \quad (\text{E.3})$$

We see that there are three integrals to evaluate.

E.1 $I_1 = \int x \sqrt{x^2 - 1} dx$

This integral can be solved with a simple substitution $u = x^2 - 1$, $dy = 2x dx$. Then,

$$\begin{aligned} I_1 &= \frac{1}{2} \int \sqrt{u} du \\ &= \frac{1}{3} u^{3/2} \\ &= \frac{1}{3} (x^2 - 1)^{3/2}. \end{aligned} \quad (\text{E.4})$$

$$\mathbf{E.2} \quad I_2 = \int x^2 \sqrt{x^2 - 1} dx$$

For I_2 , we perform the substitution $x = \cosh u$, $dx = \sinh u du$. Then $\sqrt{\cosh^2 u - 1} = \sinh u$ and (using $\sinh 2u = 2 \sinh u \cosh u$ and $2 \sinh^2 u = \cosh 2u - 1$, $2 \cosh^2 u = \cosh 2u + 1$) the integral is given by,

$$\begin{aligned} I_2 &= \int \cosh^2 u \sinh^2 u du \\ &= \frac{1}{4} \int \sinh^2 2u du \\ &= \frac{1}{8} \int \cosh 4u - u du \\ &= \frac{1}{32} (\sinh 4u - 4u) \\ &= \frac{1}{16} (\sinh 2u \cosh 2u - 2u) \\ &= \frac{1}{8} [\sinh u \cosh u (2 \cosh^2 u - 1) - u] \\ &= \frac{1}{8} [\sqrt{\cosh^2 u - 1} \cosh u (2 \cosh^2 u - 1) - u] \\ &= \frac{1}{8} [\sqrt{x^2 - 1} (2x^3 - x) - \cosh^{-1}(x)]. \end{aligned} \tag{E.5}$$

We could leave I_2 in terms of the inverse hyperbolic cosine, but the standard answer (see [50]) writes this terms using natural logarithms. We can use the definition of the hyperbolic cosine, $\cosh u = (e^u + e^{-u})/2$ to write

$$\begin{aligned} \cosh u &= x \\ \frac{e^u + e^{-u}}{2} &= x. \end{aligned} \tag{E.6}$$

Let $z = e^u$, then

$$\begin{aligned} z + z^{-1} &= 2x \\ z^2 - 2xz + 1 &= 0 \\ \rightarrow z &= x \pm \sqrt{x^2 - 1} \\ \rightarrow u &= \cosh^{-1} x = \ln(x + \sqrt{x^2 - 1}). \end{aligned} \tag{E.7}$$

where we have taken the positive solution. The solution to I_2 is then

$$I_2 = \frac{1}{8} \left[\sqrt{x^2 - 1} (2x^3 - x) - \ln(x + \sqrt{x^2 - 1}) \right]. \quad (\text{E.8})$$

E.3 $I_3 = \int x^3 \sqrt{x^2 - 1} dx$

We begin by integrating by parts: We let $u = x^2$ and $dv = x\sqrt{x^2 - 1}dx$. Then, $du = 2xdx$, and we use the solution to I_1 (Eq. E.4) to set $v = \frac{1}{3}(x^2 - 1)^{3/2}$. Then the integral becomes

$$I_3 = \frac{1}{3}x^2(x^2 - 1)^{3/2} - \int \frac{2}{3}x(x^2 - 1)^{3/2} dx. \quad (\text{E.9})$$

We can solve this new integral with another the same substitution as I_1

$$\begin{aligned} I_{3b} &= \frac{2}{3} \int x(x^2 - 1)^{3/2} dx \\ &= \frac{1}{3} \int (u)^{3/2} du \\ &= \frac{2}{15} (u)^{5/2} \\ &= \frac{2}{15} (x^2 - 1)^{5/2}. \end{aligned} \quad (\text{E.10})$$

Then I_3 becomes

$$\begin{aligned} I_3 &= \frac{1}{3}x^2(x^2 - 1)^{3/2} - \frac{2}{15}(x^2 - 1)^{5/2} \\ &= \frac{1}{15}\sqrt{x^2 - 1} [(5x^4 - 5x^2) - 2(x^4 - 2x^2 + 1)] \\ &= \frac{1}{15}\sqrt{x^2 - 1} (3x^4 - x^2 - 2). \end{aligned} \quad (\text{E.11})$$

E.4 Full Results

Combining Eqs. (E.4), (E.8), and (E.11), the total integral is given by

$$\begin{aligned} I &= \frac{a^2}{3}\sqrt{x^2 - 1}(x^2 - 1) - \frac{a}{4}\sqrt{x^2 - 1}(2x^3 - x) \\ &\quad + \frac{1}{15}\sqrt{x^2 - 1}(3x^4 - x^2 - 2) + \frac{a}{4}\ln(x + \sqrt{x^2 - 1}) \end{aligned} \quad (\text{E.12})$$

Evaluating at the endpoints, a and 1 gives $F(0, a)$

$$\begin{aligned}
 f(0, a) &= \frac{a^2}{3} \sqrt{a^2 - 1} (a^2 - 1) - \frac{a}{4} \sqrt{a^2 - 1} (2a^3 - x) \\
 &\quad + \frac{1}{15} \sqrt{a^2 - 1} (3a^4 - a^2 - 2) + \frac{a}{4} \ln(a + \sqrt{a^2 - 1}) \\
 &= \frac{1}{60} \sqrt{a^2 - 1} (20a^4 - 20a^2 - 30a^4 + 15a^2 + 12a^4 - 4a^2 - 8) \\
 &\quad + \frac{a}{4} \ln(a + \sqrt{a^2 - 1})
 \end{aligned}$$

$$\boxed{f(0, a) = \frac{1}{4} \left[\frac{1}{15} (2a^4 - 9a^2 - 8) \sqrt{a^2 - 1} + a \ln(a + \sqrt{a^2 - 1}) \right]}. \quad (\text{E.13})$$

VITA

VITA

Michael James Mueterthies was born in April of 1988 in Lawler, Iowa, a small town in Northeast Iowa. His parents are Mark and Margaret (Peg) Mueterthies and he has an older sister Megan, a younger brother Matthew, a brother-in-law Kelly, and, recently, a niece Mollie. He spent his childhood on his family's dairy farm and was a 10 year member of his local 4-H club, the Lawler Lassies and Lads. Michael graduated from Turkey Valley High School in 2006.

Michael entered Purdue's School of Aeronautics and Astronautics Engineering where he graduated with highest honors with a Bachelor's Degree in May 2010 and a Master's Degree in May 2012. During his engineering career, Michael specialized in control systems. While an undergraduate student, Michael was an intern at Rockwell Collins, Continental Airlines, and the Space Dynamics Laboratory.

In 2011, Michael was a member of the inaugural class of the NASA Space Technology Research Fellowship program. Under the fellowship, Michael worked for two years with Professor James Longuski on spacecraft propulsion via electrodynamic tethers and one year on carbon nanotube electrodes with Professor John Cushman. While a fellow, Michael spent a summer at NASA Marshall Space Flight Center, performing space environmental experiments and was part of a NASA team investigating the practicality of propelling spacecraft using the Lorentz force.

Apparently not content being a rocket scientist, Michael entered the Purdue Department of Physics and Astronomy in Fall 2012 to pursue a PhD, earning a Master's Degree in 2017, after putting it off for several years. He joined the research group of Professor Ephraim Fischbach, investigating the Eötvös experiment and time-varying nuclear decay rates. While a physics graduate student, Michael served as teaching assistant and instructor for a number of courses.

In the July of 2016, Michael co-founded the company IFBattery, Inc, to study immiscible flow batteries. He briefly served as a staff scientist before reducing his involvement in the company in 2017. Since May of 2018, Michael has been a staff scientist at Blue Wave A.I. Labs performing machine learning analysis and developing A.I. systems.

When not diligently studying and working, Michael is a space and spaceflight enthusiast and enjoys video games and all forms of science fiction (especially if set in space).